

Macrophage-Derived Mechanisms of Resolution of Environmental Lung Injury

by

Marissa A. Guttenberg

Environment
Duke University

Date: February 21, 2024

Approved:

Robert M. Tighe, Co-Supervisor

Joel N. Meyer, Co-Supervisor

Loretta G. Que

Michael B. Fessler

Amanda S. Macleod

Junfeng Zhang

Dissertation submitted in partial fulfillment of
the requirements for the degree of
Doctor of Philosophy in Environment
in the Graduate School
of Duke University

2024

ABSTRACT

Macrophage-Derived Mechanisms of Resolution of Environmental Lung Injury

by

Marissa A. Guttenberg

Environment
Duke University

Date: February 21, 2024

Approved:

Robert M. Tighe, Co-Supervisor

Joel N. Meyer, Co-Supervisor

Loretta G. Que

Michael B. Fessler

Amanda S. Macleod

Junfeng Zhang

Abstract of dissertation submitted in partial fulfillment of
the requirements for the degree of
Doctor of Philosophy in Environment
in the Graduate School
of Duke University

2024

Copyright by
Marissa A. Guttenberg
2024

Abstract

Lung inflammation, caused by acute exposure to ozone (O₃)– one of the six criteria air pollutants – is a significant source of morbidity in susceptible individuals. The adverse effects of ozone (O₃) on respiratory health and its significant impact on global public health are well-established, but the cellular mechanisms that drive these effects remain poorly understood. This study explores mechanisms that regulate resolution of O₃-induced lung inflammation, specifically focused on the function of alveolar macrophages. Alveolar macrophages (AMØs) are central regulators of lung immune responses including both the initiation and resolution of inflammation. They regulate inflammation via functions such as production of cytokines, phagocytosis, and efferocytosis. While prior O₃ exposure studies have highlighted that exposure leads to an increase in AMØs, the specific role of AMØs in promoting resolution of O₃-induced lung inflammation remains unclear.

One reason that it is challenging to define the role of AMØs following acute O₃ exposure is that within the lung, macrophages can have different origins (ontogeny). This uncertainty has motivated a series of studies focused on determining if differences in AMØ functions are due to their distinct ontogeny. While it has been observed that AMØ derived from circulating monocytes (i.e. monocyte-derived AMØs) play a critical role in

regulating chronic/severe injury, the ontogeny of AMØs (i.e. tissue-resident versus monocyte-derived) following acute O₃ exposure has been undefined. Using mouse models (lineage labeled, genetic knockouts, and wildtype), we traced the origin of AMØs and found them to be predominantly tissue-resident AMØs following acute O₃ exposure, which was then confirmed using data from O₃-exposed human volunteers. Depletion of these tissue-resident AMØs resulted in a persistence of neutrophils in the alveolar space after O₃ exposure, indicating impaired clearance and persistent inflammation. This impaired clearance was associated with reduced efferocytosis, the clearance of apoptotic cells, a process crucial for resolving inflammation. Mice with a genetic deficiency in MerTK – a key receptor regulating efferocytosis – also resulted in impaired clearance of apoptotic neutrophils following O₃ exposure. We thus defined the pivotal role of tissue-resident AMØs in resolving O₃-induced inflammation via MerTK-mediated efferocytosis.

We then focused on intracellular mechanisms of inflammation resolution that occur within AMØs. We focused on a previously established pathway of inflammation resolution regulation through the metabolism of the amino acid, L-arginine. While L-arginine metabolism by nitric oxide synthase can promote inflammatory responses, L-arginine metabolism by arginase-1 generates metabolites that have the potential to direct inflammation resolution. One such metabolite of L-arginine is spermidine, and it is of

interest due to its anti-inflammatory properties observed in many tissues (pulmonary and non-pulmonary) and macrophages. Additionally, prior research suggests that spermidine inhibits N-methyl-d-aspartate (NMDA) receptor activation. This is of interest as the NMDA receptor is a known regulator of the pro-inflammatory Nuclear factor kappa B (NF- κ B) pathway. We therefore hypothesized that the mechanism by which spermidine leads to resolution of macrophage-derived inflammation is via inhibition of NMDA, thereby reducing the activation of the pro-inflammatory NF- κ B signaling.

Here we expand the understanding of the mechanism for spermidine effect in macrophages via impact on NF- κ B signaling through the NMDA receptor. We initially utilized a mouse model to assess the concentration of L-arginine and its metabolites in BALF following acute O₃ exposure. Here, we identified a decrease of L-arginine at 12h post-exposure, with a subsequent increase in spermidine present at 24h post-exposure, a time point critical for resolution of O₃-induced lung inflammation. We then conducted a pretreatment exposure in which the mice were treated with spermidine prior to O₃ exposure to determine if there was a reduction in inflammation. Mice pretreated with spermidine, when compared to control mice, demonstrated reduced O₃-induced lung inflammation. This suggests that spermidine may drive a reduction in pro-inflammatory signaling following acute O₃ exposure.

We next sought to understand the potential intracellular mechanism driving this response. To test this, we conducted *in vitro* studies in MH-S cells, AMØ-like immortalized cells. We utilized MH-S cells to define spermidine's effect on pro-inflammatory signaling following Lipopolysaccharide (LPS) exposure. We utilized LPS as a known pro-inflammatory stimulus in AMØ and a canonical activator of NF-κB. Utilizing a rescue model, in which spermidine was given following an initial LPS exposure, we found that spermidine decreased the expression and concentration of NF-κB associated pro-inflammatory cytokines, supporting a role in the resolution of inflammation. Then we pretreated MH-S cells with spermidine and determined that spermidine decreases the activation of NF-κB. We then utilized a known agonist, NMDA, for the NMDA receptor and found that NMDA activates NF-κB. In summary, the research highlights the pivotal role of tissue-resident AMØs and explores the potential of spermidine as a therapeutic agent for resolving environmental-induced lung inflammation.

Dedication

This thesis work is dedicated to my family and friends, including the furry members. Whether facing mountains of work, global pandemics, or general neuroticism, thank you for your love, support, and patience throughout this process.

Contents

<i>Abstract</i>	<i>iv</i>
<i>List of Tables</i>	<i>xii</i>
<i>List of Figures</i>	<i>xiii</i>
<i>Acknowledgements</i>	<i>xv</i>
1. Introduction	1
1.1 Lung response to environmental air pollution	2
1.2 Ozone (O ₃) pollution impacts human health	4
1.3 Immune mechanisms of O ₃ effects.....	5
1.3.1 AMØ ontogeny	6
1.4 Mechanisms of AMØ mediated resolution	8
1.4.1 Cellular mechanism of resolution: Phagocytosis/efferocytosis	8
1.4.2 Intracellular mechanism of resolution: NMDA as a regulator of NF-κB signaling.....	9
1.5 Dissertation objectives and outline	12
2. Tissue-resident alveolar macrophages reduce O₃-induced inflammation via MerTK mediated efferocytosis	16
2.1 Introduction	16
2.2 Materials and Methods	19
2.2.1 Experimental Animals	19
2.2.2 Rodent Exposures.....	20
2.2.3 Mouse bronchoalveolar lavage and measures of inflammation and injury	21
2.2.4 Mouse lung tissue harvest and flow cytometry	22

2.2.5 Human laboratory exposure to filtered air or ozone.....	23
2.2.6 Human bronchoscopy and bronchoalveolar lavage (BAL).....	24
2.2.7 Human flow cytometry	25
2.2.8 Efferocytosis assay.....	26
2.2.9 Real-Time PCR	26
2.2.10 Statistics.....	27
2.3 Results.....	28
2.3.1 Monocyte-derived AMØs are not recruited following acute O ₃ exposure in rodents..	28
2.3.2 Monocyte-derived AMØs are not recruited following acute O ₃ exposure in healthy human volunteers.....	30
2.3.3 Tissue-resident AMØ depletion causes persistent O ₃ -induced bronchoalveolar lavage neutrophilia	31
2.3.4 Tissue-resident AMØ depletion causes persistence of BAL cytokine/chemokines and neutrophil elastase.....	33
2.3.5 Depletion of tissue-resident AMØs reduces efferocytosis in vivo.....	34
2.3.6 Mer tyrosine kinase (MerTK) null mice exhibit persistent O ₃ -induced inflammation	35
2.4 Discussion	36
2.5 Conclusion.....	45
2.6 Acknowledgements.....	46
3. Spermidine regulation of NF-κB activation via the NMDA receptor.....	64
3.1 Introduction	64
3.2 Materials and Methods	67
3.2.1 Cell Culture.....	67

3.2.2 <i>Experimental Animals</i>	68
3.2.3 <i>Rodent Exposures</i>	69
3.2.4 <i>Mouse bronchoalveolar lavage and measures of inflammation and injury</i>	69
3.2.5 <i>Metabolite Analysis</i>	69
3.2.6 <i>Western Blot</i>	71
3.2.7 <i>Real-Time PCR</i>	72
3.2.8 <i>Statistics</i>	73
3.3 <i>Results</i>	73
3.3.1 <i>Spermidine is increased in the bronchoalveolar lavage fluid following acute O₃ exposure</i>	73
3.3.2 <i>Spermidine administration reduces O₃-induced lung injury in vivo</i>	74
3.3.3 <i>Spermidine pretreatment decreases LPS-induced NF-κB activation</i>	76
3.3.4 <i>Spermidine rescue treatment decreases NF-κB associated cytokine expression and concentration</i>	77
3.3.5 <i>NMDA receptor agonist activates NF-κB</i>	79
3.4 <i>Discussion</i>	81
3.5 <i>Conclusion</i>	88
3.6 <i>Acknowledgements</i>	89
4. <i>Conclusion</i>	101
4.1 <i>Summary</i>	101
4.2 <i>Implications and Future Directions</i>	103
<i>References</i>	108
<i>Biography</i>	132

List of Tables

<i>Table 1. Immunophenotyping: Mouse: Antibodies and Staining reagents.</i>	<i>60</i>
<i>Table 2. LSRFortessa X-20 configuration.</i>	<i>62</i>
<i>Table 3. Human: Flow cytometry panel used for BAL sample phenotyping</i>	<i>63</i>
<i>Table 4. RT-PCR primer sequences used for proinflammatory cytokine expression.....</i>	<i>100</i>

List of Figures

<i>Figure 1. Schematic of dissertation aims.</i>	15
<i>Figure 2. Monocyte-derived alveolar macrophages (AMØ) are not recruited following acute O₃ exposure.</i>	47
<i>Figure 3. Mouse Flow Cytometry Gating Strategy</i>	48
<i>Figure 4. Inflammatory and constitutive monocytes are increased in lung tissue in response to acute O₃ exposure.</i>	49
<i>Figure 5. Monocyte-derived alveolar macrophages (AMØ) are not recruited following acute O₃ exposure in humans.</i>	50
<i>Figure 6. Airspace administration of clodronate (CL) depletes tissue-resident alveolar macrophages (AMØ).</i>	52
<i>Figure 7. Tissue-Resident AMØ depletion leads to persistent O₃-induced BAL neutrophilia.</i>	53
<i>Figure 8. Increased BAL cytokines associated with neutrophil recruitment in O₃-exposed tissue-resident AMØ depleted mice.</i>	54
<i>Figure 9. Neutrophil elastase is persistently elevated in tissue-resident AMØ depleted mice</i>	55
<i>Figure 10. Tissue-resident AMØ depletion increased the proportion of apoptotic neutrophils following O₃ exposure.</i>	56
<i>Figure 11. Tissue-resident alveolar macrophage (AMØ) depletion decreased efferocytosis</i>	57
<i>Figure 12. MerTK^{-/-} mice have increased O₃-induced airspace inflammation.</i>	58
<i>Figure 13. Increased BAL cytokines associated with neutrophil recruitment in O₃-exposed MerTK^{-/-} mice</i>	59
<i>Figure 14. L-Arginine metabolites fluctuated following O₃ exposure</i>	90
<i>Figure 15. In vivo spermidine treatment trended toward decreased inflammatory cell recruitment.</i>	91
<i>Figure 16. Spermidine treatment decreased total protein and albumin in the airspace following O₃ exposure.</i>	92

<i>Figure 17. Pretreatment of spermidine decreased NF-κB activation.</i>	<i>93</i>
<i>Figure 18. Rescue treatment of spermidine decreased expression of NF-κB associated cytokines.</i>	<i>94</i>
<i>Figure 19. Decrease of inflammatory cytokines following a 2h spermidine rescue treatment.....</i>	<i>95</i>
<i>Figure 20. Decrease of inflammatory cytokines following a 3h spermidine rescue treatment.....</i>	<i>96</i>
<i>Figure 21. NMDA activates NF-κB.....</i>	<i>97</i>
<i>Figure 22. Technical limitations in showing D-AP5 decreases LPS-induced NF-κB activation and spermidine decreases NMDA-induced NF-κB activation.....</i>	<i>98</i>

Acknowledgements

I consider myself incredibly fortunate to have had remarkable mentors who played a pivotal role in my academic growth. To each person who has impacted me along the way, I am deeply grateful for your unwavering support and encouragement throughout my scientific journey. Linda Stollow and Mary Hendrickson, during my time at Syosset Middle and High School, your infectious passion for science ignited my interests and motivated me to step out of my comfort zone. Your encouragement to question and explore has been instrumental in shaping my path, and I am indebted to both of you for leading me to future mentors. A heartfelt thank you to Sara Brenner and Nicole Neu-Baker for taking a chance on a 15-year-old in your research lab. Your mentorship not only inspired me but also fueled my aspiration to become a mentor and researcher of your caliber. To my thesis committee, your valuable insights and collaborative spirit have not only influenced my dissertation work but have also contributed significantly to my development as a scientist. To my graduate research mentor, Robert Tighe, I extend my deepest gratitude for your consistent support, guidance, and encouragement. Your rare combination of kindness, intelligence, and genuine enjoyment of mentoring has created an environment where I thrived in clinical, laboratory, and conference-based settings. This environment has not only defined my identity as a scientist but will also continue to shape my future career and life. Thank you for being an exceptional mentor and human being.

I would also like to thank my exceptional lab and the QuIT Group (Que, Ingram, and Tighe Labs), past and present. Being a part of this lab and group has not only afforded me the opportunity to collaborate with brilliant scientists and students but also provided me with a supportive work family. A special thank you goes to my outstanding lab manager Anastasiya Birukova, who consistently challenges me, answers my questions, and graciously helps me troubleshoot any protocol, even at unconventional times—sometimes with the help of her husband, Ivan. Each of you has made a lasting impact on my life.

1. Introduction

Excerpts from this section are from an accepted peer-reviewed manuscript published by Springer in Current Allergy and Asthma Reports on April 7th, 2021, as Role of Innate Immune System in Environmental Lung Diseases written by M.A. Guttenberg, A.T. Vose, and R.M. Tighe. Available at <https://doi.org/10.1007/s11882-021-01011-0>.

Pollution is a ubiquitous effector to the health and well-being of individuals. In 2015, environmental pollution was responsible for 16% of all global deaths, with the vast majority, approximately 6.5 million deaths, directly attributed to air pollution [1]. Because of the high mortality attributed to air pollution, governmental entities have focused extensively on regulations and interventions to limit exposure to air pollutants. The six criterion air pollutants defined by the US Environmental Protection Agency in the 1970 Clean Air Act, revised in 1977 and 1990, are ozone (O₃), particulate matter, carbon monoxide, sulfur dioxide, nitrogen dioxide, and lead [2]. Levels of these pollutants are commonly reported using the air quality index (AQI), a tool developed by the US Environmental Protection Agency that ranges from good (0) to hazardous (301 or higher) [3,4]. Importantly, elevated AQI levels are associated with increased morbidity and mortality due to acute exposure to pollutants, inclusive of O₃, which is linked to many of the adverse health effects caused by air pollution [4]. Despite efforts to define and regulate acute air pollution events, these exposures remain a concern and will only further increase due to extreme global climate events [1,5].

1.1 Lung response to environmental air pollution

As a mucosal surface, the lung is at the interface between the external and internal environments and is continuously exposed to a variety of foreign materials including pathogens, particulates, and toxicants. Addressing these exposures while maintaining homeostasis to preserve principal functions (e.g. gas exchange) requires highly coordinated immune surveillance. This surveillance directs targeted and appropriate responses to foreign materials while limiting excessive inflammation that can lead to tissue damage and disease. This effort largely is the role of the innate immune system.

The innate immune system is composed of cellular and humoral components that are responsible for initial responses to inhaled foreign materials [6]. These responses are germline encoded, meaning that they are genetically inherited and do not require prior exposure to initiate immune responses. Innate immunity includes physical and mechanical barriers, pattern recognition receptors, and cellular/humoral signaling. Innate immune activation directs targeted inflammatory cascades that initiate inflammation to pathogens while also facilitating resolution to limit lung injury. When functioning appropriately the innate immune system allows the lung to appropriately defend itself while also maintaining homeostasis.

To a large extent, lung disease reflects a failure of normal immune mechanisms that maintain homeostasis. When homeostasis is not maintained, inflammation becomes

dysregulated and can persist. This chronic inflammation can then result in ongoing lung damage frequently observed in chronic lung disease. This process has been observed with innate immune system dysregulation. Research continues to demonstrate that dysregulated innate immunity occurs in response to environmental pollutants, appearing to be the result of pollutants coopting normal innate immune signaling pathways [7,8].

A consequence of innate immunity being germline encoded is that innate immunity has not adapted to evolutionarily novel exposures such as products of combustion and other industrial materials that have become essential parts of modern life. Meaning rather than a specific and precise mechanism, the innate immune system bluntly and broadly addresses pollutants in the airspace. The consequence of this can be inappropriate or prolonged inflammation that can cause incident respiratory disease or exacerbate established disease. This is best evidenced by clear associations between ambient air pollution exposures and airway diseases such as asthma [9–13], chronic obstructive pulmonary disease (COPD) [14–18], and cystic fibrosis [19–21]. Much of this epidemiology has focused on exacerbations of these diseases, however, there is developing evidence that suggests air pollution may cause incident airway disease (as discussed in a recent American Thoracic Society report [22]). Therefore, understanding the interactions between environmental exposures and the innate immune system is

critical to improving the care of these diseases and limiting the severity of their clinical course.

1.2 Ozone (O₃) pollution impacts human health

O₃ is a highly reactive gaseous air pollutant, which when present at ground-level can be a respiratory health hazard. O₃ exists at varying levels in the atmosphere; while in the stratosphere, O₃ limits human exposure to harmful cosmic ultraviolet radiation [23–25]. Alternatively, tropospheric or ground-level O₃ causes harmful health impacts, as humans interact more directly with it, and is often what is discussed when addressing O₃ pollution [25]. The production of O₃ occurs through a photochemical reaction in which a dioxygen molecule binds with an oxygen singlet atom. This reaction involves the photolysis of volatile organic compounds and oxides of nitrogen in the air, components of emissions from combustion [23,24].

Increased ambient O₃ associates with enhanced morbidity and mortality and lung disease severity [24,26]. Increased concentrations of ground-level O₃ lead to a notable rise in hospitalizations, causing considerable health and economic challenges [14,27–29]. In a study sampling 95 large US urban communities, an increase in 10 parts per billion (ppb) in daily O₃ exposure led to an approximately 0.87% increase in total mortality, including enhanced mortality at exposure doses well below current regulatory standards [30]. This data suggests that there is no “safe” O₃ exposure level. Furthermore, regulation of O₃ levels will become increasingly difficult as ambient levels

increase with rising global temperatures, as ozone production increases at higher temperatures [5,31]. Thus, this public health burden from O₃ exposure will be difficult to completely alleviate solely by regulatory action. Rather, it requires an understanding of the underlying effects of exposure on lung immunity to define strategies, in addition to mitigation, that reduce health effects.

1.3 Immune mechanisms of O₃ effects

O₃ alters normal lung immune responses through effects on the innate immune system. We are particularly focused on the impact of O₃ on a central cellular component of the pulmonary innate immune system, AMØs. Macrophages play a critical role in clearance of pathogens, xenobiotics, apoptotic cells, as well as cytokine production, and neutrophil recruitment [32–34]. Due to their central role in lung inflammation, AMØs have diverse roles; responsible for both the initiation of inflammation as well as directing resolution of inflammation and limiting excessive inflammation [35–37]. During the initiation of lung inflammation, AMØ activation leads to the production of pro-inflammatory cytokines and mediators that direct leukocyte recruitment [38,39]. Following initiation and propagation of inflammation, resolution of inflammation is required to limit lung damage. Previously, resolution has been considered a passive function where it was thought that cytokine production and responses gradually diminished, with associated reductions in leukocyte recruitment and a gradual return to homeostasis. However, recent work has challenged this dogma, identifying that

resolution is an active component of the immune response. Furthermore, defective resolution can lead to uncontrolled and unresolved inflammation potentiating chronic and exacerbated diseases and even autoimmunity [40,41]. Critically, resolution mechanisms are defined by the production of pro-resolving mediators, down-regulation of pro-inflammatory cytokines and chemokines, neutrophil apoptosis, and clearance of apoptotic bodies (efferocytosis) [39,42].

AMØ functions are impacted by exposure to air pollutants and other environmental exposures, altering normal lung inflammation and resolution responses [36,37,42,43]. Broadly, these effects have been observed with a variety of air pollutants, including particulate matter as well as O₃ [43–46]. The effects include enhanced pro-inflammatory cytokine production and reduced phagocytosis and efferocytosis. Studies continue to dissect these functional AMØ responses and the impact of environmental exposures to understand how dysregulated functions can affect pulmonary diseases such as asthma and allergy. Improved understanding of O₃'s impact on cellular components of innate immunity, and particularly AMØs' functions in resolution of inflammation, has the potential to define interventions that could alleviate O₃-induced adverse health effects.

1.3.1 AMØ ontogeny

Increasingly, macrophage functions are considered in the context of their origin and tissue location [47,48]. In the lung, macrophages are present both in the airspace and

the interstitium (fluid-filled space between alveolus and vasculature), exhibiting distinct gene expression patterns and cell surface markers based on their location [49–51].

Additionally, there is evidence suggesting distinct AMØ subsets are present within the lung. Detailed evaluation of AMØs by single cell RNA sequencing identified unique AMØ subsets that were conserved across individuals and between sexes, including a subset with elevated metal binding gene expression [52]. The functions of these individual subsets were not clearly defined but support other studies identifying that AMØs from the upper (nose, mouth, sinuses, pharynx, and larynx) and lower (trachea, bronchial tubes, and lungs) respiratory tract had distinct bioenergetics at baseline and response to phorbol 12-myristate 13-acetate (PMA) or 1,2-naphthoquinone [53]. In the interstitium, detailed stereology of interstitial MØs in lung tissue, defined distinct interstitial MØs are located along the bronchi (termed peribronchial), in the alveolar interstitium and also around the vasculature [54]. This supports that there are heterogeneous IMØ populations not only in the alveolar space, but also in the surrounding lung space. The specific functions of these subsets require further study to determine their role in inflammation and homeostasis.

Beyond tissue location, lung macrophages can also be defined based on their origin. Lung macrophage can be tissue-resident (i.e. macrophages deposited in the lung during early embryologic development) or those derived from circulating monocytes (i.e. monocyte-derived). Monocyte-derived macrophages are derived from CCR2

dependent recruitment of monocytes that then differentiate in the lung into AMØs. Furthermore, it has been suggested that circulating monocytes traffic to the spleen prior to recruitment to the lung and then differentiation into monocyte-derived AMØs [55]. Prior research has demonstrated that following chronic PM_{2.5} exposure monocyte-derived AMØs can replace tissue-resident AMØs and may function to perpetuate chronic inflammation [43].

These efforts, along with others, have begun to untangle the heterogeneity that exists in the lung and defines how the diversity of AMØs functions and origin drive responses to environmental pollutants and environmental lung disease [43,56–59]. The work undertaken in this thesis investigates the specific AMØ subset that is responsible for resolution acute O₃-induced lung inflammation as well as probes a potential intracellular pathway that mediates this response; offering a foundation for future research and the development of therapeutic targets to alleviate health effects of air pollution.

1.4 Mechanisms of AMØ mediated resolution

1.4.1 Cellular mechanism of resolution: Phagocytosis/efferocytosis

The clearance of debris and pathogens through phagocytosis, as well as clearance of apoptotic cells via efferocytosis, are critical functions that macrophages perform to maintain homeostasis [60,61]. Prior work supports that macrophage phagocytosis is altered by exposure to pollutants. This includes studies with murine and human

exposures to O₃ [62], PM [63], and engineered nanomaterials [64]. Beyond clearance of bacteria and/or debris, macrophages are critical to the clearance of immune cells, particularly those that are apoptotic, through a process termed efferocytosis [65]. Recent data suggests that AMØ efferocytosis is dysregulated in chronic lung diseases such as asthma [66]. Additionally, it is becoming clear that environmental exposures can reduce efferocytosis [67]. A recent study by Hodge et. al. developed a protocol to assess AMØ efferocytosis *in vivo* and noted decreased AMØ efferocytosis following O₃ exposure [68]. Though the data supports that environmental exposures impact phagocytosis and efferocytosis, the specific mechanisms remain largely understudied.

1.4.2 Intracellular mechanism of resolution: NMDA as a regulator of NF-κB signaling

Regulation of innate immune activation in the AMØs is largely via canonical Nuclear-Factor kappa B (NF-κB) signaling [69]. NF-κB signaling can proceed through either a canonical or a non-canonical pathways; however, Immunological responses are largely attributed to the canonical pathway and therefore will be referred to as the NF-κB pathway [70]. Activation of the NF-κB pathway results in the induction of transcription factors that support initiation and propagation of inflammation. NF-κB activation is initiated by exposure to an infection, cytokines, or genotoxic stresses, such as reactive oxygen species, which lead to phosphorylation of IκBα via the IκB kinase complex [71,72]. Following phosphorylation, IκBα degradation is triggered through ubiquitination via the proteasome, which then liberates NF-κB transcription factors for

translocation from the cytoplasm into the nucleus. The predominant heterodimer p50/p65(RelA) then binds to DNA which leads to cytokine production/release and recruitment of immune cells [71,72]. Key to the resolution of inflammation is reduction in NF- κ B activation. Since O₃ induces activation of NF- κ B [69,73], understanding regulators of NF- κ B activation is important not only for limiting O₃-induced inflammation, but also for promoting inflammation resolution. An established regulator of NF- κ B activation is the N-methyl D-aspartate (NMDA) receptor [74]. The NMDA receptor has been principally studied as a neurotransmitter due to its role as a receptor for one of the major excitatory amino acids, glutamate [75]. While glutamate plays critical roles in memory and learning, the dysfunction of glutamate receptors, such as the NMDA receptor, can lead to neuronal degeneration [76]. Recently, research has begun to define the role of NMDA in non-neuronal tissues including the lungs. Data suggests that the NMDA receptor is expressed in various pulmonary tissues including AMØs, alveolar type 2 cells, and the airway epithelium [77,78]. Furthermore, prior data has demonstrated that the NMDA receptor and glutamate signaling is involved in the regulation inflammation and pulmonary lung injury [79,80]. The receptor is a heterotetrameric transmembrane ion channel which regulates intracellular calcium flux. Binding of glutamate to the NMDA receptor causes a conformational change, opening the channel and facilitating calcium influx to generate reactive oxygen species; leading to the activation of NF- κ B and pro-inflammatory cytokine release [74,80,81]. Presently,

the mechanism linking the activation of NMDA and activation of NF- κ B in AM \emptyset inflammation resolution signaling is not defined.

Endogenous antagonists of NMDA can inhibit glutamate binding and reduce NMDA receptor activity. Included in these are metabolites of L-arginine, an amino acid which is critical to induction, persistence, and resolution of inflammation [82,83]. L-arginine metabolism via distinct enzymes favors either pro-inflammatory or anti-inflammatory signaling. Pro-inflammatory signaling occurs via L-arginine metabolism by nitric oxide synthase 2 (NOS2), or inducible NOS (iNOS). NOS2-generated metabolites include L-citrulline and reactive nitrogen species, which induce and propagate inflammation [84]. While NOS2 functions in other cells, it has largely been described to be induced in macrophages in response to pro-inflammatory cytokines such as interferon gamma (IFN γ), tumor necrosis factor alpha (TNF α), and bacterial lipopolysaccharide (LPS), an agonist of Toll-like receptor 4 (TLR4) [82,85]. Alternatively, anti-inflammatory signaling occurs via L-arginine metabolism by arginase-1. Arginase-1 metabolism generates polyamines, which exhibit anti-inflammatory properties [84,86]. Arginase 1 has been found to be expressed in myeloid cells, such as macrophages. Arginase-1 expression is induced by cytokines such as T helper 2 cytokines, interleukin 4 (IL-4) and interleukin 13 (IL-13), as well as granulocyte-macrophage colony-stimulating factor (GM-CSF), transforming growth factor β (TGF β), and toll-like receptor agonists [87–89]. One of the arginase-1 derived metabolites is spermidine.

administration, following exposure to a canonical NF- κ B activator, lipopolysaccharide (LPS), reduces NF- κ B activation and cytokine release [90,91], supporting its role as an anti-inflammatory metabolite. However, the mechanism for this effect has not been determined. We hypothesized that spermidine's anti-inflammatory effects are via inhibition of NMDA receptor activation that limits NF- κ B activation.

Based on prior research that identified spermidine as a ligand to a polyamine allosteric binding site on the NMDA receptor, our studies assessed whether spermidine binding to NMDA will then reduce agonist affinity and decrease NMDA receptor activation [92,93]. While individual components of this pathway have been studied, no one has connected them together into a comprehensive pathway [89,90,94]. Defining spermidine effects on NF- κ B activation via the NMDA receptor has the potential to identify a novel mechanism which can promote AM \emptyset -regulated resolution of environmentally-induced inflammation. This finding can also be more broadly applicable to other forms of oxidative lung injury.

1.5 Dissertation objectives and outline

The overall aim of this dissertation is to define cellular and intracellular AM \emptyset mechanisms of inflammation resolution following pulmonary environmental exposures. From a cellular perspective, we hypothesized that AM \emptyset ontogeny has an essential role in resolution of O₃-induced lung inflammation via its functions in efferocytosis. We also focused on intracellular mechanisms in AM \emptyset s that drive signaling that promotes

resolution of pro-inflammatory AMØ signaling. We hypothesized that spermidine promotes resolution of LPS-induced NF-κB activation in AMØ via inhibition of NMDA receptor activation (Figure 1).

This dissertation is organized into the following chapters which address independent objectives and hypothesis (research schematic depicted in Figure 1):

Chapter 2: Tissue-resident alveolar macrophages reduce O₃-induced inflammation via MerTK mediated efferocytosis

AMØ composition and role was assessed following acute murine O₃ exposure. Utilizing lineage reporting and genetically deficient mouse strains, we defined an essential role for tissue-resident AMØs in the resolution of O₃-induced lung inflammation via MerTK mediated efferocytosis.

Chapter 3: Spermidine regulation of NF-κB activation via the NMDA receptor

Mechanistic studies were conducted to assess spermidine treatments in the reduction of LPS-mediated AMØ cytokine production via reduced NF-κB activation. Further studies identified that LPS activated NMDA which led to the activation of NF-κB. In an effort to connect these mechanistic observations, we utilized an NMDA agonist, NMDA, and antagonist, D-AP5, to assess if LPS-induced NF-κB activation is predominantly through the NMDA receptor as well as if reduction of NMDA receptor

activity corresponds with reduction of NF- κ B activation. Due to technical issues, we are limited in defining spermidine as a regulator of NF- κ B activation via the NMDA receptor.

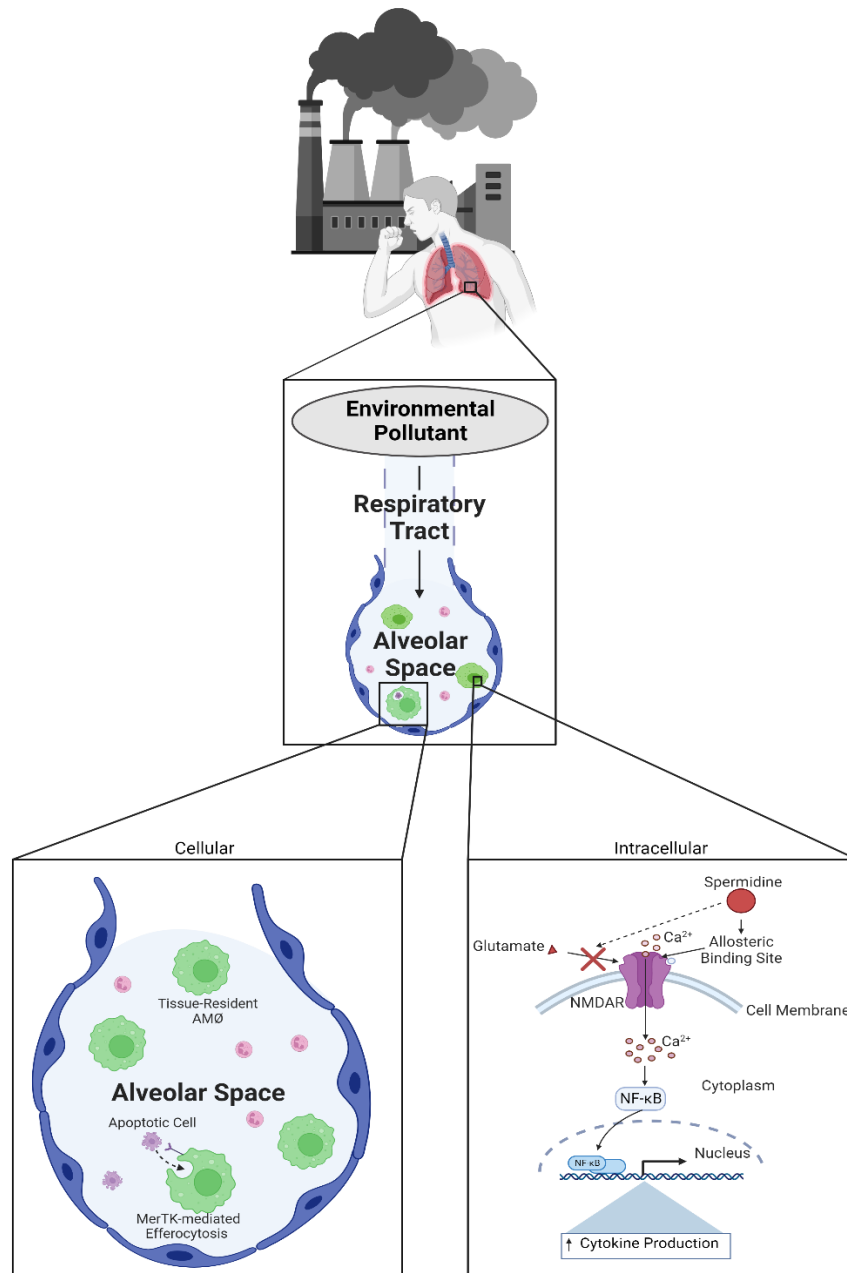


Figure 1. Schematic of dissertation aims.

This thesis will uncover the role and composition of AMØs following O₃ exposure. In addition, we explore a specific mechanism in AMØs, where spermidine can reduce NF-κB activation via the NMDA receptor to promote resolution of inflammation. Graphic created using Biorender.com.

2. Tissue-resident alveolar macrophages reduce O₃-induced inflammation via MerTK mediated efferocytosis

This chapter is from a manuscript in-review for publication in The American Journal of Respiratory Cell and Molecular Biology which was submitted November 8th, 2023, as Tissue-resident alveolar macrophages reduce O₃-induced inflammation via MerTK mediated efferocytosis written by M.A. Guttenberg, A.T. Vose, A. Birukova, K. Lewars, R.I. Cumming, M.C. Albright, J.I. Mark, C.J. Salazar, S. Swaminathan, Z. Yu, Y. Sokolenko, E. Bunyan, M.J. Yaeger, M.B. Fessler, L.G. Que, K.M. Gowdy, A.V. Misharin, and R.M. Tighe. Preprint is available on BioRxiv <https://www.biorxiv.org/content/10.1101/2023.11.06.565865v1>.

2.1 Introduction

Air pollution is responsible for a significant number of premature deaths globally with an average mortality of 6.5 million individuals per year [1]. Despite an already significant impact on rates of global morbidity and mortality, air pollution associated mortality will continue to rise with climate change. Furthermore, current regulatory efforts will not eliminate air pollution-associated morbidity and mortality, particularly in sensitive individuals [1,5]. Understanding the mechanisms that drive air pollution-mediated health effects is therefore critical to better target mechanisms that mitigate its adverse effects.

When ground-level ozone (O₃) exposures increase, as with other criterion air pollutants, the risk of respiratory-related morbidity and mortality increases [95–97]. A principal lung effect of O₃ exposure is the generation of lung inflammation and injury. Generally, O₃-induced lung inflammation and injury is considered mild and resolving; however, in sensitive individuals or those with underlying lung disease this can lead to exacerbated or prolonged inflammation and injury responses [98]. Lung inflammation is a highly regulated process that includes both initiation and resolution phases that are regulated, in part, by signaling of alveolar macrophages (AMØ) [95,99]. Prior research underscores the critical roles of AMØs in O₃-induced lung injury. This includes well-characterized pro-inflammatory effects including cytokine generation [33], and airspace neutrophil influx [34]. Conversely, AMØs can function in the resolution of lung inflammation via functions such as phagocytosis and efferocytosis that clear pathogens, cellular debris, and apoptotic immune cells [42]. This diversity of AMØs functions has made them a challenge to study and has limited efforts to target them therapeutically. Thus, a better understanding of the context-dependent functions of AMØs following O₃ exposure are required to target them with precision.

AMØ functions can depend on their specific origin (i.e., ontogeny). In naïve mice, all AMØs are of tissue-resident origin. Tissue-resident AMØs populate the lung during the early postnatal period and, in the absence of lung injury, maintain

themselves via proliferation in situ for the life of the animal [100,101]. Alternatively, following lung injury, monocytes are recruited to the lung and differentiate into monocyte-derived AMØ [102,103]. Though tissue-resident and monocyte-derived AMØs share some common macrophage functions, they also exhibit distinct metabolism, activation markers, and cytokine profiles suggesting different functional roles in lung injury and repair [104]. While monocyte-derived AMØs have clearly documented roles in promoting lung injury, inflammation, and fibrosis, [104–106] the role of tissue-resident AMØs is less understood. Furthermore, the composition and function of AMØs following the mild and resolving acute lung injury with acute O₃ exposure has not been clearly defined.

To address this question, we defined the composition of AMØs following filtered air (FA) and O₃ exposure using a lineage-tracing mouse system which labels monocytes and monocyte-derived AMØs but not tissue-resident AMØs [106,107]. Following O₃ exposure in these mice, we did not identify an increase in monocyte-derived AMØs. Additionally, in healthy human volunteers undergoing laboratory FA and O₃ exposure, we also did not observe an increase in monocyte-derived AMØs. To define tissue-resident AMØ functions in O₃-induced lung injury, we administered intratracheal clodronate-loaded liposomes to deplete tissue-resident AMØs [105] and then exposed them to FA or O₃. Depletion of tissue-resident AMØs resulted in persistence of O₃-

induced airspace neutrophilia, suggesting a defect in clearance of apoptotic neutrophils (i.e., efferocytosis). We confirmed the direct effect of tissue-resident AMØs on efferocytosis by demonstrating reduced clearance of apoptotic Jurkat cells following clodronate-mediated depletion of tissue-resident AMØ. Finally, in MerTK^{-/-} mice, which have defective efferocytosis [108,109], we defined the impact of reduced efferocytosis on O₃-induced lung inflammation. Consistent with tissue-resident AMØ-depleted mice, O₃-exposed MerTK^{-/-} mice exhibited persistent airspace neutrophil inflammation. These data support that tissue-resident AMØs promote resolution of O₃-induced lung inflammation via MerTK-mediated efferocytosis of neutrophils.

2.2 Materials and Methods

2.2.1 Experimental Animals

C57Bl/6J mice were purchased from Jackson Laboratories. The mice were a mix of males and females, group specific composition listed in the figure legends. MerTK^{-/-} and Cx3cr1^{ERcre} zsGreen mice were bred in-house. MerTK^{-/-} mice were a kind gift from Dr. Edward Thorp, Northwestern University; originally from The Jackson Laboratory (stock 011122 on mixed genetic background). They were backcrossed on B6 background for more than 10 generations. All mice were 8-10 weeks old at the time of exposure. Animal breeding and study procedures were performed under an approved institutional animal care and use committee (IACUC) protocol at Duke University

(A053-21-03). All animal experiments were conducted in accordance with the American Association for the Accreditation of Laboratory Animal Care guidelines.

2.2.2 Rodent Exposures

Filtered air (FA) and ozone (O₃) exposures followed published protocols [58,110–112]. Exposures to FA or O₃ (2 parts per million) for 3h were performed in 55-liter Hinners-style exposure chambers. The mice were exposed in stainless steel wire mesh cages inside the exposure chamber with dividers to prevent congregating. Chamber air was maintained at 20–22°C with 40–60% relative humidity and supplied at a rate of 20 changes/hour. O₃ was generated by directing 100% oxygen through ultraviolet light. O₃ concentration was continuously monitored by an O₃ ultraviolet light photometer (Teledyne Instruments, model 400E). After 3h, the mice were removed from the chamber. For the lineage labeling experiments, Cx3cr1^{ERcre} zsGreen mice were administered 2 mg of tamoxifen via oral gavage. 24h after tamoxifen induction, the mice were exposed to FA or O₃ and lungs were harvested 12, 24, or 72h post-exposure for flow cytometry to define lineage reporter expression. For clodronate studies, C57Bl/6J mice were dosed with 50uL of 5mg/mL clodronate-loaded liposomes (batch No. C12J0321 & C18E0422) (Liposoma BV) or PBS by oropharyngeal aspiration. 72h after clodronate or PBS, mice were exposed to FA or O₃ and sacrificed 12 or 24h post-

exposure. MerTK^{-/-} mice and control C57Bl/6J mice were exposed to FA or O₃ (2 ppm x 3h) and harvested 24h post-exposure.

2.2.3 Mouse bronchoalveolar lavage and measures of inflammation and injury

Bronchoalveolar lavage (BAL) was performed as outlined in prior publications [58,110]. In brief, for BAL, mice were deeply anesthetized with an intraperitoneal injection of ketamine (100 mg/kg), xylazine (100 mg/kg), and saline (0.9%), dosed by weight (~350-500 μ L/mouse). Following anesthesia, the chest and trachea were exposed by dissection and a small nick was made in the trachea. PE-60 tubing (Clay Adams) was used to cannulate the trachea. The tubing was connected to 12-inch tubing from an infusion set (Terumo). PBS was infused via the tubing to 20 cm H₂O via connection to syringe on a ring stand until the lung reached total lung capacity. The fluid was then passively drained and the volume was recorded. The BAL cells were isolated from the fluid by centrifugation, (Eppendorf centrifuge 5424 R) (1,500 rpm, 10 min, 4°C). BAL fluid was decanted and used for measures of lung inflammation and injury including neutrophil elastase (cat#: ab252356) and multiplex ELISA for cytokines/chemokines (#cat: PPX-08-MX47XMC) following the manufacture's protocols. To enumerate BAL cells, cells underwent red blood cell lysis with RBC lysis buffer (Biolegend, #420302) and the number of live cells were determined using a Cellometer K2 (Nexcelom Bioscience). Following total cell count, cells were immobilized by cytospin, stained with Diff-Quik

(Fisher Scientific), and counted in a blinded fashion to determine exposure changes in cell differentials.

2.2.4 Mouse lung tissue harvest and flow cytometry

Flow cytometry was performed on whole lung tissue using a previously published protocol with modifications, as described below [58,113]. In brief, mice were pre-treated subcutaneously with 50 μ L of 1000/mL heparin. Approximately 10min after the injection, the mice were euthanized with isoflurane. The chest wall was opened, and the trachea cannulated. Following cardiac perfusion with 10 mL of PBS to remove intravascular red blood cells, the lung was insufflated just past total lung capacity with a digestion solution (1.5mg/mL of Collagenase A [Roche] and 0.4mg/mL DNase I [Roche] in HBSS plus 5% fetal bovine serum and 10mM HEPES). The lung tissue was excised and then incubated at 37°C for 30 min in the digestion solution with intermittent vortexing. Enzyme activity was halted by mixing the digestion mix with cold PBS then the mixture passed through a 70 μ M cell strainer (Olympus Plastics, Genesee Scientific) and centrifuged (350 x g for 6-8 min at 4°C). Cell pellets were re-suspended in Red Blood Cell lysis buffer and incubated on ice and washed per manufacturer's instructions for 2-3 cycles as needed (RBC Lysis Buffer, Biolegend). The cells were re-suspended in cold PBS and kept on ice while aliquots were counted then apportioned for live/dead staining (Zombie UV, Biolegend) followed by cell surface staining with an optimized antibody

panel (Table 1). Stained cells were fixed (0.4% paraformaldehyde in PBS) for later acquisition (within 1 week of initial harvest). Lung cells from control animals (C57Bl/6J) were stained similarly & used for single-color controls. See Table 1 for antibody list. Data was collected on a BD LSR Fortessa X-20 using the configuration noted in Table 2 and analyzed using FlowJo™ version 10 software (BD Life Sciences).

2.2.5 Human laboratory exposure to filtered air or ozone

Human exposure studies were performed after informed consent through Duke Institutional Review Board approved protocols (Pro00088966 and Pro00100375). Healthy human subjects were recruited for inclusion in this study through advertisements. No study procedures were performed before obtaining informed consent. Requirements for inclusion included normal range of body mass index, no evidence of respiratory disease, and non- smoking. Exclusion criteria included a recent respiratory infection (within 4 weeks), history of smoking, pregnancy, ages less than 18 or greater than 50 years, and BMI > 35.0 and failure to understand the study protocol. Additionally, participants could not be taking antihistamines, non-steroidal anti-inflammatory drugs, or supplemental vitamins for one week prior to the study, and throughout the study's duration.

Subject exposures to filtered air or ozone were performed in a custom designed 730 cubic feet exposure room that included an HEPA air ventilation system to remove particulates. The air supply was set to a selected range of temperatures (20-23°C) and

relative humidity (45-22 55%). Exposures lasted 135 minutes in duration, during which participants alternated between resting and walking on a treadmill at 2-3 mph to mimic an individual performing mildly strenuous activity under ambient conditions. Ozone exposure consisted of a dose of 200 ppb and was continuously monitored. This concentration of ozone exposure exceeds the federal government's standard (80 ppb for 8-hour average) but is similar to ambient ozone levels in the Research Triangle area during ozone alert days. Ozone was created from a 100% O₂ source by cold plasma corona discharge (Ozotech, Yreka CA), and mixed with filtered air before addition to chamber. The order of filtered air or ozone exposure was randomized for every participant, with at least a 21-day washout period between exposures.

2.2.6 Human bronchoscopy and bronchoalveolar lavage (BAL)

On the day following filtered air or ozone exposure, approximately 21 hours after exposure, participants underwent a flexible bronchoscopy with bronchoalveolar lavage. Subjects received sedation with midazolam (Versed) and fentanyl (Sublimaze), and topical anesthetic lidocaine prior to bronchoscopy. A flexible bronchoscope was inserted through the mouth, past the vocal cords, into the lungs. The bronchoscope was wedged into the right middle lobe and 150 mL of sterile saline was discharged into the lungs and subsequently removed with gentle syringe suction in order to obtain bronchoalveolar lavage fluid (BALF). BALF was passed through a strainer and 10mL of

the sample was separated. The sample was then mixed 1:1 with HypoThermasol FRS (StemCell Technologies, USA) and then sent overnight to Northwestern University for flow cytometry and cell sorting.

2.2.7 Human flow cytometry

BALF samples were filtered through a 70 μ m cell strainer, pelleted by centrifugation at 400rcf for 10 min at 4°C, followed by hypotonic lysis of red blood cells with 2 mL of PharmLyse (BD Biosciences) reagent for 2 minutes. Lysis was stopped by adding 13 mL of MACS buffer (Miltenyi Biotech). Cells were pelleted again and re-suspended in 100 μ L of 1:10 dilution of Human TruStain FcX (Biolegend) in MACS buffer, and a 10 μ L aliquot was taken for counting using K2 Cellometer (Nexcelom) with AO/PI reagent. The cell suspension volume was adjusted so the concentration of cells was always less than 5x10⁷ cells/mL and the fluorophore-conjugated antibody cocktail was added in 1:1 ratio (Table 3). After incubation at 4°C for 30 minutes, cells were washed with 5 mL of MACS buffer, pelleted by centrifugation, and re-suspended in 500 μ L of MACS buffer with 2 μ L of SYTOX Green viability dye (ThermoFisher). Cells were analyzed by a FACS Aria III SORP instrument. Sample processing was performed in a BSL-2 facility using BSL-3 practices. Analysis of the flow cytometry data was performed using FlowJo 10.6.2. using uniform sequential gating strategy reported in a previous publication by the Misharin group [114] and reviewed by two investigators (SS, AVM).

Relative cell type abundance was calculated as a percentage of all singlets/live/CD45+ cells.

2.2.8 Efferocytosis assay

Immortalized human T lymphocytes (Jurkat cells) (ATCC) were stained with Calcein AM (ThermoFisher) (20 uL dye per 30 million cells) and incubated for 1.5h at 37°C. The cells were then re-counted and re-constituted in Jurkat cell complete media (RPMI1640 + GlutaMax, Gibco #61870-036, 10% FBS HI, 5mL A/A) at 1.5 million cells per 10 cm dish. The cells were then irradiated in the UV Stratalinker 1800 at 400 µjoules (10-15sec). The following day the cells were spun down (1,200rpm X 6min) and re-suspended at a concentration of 4 million cells in 50 uL in PBS. Jurkat cells (4 million cells, in 50 uL of PBS) or PBS control were instilled in C57Bl/6J mice by oropharyngeal aspiration for 1.5h prior to the harvest [68]. Following the harvest, BAL fluid was collected and single-color flow cytometry was performed by flow cytometry to define the number of Calcein AM-positive cells. Data was expressed as a ratio of the number of recovered Jurkat cells versus the total number of Calcein AM positive Jurkat cells initially instilled.

2.2.9 Real-Time PCR

Total RNA was collected utilizing RNeasy Plus Mini Kit (Qiagen) per manufacturer protocol. RNA samples were then reverse transcribed into cDNA using

Maxima H Minus cDNA Synthesis Master Mix (thermo scientific). PCR amplification was completed using the following program: 20 uL reaction volume; 50°C, 2min; 95°C, 2min; 40 cycles, 95°C 1 sec, 60°C 30 sec. All real time quantitative PCR reactions were completed using the Quant Studio 6 Flex (Applied Biosystems). The reactions utilized SyBR Green reagent (Applied Biosystems), sterile UltraPure Distilled water (Invitrogen), and primers, as listed below. MerTK forward (Sigma-Aldrich), 5'-CTGGATATTAGATGGACGAAG-3', MerTK reverse (Sigma-Aldrich), 5'-AGAAAGCTCTTTGTAAGTCC-3', 18S forward (Integrated DNA Technologies), 5'-TTGACGGAAGGGCACCACCAG-3', 18S reverse (Integrated DNA Technologies), and 5'-GCACCACCACCCACGGAATCG-3'. Gene expression values were normalized to 18S as a housekeeper and presented as a fold change normalized again to FA.

2.2.10 Statistics

Statistical testing is as noted in the figure legends. In most settings, an ANOVA with post-hoc multiple comparisons analysis was conducted in PRISM 9 (GraphPad, Boston, MA) using Tukey's Honestly Significant Difference Test to reveal individual comparisons within groups on both cell types and cytokines. A p-value of less than 0.05 was considered statistically significant. Data in figures are presented as individual data points \pm standard error of the mean. To account for any variability within experiments and samples, we performed an additional secondary analysis. This used mixed effects

linear regressions performed in MATLAB 2017b (MathWorks, Natick, MA). We assessed the effects of timepoint (12, 24h), exposure (FA, O₃ (2 ppm × 3h)), and treatment (CL, PBS), and all 2- and 3-way interaction effects, on cell differentials, individual cytokines, and neutrophil elastase. The Robust Regression was fit using a bisquare weighting function that assigns observations with larger residuals a weight trending towards zero. The analysis conducted in MATLAB confirmed and validated the statistics run in PRISM.

2.3 Results

2.3.1 Monocyte-derived AMØs are not recruited following acute O₃ exposure in rodents

To define AMØ composition following acute O₃ exposure in rodents, we utilized an established inducible monocyte/macrophage lineage tracing system (Cx3cr1^{ERcre} crossed to zsGreen mice) [106,107]. In this system, tamoxifen administration permanently labels nearly 100% of circulating monocytes, which express *Cx3cr1*, and their progeny (i.e. monocyte-derived AMØs), with a green fluorescent protein (GFP) [106]. In contrast, in Cx3cr1^{ERcre} zsGreen mice, tissue-resident AMØ, which do not express *Cx3cr1* in adulthood, are not labeled. Therefore, the Cx3cr1^{ERcre} zsGreen mice allow clear segregation of tissue-resident from monocyte-derived AMØs. To induce lineage tracing, tamoxifen was administered via oral gavage 24h prior to FA or O₃ exposure (Figure 2A). The mice were harvested at 12, 24, and 72h post-exposure based

on our and others' prior studies defining peak and resolving time points of O₃-induced inflammation and injury [58,115,116]. Whole lung tissue was harvested and digested to obtain a single cell suspension and the cells were processed for flow cytometry using a previously published protocol (See Table 1 and 2 for antibodies and cytometer configuration) [58]. Lung MØs were defined as live, CD45⁺, Ly6G⁻, CD64⁺, CD24⁻ cells (Figure 3). Based on CD11c versus CD11b expression, AMØs (CD11c⁺, CD11b⁻) were delineated from IMØs (CD11c^{+/+}, CD11b⁺). AMØ definition was further confirmed using CD169 or CD206 (data not shown) and Siglec-F versus Ly6C (Figure 3, blue panel). AMØs were then segregated by GFP expression to define tissue-resident AMØs (live, CD11c⁺, CD11b⁻, GFP⁻) versus monocyte-derived AMØs (live, CD11c^{dim/+}, CD11b⁺, GFP⁺). Comparing GFP⁺ and GFP⁻ expression of AMØ in O₃-exposed mice (Figure 2B and 2C), we observed that the majority of AMØs were GFP⁻, suggesting a predominance of tissue-resident AMØs and a lack of flux of monocyte-derived AMØs following O₃ exposure. The red boxes depict the average percentage of monocyte-derived AMØ present in the FA (mean 1.154% +/- 0.1724, n=3), 12h (mean 0.6352% +/- 0.0765, n=5), 24h (mean 0.7240% +/- 0.1201, n=4), and 72h (mean 0.1068% +/- 0.1341, n=6) post-O₃ exposure (Figure 2C). Despite the lack of monocyte-derived AMØ recruitment (Figure 2B), we did observe influx of monocytes following O₃ exposure suggesting that monocytes traffic into the lung following exposure but do not differentiate into AMØs (Figure 4). Overall,

the data collected with an inducible monocyte lineage tracing mice show no evidence for lung recruitment of monocyte-derived AMØs following O₃ exposure.

2.3.2 Monocyte-derived AMØs are not recruited following acute O₃ exposure in healthy human volunteers

Given the lack of monocyte-derived AMØ recruitment following acute O₃ exposure in rodents, we wanted to translate this observation to humans undergoing acute laboratory O₃ exposure. Healthy human volunteers (n=12) without a history of chronic cardiopulmonary disease (Figure 5A) were exposed to FA or O₃ (200 ppb) for 135 minutes with intermittent exercise in a randomized crossover study design with an 18–20 day washout period between exposures. Approximately 21h following each exposure, the subjects underwent a bronchoscopy with bronchoalveolar lavage (BAL). 10mL of BAL fluid was aliquoted per exposure and processed/stained/analyzed by flow cytometry to define AMØ composition. Human AMØs were defined as singlets, live, CD45⁺, CD3⁻, CD15⁻, CD206⁺ cells (Figure 5B and Table 3). Segregation of human tissue-resident from monocyte-derived AMØs was defined by the extent of CD206 and CD14 staining where tissue-resident AMØs are CD206^{Hi}, CD14^{Lo} and monocyte-derived AMØs are CD206^{Lo}, CD14^{Hi} (Figure 5B). Monocytes were segregated and identified as CD14^{Hi}, finding no significant monocyte recruitment following O₃ exposure (Figure 5B and 5C). Consistent with prior human data [117], healthy human volunteers had monocyte-derived AMØs in the FA exposure samples (Figure 5C). However, following O₃

exposure there was no significant recruitment of monocyte-derived AMØs (Figure 5B and 5C). Despite the lack of overall evidence for recruitment of monocytes or monocyte-derived AMØs, we did observe significant intra-individual variability in filtered air and O₃ exposure immune cell profiles, suggesting differences in basal airspace immune cell composition and response to exposure between study subjects (Figure 5D). Overall, this data suggests that similar to mice, healthy human volunteers do not recruit monocyte-derived AMØs following acute laboratory O₃ exposure.

2.3.3 Tissue-resident AMØ depletion causes persistent O₃-induced bronchoalveolar lavage neutrophilia

Given the lack of monocyte-derived AMØ recruitment following O₃ exposure in rodents or humans, we focused on defining a role of tissue-resident AMØs in acute O₃ exposure. Following previously published protocols [105], tissue-resident AMØs were depleted using administration of intra-tracheal clodronate-loaded liposomes. To confirm specificity of this clodronate-mediated depletion, we performed whole lung flow cytometry assessment of immune cells, identifying that clodronate-loaded liposomes led to AMØ-specific depletion (Figure 6A). Administering clodronate-loaded liposomes to tamoxifen-induced Cx3cr1^{ERcre} zsGreen mice, we also confirmed that clodronate administration did not cause recruitment of monocyte-derived AMØs during the timescale of our exposure experiments (Figure 6B). The red boxes depict the average percentage of monocyte-derived AMØ present (mean 0.9200% +/- 0.3107, n=4). This data

demonstrates that clodronate-mediated depletion was specific to AMØs and resulted in depletion of tissue-resident AMØs without subsequent recruitment of monocyte-derived AMØs.

Next, we assessed the impact of clodronate-mediated depletion of tissue-resident AMØs on acute O₃-induced lung inflammation and injury. C57BL/6J mice were administered PBS or clodronate and then 72h post-administration were exposed to FA or O₃ (2 ppm) for 3h (Figure 7A). At 12h or 24h post-exposure, mice were harvested and assessed for airspace inflammation. No differences in total cells, macrophages, or neutrophils were observed in the filtered air groups (Figure 7B, FA). In PBS-administered, O₃-exposed mice, there was an increase in BAL total cells at both 12 and 24h post-exposure (Figure 7B). Cell differentials revealed an increase in airspace neutrophils that peaked at 12h and had started to decline by 24h post-exposure. In contrast, in the clodronate-administered, O₃-exposed mice, neutrophils increased at 12h post-exposure but then remained persistently elevated at 24h post-exposure (Figure 7B). As expected, AMØs were reduced at 12h and remained so through 24h post-exposure in mice given clodronate administration prior to O₃. In contrast, there was a significant difference in the amount of airspace neutrophils 24h post-exposure in the PBS and clodronate administered mice exposed to O₃, where the clodronate administered mice demonstrated persistent airspace neutrophilia.

2.3.4 Tissue-resident AMØ depletion causes persistence of BAL cytokine/chemokines and neutrophil elastase

In addition to airspace inflammation, we also assessed the impact of tissue-resident AMØ depletion on other measures of O₃-induced lung inflammation and injury. BAL fluid cytokines and chemokines levels were measured by multiplex ELISA with a focus on neutrophil factors. These included Granulocyte colony-stimulating factor (G-CSF), Leukemia inhibitory factor (LIF), IP-10 (also known as CXCL10), interleukin (IL)-6, GRO α (also known as CXCL1), Monocyte chemoattractant protein-1 (MCP-1 or CCL2), Macrophage inflammatory protein 2-alpha (MIP-2 α), and Macrophage inflammatory protein-2 beta (MIP-2 β). At 12h post-exposure, LIF, IL-6, GRO α , MIP-2 α , and MIP-2 β were increased when compared to FA groups but no difference was observed between PBS or clodronate administered groups. Alternatively, at 24h post-O₃ exposure, differences were present in the cytokine responses between PBS and clodronate administered groups (Figure 8), where IP-10, IL-6, GRO α , MCP-1, MIP-2 α , and MIP-2 β were all elevated in clodronate administered but not control mice. Similar to cytokine responses, BAL neutrophil elastase was elevated in O₃ exposed mice at 12h when compared to FA but not different based on clodronate administration (Figure 9). However, neutrophil elastase was persistently increased at the 24h post-exposure time point in the clodronate administered versus control mice. This data supports that in tissue-resident AMØ-depleted mice, the O₃ exposure induced

persistence in airspace neutrophils associates with a similar persistence in pro-inflammatory cytokines and neutrophil elastase suggesting failed resolution of O₃-induced inflammation.

2.3.5 Depletion of tissue-resident AMØs reduces efferocytosis *in vivo*

The persistence of airspace neutrophils following O₃ exposure in tissue-resident AMØ-depleted mice suggests failed clearance of apoptotic neutrophils. To determine if neutrophils exhibit increased apoptosis following clodronate-loaded liposome administration, we assessed apoptosis markers (7AAD and Annexin V) by flow cytometry in Ly6G⁺ BAL neutrophils. We observed that O₃ exposed PBS administered control mice had a higher portion of “Live” neutrophils (Ly6G⁺, 7AAD⁻, Annexin V⁻) and reduced “Early Apoptosis” neutrophils (Ly6G⁺, 7AAD⁻, Annexin V⁺) than O₃ exposed clodronate-loaded liposome administered mice (Figure 10). This finding suggests that depletion of tissue-resident AMØs resulted in increased apoptotic neutrophils following O₃ exposure, supporting defective efferocytosis. To confirm the requirement of tissue-resident AMØs for *in vivo* efferocytosis, we adapted a method from Hodge et al. to assess efferocytotic function *in vivo* [68]. Apoptotic cells were generated by UV irradiating immortalized T cells (Jurkat cells) and were labeled with Calcein AM dye to track their clearance. Prior to dosing, the extent of Jurkat cell apoptosis was confirmed by viability staining (data not shown). PBS or clodronate was administered to C57Bl/6J

mice as described above. 72h after administration, apoptotic labeled Jurkat cells, were instilled via oropharyngeal aspiration and 1.5h later mice were harvested for BAL allowing for the number of labeled Jurkat cells to be measured by flow cytometry (Figure 11A). To assess *in vivo* efferocytosis we created a ratio of the number of recovered labeled Jurkat cells in the BAL over the number of instilled Jurkat cells. We observed that the mice with tissue-resident AMØ depletion exhibited decreased efferocytosis, as evidenced by an increased number of Jurkat cells recovered from BAL fluid (Figure 11B). This supports that tissue-resident AMØ facilitate effective efferocytosis.

2.3.6 Mer tyrosine kinase (MerTK) null mice exhibit persistent O₃-induced inflammation

As tissue-resident AMØs depleted mice exhibited decreased efferocytosis, we wanted to validate the role of efferocytosis in acute O₃ exposure responses. To perform this, we assessed O₃ exposure responses in MerTK null (MerTK^{-/-}) mice. MerTK cell surface staining is a defining feature of AMØs and is frequently used in flow cytometry studies to segregate AMØs from other lung immune cells [51]. In addition, MerTK regulates efferocytosis and MerTK^{-/-} mice are noted to have ineffective efferocytosis [108,109]. We first assessed if MerTK expression was modified by O₃ exposure. We measured MerTK expression by real time PCR from BAL cells at 6h, 12h, 24h, 48h, 72h and 7 days post-acute O₃ exposure (2 ppm for 3h). Overall, there was minimal overall

change in MerTK expression (Figure 12A). We then compared O₃-induced lung inflammation and injury responses in C57Bl/6J (WT) and MerTK^{-/-} mice. WT and MerTK^{-/-} mice were exposed to FA or O₃ (2 ppm) for 3h and then harvested 24h post-exposure. We focused on the 24h time point since this is where we identified differences in the resolution of O₃-induced neutrophilic inflammation. No differences were observed in BAL immune cells in FA exposed WT and MerTK^{-/-} mice. Following O₃ exposure, MerTK^{-/-} mice, compared to WT mice, demonstrated increased total cells, macrophages, and neutrophils (Figure 12B). Furthermore, BAL cytokine and chemokine profiles were enhanced in the O₃ exposed MerTK^{-/-} mice when compared to WT mice (Figure 13). This included elevations in IP-10, IL-6, GRO α and MIP-2 β . This suggests that MerTK promotes resolution of O₃-induced inflammation.

2.4 Discussion

AM \emptyset s are critical to the initiation, propagation and resolution of lung inflammation and injury. Therefore, defining specific AM \emptyset functions in diverse lung injury responses remains an important research question. In the present study, we focused on defining the role of AM \emptyset s in O₃-induced lung injury. We performed detailed lineage tracing of AM \emptyset s following O₃ exposure to define the origin of AM \emptyset s. We identified that following O₃ exposure AM \emptyset s are of tissue-resident origin without a predominance of monocyte-derived AM \emptyset s. Similar to observations in rodents, healthy

humans exposed to O₃ also did not have an increase in monocyte-derived AMØs. To define the function of tissue-resident AMØs, we performed a series of experiments using a clodronate-mediated tissue-resident AMØ depletion model to demonstrate that tissue-resident AMØs facilitate efferocytosis following O₃ exposure and that efferocytosis promotes resolution of O₃-induced lung injury. To confirm the requirement of effective efferocytosis in the resolution of O₃-induced lung inflammation, we performed O₃ exposure studies in MerTK^{-/-} mice, which have a genetic deficiency in efferocytosis. Following O₃ exposure, MerTK^{-/-} mice exhibited persistent airspace neutrophils and cytokine responses similar to exposed tissue-resident AMØ depleted mice. Overall, the data support that O₃ exposure does not recruit monocyte-derived AMØs and tissue-resident AMØs appear to promote resolution of O₃-induced lung injury through efferocytosis via MerTK.

Acute O₃-induced lung injury is regulated by AMØ functions, with data supporting both pro-inflammatory and protective/pro-resolving functions [26,36,95,118]. While AMØ origin may offer one potential explanation for differing functions of AMØs following O₃ exposure, there have been inconsistent findings in the literature about AMØ composition following O₃ exposure. Francis et al. defined populations of pro-inflammatory (CD11b⁺ Ly6C^{Hi} and iNOS⁺) and anti-inflammatory (CD11b⁺ Ly6C^{Lo}) AMØs present in the lung following O₃ exposure, which required CCR2 for their

recruitment [119]. In addition, another study by this group identified that these O₃-induced pro-inflammatory AMØs were reduced in splenectomized mice suggesting these pro-inflammatory AMØs are derived from a splenic intermediate [120]. Overall, their data on pro-inflammatory AMØs suggests these cells are monocyte-derived in origin (i.e. monocyte-derived AMØ) due to their CCR2 requirement and origin from a splenic intermediate. As CCR2-null or splenectomized mice exhibited reduced O₃-induced inflammation and injury, the authors argued that these pro-inflammatory AMØ were driving O₃-induced pathobiology. Alternatively, our prior work suggests that O₃-derived AMØs are principally tissue-resident in origin and exhibit a protective role in O₃-induced lung injury [111]. We defined expansion of a Cx3cr1-mediated tissue-resident AMØ subset following O₃ and loss of this subset in Cx3cr1-null mice exacerbated O₃-induced lung inflammation and airway hyperresponsiveness [111]. In a separate study, we compared O₃ exposure responses in male and female mice using a more extensive immune phenotyping flow cytometry panel and also did not identify monocyte-derived AMØs [58]. However, none of these studies relied on lineage tracing strategies that clearly define AMØ origin. To address this, the present study used lineage tracing with inducible Cx3cr1^{ERcre} zsGreen mice, which distinguishes tissue-resident AMØ from monocyte-derived AMØs [106]. We identified that AMØs following O₃ exposure are predominantly tissue-resident in origin with minimal to no monocyte-

derived AMØs (Figure 2C). This supports that macrophage-derived effects in lung O₃ responses are restricted to tissue-resident AMØs.

Though we did not observe an influx of monocyte-derived AMØs, we did observe an influx of monocytes, but these monocytes did not differentiate into macrophages (Figure 4). Prior work by Jakubzick et al. identified that monocytes can traffic through lung tissues without differentiation into macrophages and have antigen presentation functions [121,122]. Presently, we do not know the specific functions of monocytes present following O₃ exposure although it is possible that they could be driving some of the pro-inflammatory functions ascribed to macrophages following O₃ exposure. Future studies will need to consider the functions of these monocytes in O₃-induced lung inflammation and injury.

Due to the lack of monocyte-derived AMØ recruitment following acute O₃ exposure in rodents, we were interested to define if a similar AMØ response would be seen in human subjects. Using BAL cells obtained by bronchoscopy from a cohort of healthy human volunteers exposed to FA and O₃, we were able to confirm that monocyte-derived AMØs were not recruited (Figure 5C). Consistent with other healthy human BAL studies, we observed that monocyte-derived AMØ subsets are present in control human BALs [117,123]. This is different from rodents, where AMØs have been shown to be solely of tissue-resident origin. This has been hypothesized to be a

consequence of differences between laboratory rodents living in largely sterile housing environments and human volunteers living in non-sterile environments with exposures to pathogens and irritants [124]. Understanding if these human monocyte-derived cells are hyper-responsive to subsequent exposures and/or pathogens remains an unanswered question and will need to be considered in future studies. One limitation of our flow cytometry analysis is that we did not define subsets of tissue-resident and/or monocyte-derived AMØs. This is despite single cell RNA-sequencing identifying 2 or more unique subsets of distinct clusters of tissue-resident and monocyte-derived AMØs with the potential to have distinct functions [117,125]. Future single cell RNA-sequencing studies will need to consider if there are distinct exposure related subsets of AMØs and their role in exposure human exposure responses.

Though we did not observe an overall difference in monocyte-derived AMØs following O₃ exposure, evaluation of the immune cell profiles between individuals suggested significant diversity in immune cell profiles (Figure 5D). Comparing profiles across individuals in the FA controls, we observed significant differences in immune cell profiles, highlighting baseline intra-individual variability in airspace immune cell composition. Furthermore, we observed additional variability in FA to O₃ exposure responses, where some individuals had minimal change and others clear immune profile differences between their FA and O₃ exposures. This highlights intra-individual

variability in baseline immune cell composition and in exposure responses. Future studies will consider if this baseline composition predicts the exposure responses or if exposure immune cell profiles predict individuals with adverse outcomes to exposure.

An interesting aspect of the present study was the observation that monocyte-derived AMØs were not recruited following acute O₃-induced lung injury (Figure 2B and 2C). This is counter to other lung injury models where monocyte-derived AMØs predominate both in cell numbers and injury-regulating functions [105,106]. This may reflect the relative severity of O₃-induced lung injury versus other lung injury models. In C57Bl/6J mice, O₃ exposure is typically associated with mild resolving lung injury [118]. This is in contrast to other commonly used lung injury models such as LPS, bleomycin, and influenza infection, which are associated with extensive tissue injury and destruction [102,126,127]. Generally, in these lung injury models, tissue-resident AMØs are largely dispensable, and principal injury-regulating effects have been ascribed to monocyte-derived AMØs. Although not specifically evaluated in the present study, it is possible that different mechanisms regulate responses in these more severe forms of lung injury than responses to mild and resolving lung injuries. This has important potential human health implications as mild lung injuries, such as those experienced following O₃ exposure, are ubiquitous and therefore more commonly experienced than severe lung injuries. Understanding distinct mechanisms driving mild versus more

severe lung injuries could shed light on how mild, normally resolving lung injury responses can become more severe and/or persistent. This insight may help us comprehend how ubiquitous injuries that typically resolve, like O₃ exposure, can cause or exacerbate lung diseases. Consistent with this, specific genetic mouse strains exhibit enhanced sensitivity to O₃ exposure, driving enhanced lung injury, and in some cases the development of lung fibrosis [128,129]. Given this importance, future studies will need to consider additional mechanisms regulating mild lung injury that favor return to homeostasis and how these might be dysregulated under certain conditions to promote lung disease.

To address the specific functions of tissue-resident AMØs following O₃ exposure, we depleted these AMØs using intratracheal administration of clodronate-loaded liposomes. We confirmed the specificity of clodronate to deplete tissue-resident AMØs (Figure 6A) and also ensured that clodronate administration did not cause recruitment of monocyte-derived AMØs to the empty niche as others have previously demonstrated (Figure 6B) [130]. When we exposed tissue-resident AMØ depleted and non-depleted control mice to O₃, the non-depleted control mice and the tissue-resident AMØ-depleted mice demonstrated similar initial O₃ inflammatory responses. However, at a later time point following exposure, tissue-resident AMØ-depleted mice, when compared to the non-depleted mice, had persistent elevation of airspace neutrophilia (Figure 7B). We also

observed persistence of BAL cytokine responses and evidence of increased neutrophil elastase (Figure 9). Interestingly, this occurred at a timeframe where inflammation is resolving in non-depleted control mice. This suggests that tissue-resident AMØ are participating in the resolution of acute O₃-induced lung inflammation. Consistent with this, we identified that O₃-exposed tissue-resident AMØ-depleted mice had increased proportions of neutrophils exhibiting markers of apoptosis (Figure 10). This suggested a defect in apoptotic neutrophil clearance. To confirm this, we assessed *in vivo* efferocytosis in control versus tissue-resident AMØ-depleted mice (Figure 11), observing a defect in efferocytosis. This suggests tissue-resident AMØ function in O₃-induced lung injury by performing efferocytosis, and thereby promoting resolution of lung inflammation.

To further clarify the role of efferocytosis in O₃-induced lung injury, we assessed O₃ responses in MerTK^{-/-} mice. MerTK is a cell surface marker and a member of the TAM receptor tyrosine kinase family. While many cells express members of the TAM family, Axl and MerTK are predominantly expressed on AMØ [131]. MerTK is known to regulate efferocytosis via binding of Protein S or Gas6, which bind phosphatidylserine on the surface of the apoptotic cell, thus facilitating apoptotic cell recognition for efferocytosis [132]. There is limited information on the impact of air pollution on MerTK and MerTK-mediated responses. A study by Liang et al., found PM_{2.5} exposure to

decrease MerTK expression and cause increased cleavage of MerTK, leading to decreased efferocytosis [133]. However, to our understanding, this is the first description of MerTK following acute O₃-exposure. We first defined AMØs MerTK expression over a time course following O₃ exposure (Figure 12A). Although we did not identify any statistical difference across the time course, there was evidence of a biological trend where MerTK expression initially increased and then decreased by 24h post exposure. Interestingly, the relative decrease in MerTK at 24h is the same time point where prior data has identified O₃-induced reductions in efferocytosis [68]. It is possible this reduction in efferocytosis could be a result of our observed changes in MerTK expression. Future studies could consider if augmentation of MerTK expression at this time point could improve O₃-induced reductions in efferocytosis. Using MerTK^{-/-} mice, we identified that MerTK^{-/-} compared to C57Bl/6 mice had persistent O₃-induced airspace neutrophilia (Figure 12B) and cytokine/chemokine responses (Figure 13). This largely phenocopied the results of O₃ exposed tissue-resident AMØ-depleted mice. This suggests that tissue-resident AMØ promote the resolution of O₃-induced lung inflammation via efferocytosis, and this occurs via a MerTK-mediated mechanism.

There are limitations to our study that should be considered. Despite the lack of clodronate-mediated impact on immune cell composition (Figure 5A), it is possible that clodronate might impact the function of non-AMØ immune cell subsets. Consistent with

this, Culemann et al. recently identified that clodronate ingestion by neutrophils led to a decrease in neutrophil inflammatory functions including reduced ROS production, NETosis, migration, and cytokine release, which they described as neutrophil “stunning” [134]. Contrary to their published data, we identify that neutrophil functions are enhanced, and not suppressed. In addition, the depletion of tissue-resident AMØs occurs prior to O₃ exposure and appears to have a direct impact on efferocytosis, independent of neutrophil function. This suggests that “stunning” of neutrophils is not driving our O₃ phenotype. Additionally, recent data from Akalu et al.[135] identified that commercially available MerTK^{-/-} mouse lines are not specific to MerTK and also delete non-MerTK gene sequences. Using a newly developed MerTK-null mouse, they demonstrated that some phenotypes previously ascribed to MerTK are no longer observed, specifically non-efferocytosis phenotypes. They did identify that efferocytosis effects appeared consistent across the various MerTK^{-/-} strains. Since our focus was on efferocytosis, we feel the use of our MerTK strain to assess O₃-exposure responses is justified.

2.5 Conclusion

In summary, our results show that monocyte-derived AMØs are not recruited following O₃ exposure. We further define that tissue-resident AMØs function in clearance of apoptotic neutrophils, which facilitates the resolution of O₃-induced lung

inflammation via MerTK. This study defines the importance of tissue-resident AMØ-mediated efferocytosis in mild resolving lung injury. Furthermore, it highlights the importance of defining distinct roles of AMØ subtypes as a means of understanding their distinct roles in lung injury and its resolution.

2.6 Acknowledgements

The authors acknowledge the contributions of the Duke Cancer Institute Flow Cytometry Facility and the Rodent Inhalation Core at Duke University, Durham, NC. Flow cytometric analysis of the human BAL specimens was performed at Northwestern University Flow Cytometry Core Facility. Northwestern University Flow Cytometry Core Facility is supported by NCI Cancer Center Support Grant P30 CA060553 awarded to the Robert H. Lurie Comprehensive Cancer Center. Cell sorting was performed on a BD FACSAria SORP cell sorter purchased through the support of NIH 1S10OD011996-01.

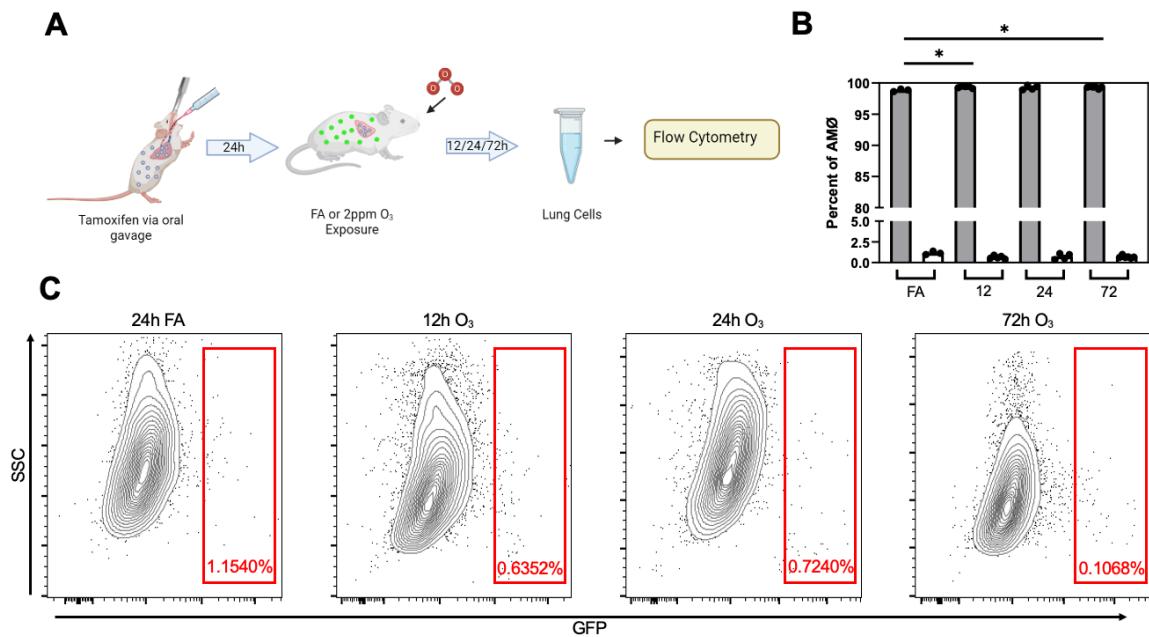


Figure 2. Monocyte-derived alveolar macrophages (AMØ) are not recruited following acute O₃ exposure.

A. Cx3cr1^{ERCre} × zsGreen mouse model was used. Circulating blood monocytes and monocyte-derived AMØ express Cx3cr1, and after tamoxifen induction are GFP⁺, while tissue-resident AMØ remain unlabeled. Lineage label was induced with tamoxifen 24h prior to exposure with filtered air or O₃ (2 ppm) for 3h. 12, 24, or 72h-post exposure, whole lungs were processed and analyzed by flow cytometry. Schematic made using BioRender.com. **B.** Bar plots represent individual mouse GFP⁻ (tissue-resident AMØ, grey) and GFP⁺ (monocyte-derived AMØ, white) populations. ANOVA analysis was conducted using Tukey’s Honestly Significant Difference Test post-hoc. Data points represented with SEM; showing significant increase of tissue-resident AMØ from FA to 12 and 72h post O₃ exposure. *p<0.05. **C.** Acute O₃ exposure does not induce recruitment/differentiation of monocyte-derived AMØ. Representative flow cytometry plots of AMØs were negative for zsGreen/GFP positive cells, supporting no evidence of monocyte-derived AMØ recruitment. The red boxes indicate where GFP⁺ cells (monocyte-derived AMØ) would be observed if they were present in these samples. Percent GFP⁺ indicated within the respective box in red. Full flow cytometry gating strategy and antibodies can be found in the supplements (Figure 3). Flow plots are representative of n=3-6 mice per timepoint and replicated x1. Mice used include 4 females at 12h, with all other mice being male.

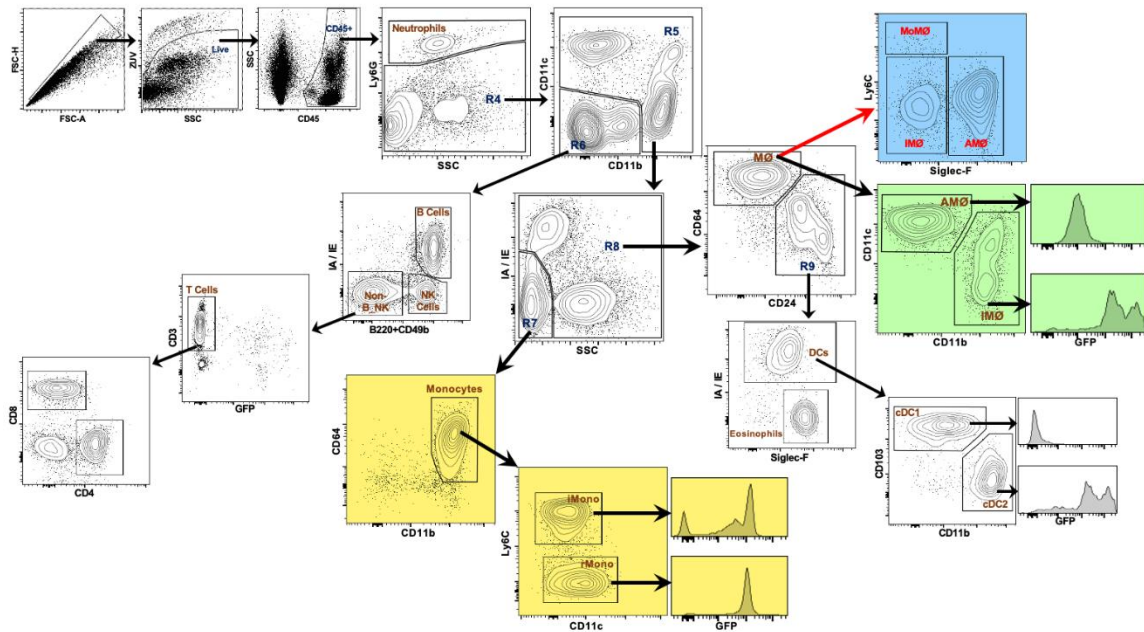


Figure 3. Mouse Flow Cytometry Gating Strategy.

Whole lung tissue was digested and stained for flow cytometry. Individual immune cells were defined based on specific cell surface markers based on prior published protocols (representative sample). Color gating indicates cellular and lineage tracking of specific cell populations of interest: yellow (monocytes), green (macrophages), blue (alternative macrophage gating to segregate monocyte-derived macrophages (MoMØ) from interstitial macrophages (IMØ) and alveolar macrophages (AMØ)).

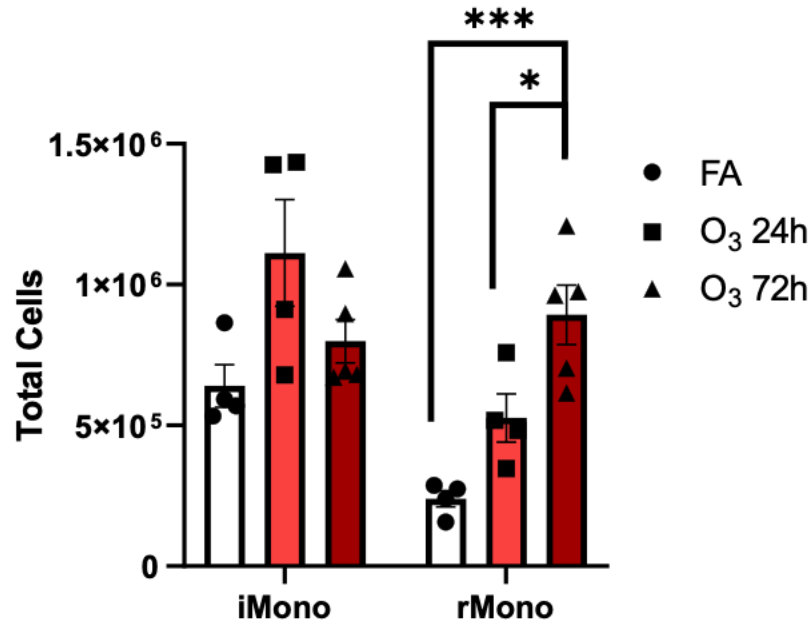


Figure 4. Inflammatory and constitutive monocytes are increased in lung tissue in response to acute O₃ exposure.

Monocyte lineage labeling was induced in Cx3cr1^{ERCre} × zsGreen mice with tamoxifen. Lineage label was induced with tamoxifen 24h prior to exposure with filtered air or O₃ (2 ppm) for 3h. 24 or 72h post exposure whole lungs were processed, stained, and analyzed by flow cytometry. Following O₃ exposure GFP⁺ inflammatory (iMono) and constitutive monocytes (rMono) were increased. n=4-5 mice per group and replicated × 1. *p<0.05. ANOVA analysis was conducted using Tukey's Honestly Significant Difference Test post-hoc.

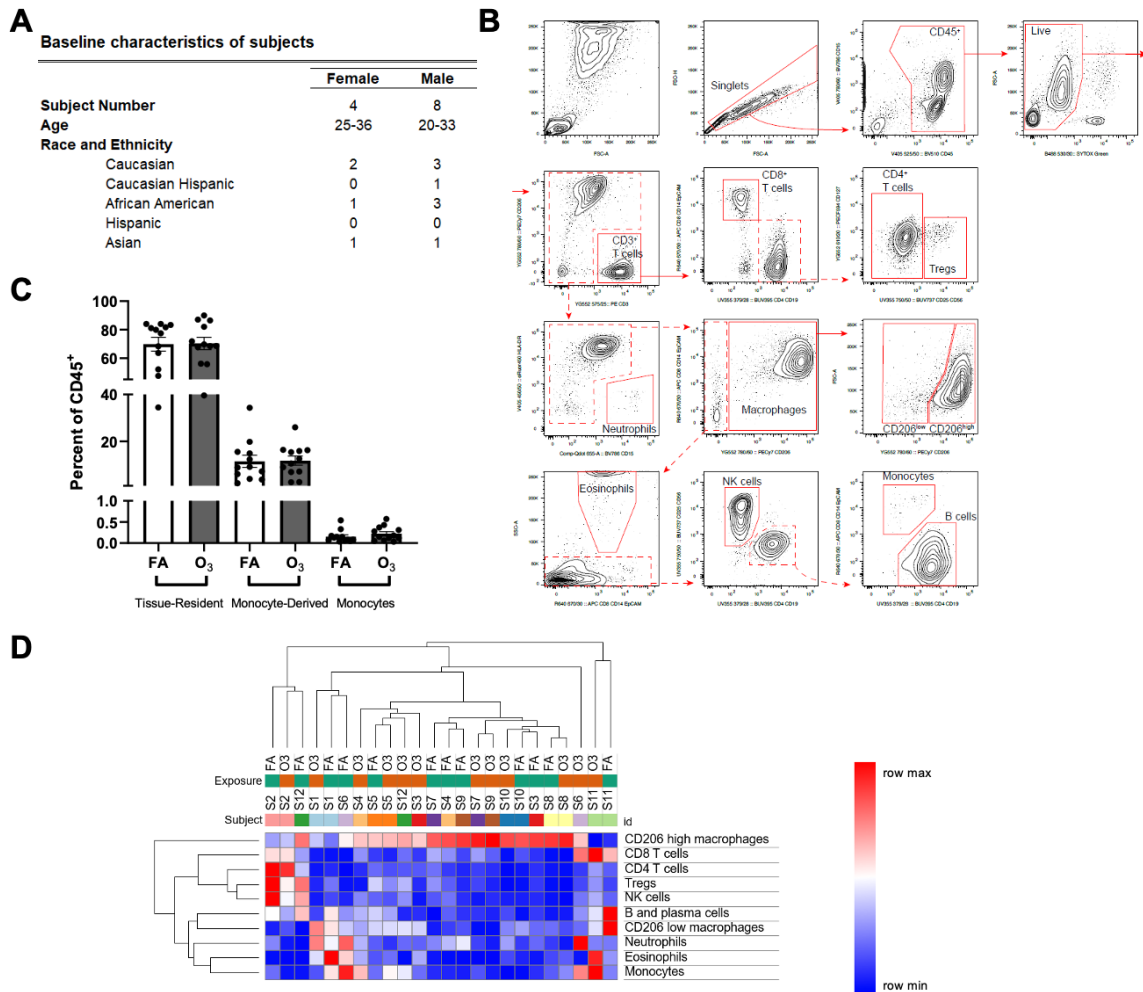


Figure 5. Monocyte-derived alveolar macrophages (AMØ) are not recruited following acute O₃ exposure in humans.

A. Human subjects were exposed to FA and O₃ (2ppm) for 3h in separate visits. They then underwent a bronchoscopy in which BAL fluid was collected and processed and analyzed by flow cytometry. Demographic information is listed for all human subjects including sex, age, and ethnicity. **B.** Representative flow cytometry plots of the gating strategy used to identify alveolar macrophages were generated demonstrating populations of CD206^{Lo}, monocyte-derived AMØ, and CD206^{Hi}, tissue-resident AMØ, populations. The CD206^{Lo} population did not increase following acute O₃ exposure, supporting no evidence of monocyte-derived AMØ function in this context. The red boxes indicate where GFP⁺ monocyte-derived AMØ would be observed if they were present in these samples. **C.** Acute O₃ exposure does not induce recruitment of

monocyte-derived AMØ. Bar plots represent human cellular response to FA (white) and O₃ (grey) populations. Paired t-test analysis was conducted and data points are represented with SEM. No significant difference seen in tissue-resident AMØ, monocyte-derived AMØ, and monocyte populations post O₃ exposure. **D.** Hierarchical clustering of the flow cytometry data from BAL samples. Column headers are color-coded by the exposure type (FA or O₃) and subject. Samples were clustered by Euclidean distance using average linkage method. *p<0.05 Flow plots are representative of n=12 human subjects.

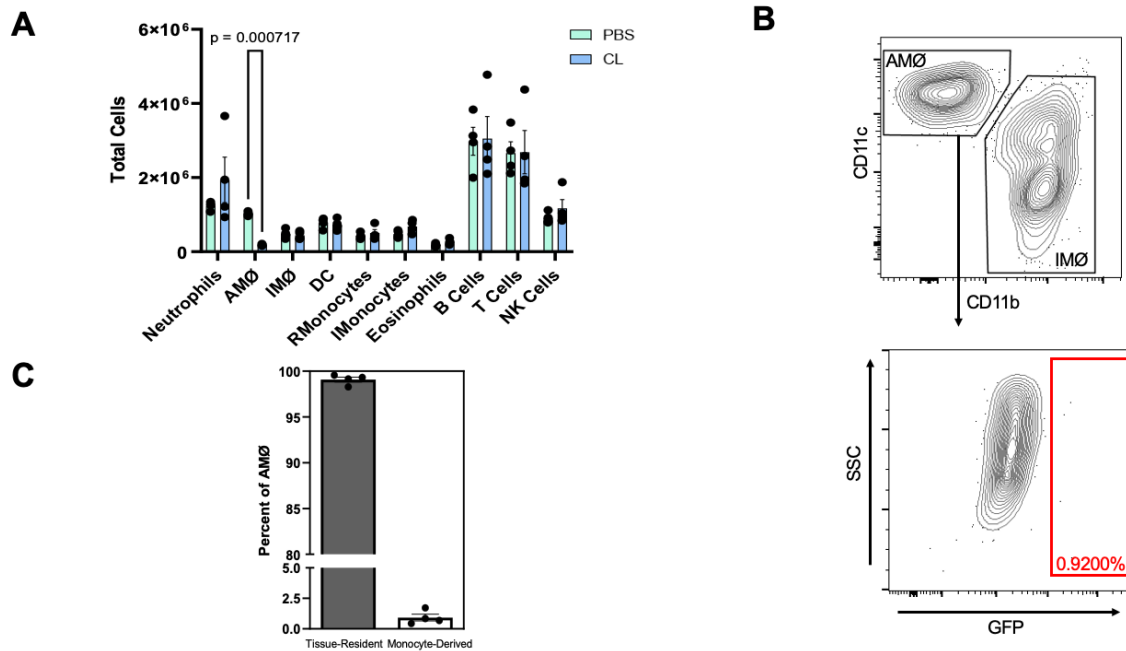


Figure 6. Airspace administration of clodronate (CL) depletes tissue-resident alveolar macrophages (AMØ).

A. C57Bl/6J female mice were dosed with clodronate or PBS (control) were harvested 72h post-dosing. The whole lung tissue samples were perfused, digested, and stained to identify the individual cells via flow cytometry. Bars shaded green indicate PBS/vehicle control while blue indicates CL administration. Data is from n=4 mice per group, p value is as identified. **B.** Cx3cr1^{ERCre} x zsGreen mice were dosed with CL 72h before harvest then underwent lineage labeling with tamoxifen 48h post-dosing. They were then harvested and processed for flow cytometry. The lack of GFP⁺ AMØ (red box) suggests a lack of Cx3cr1^{ERCre} x GFP⁺ monocyte-derived AMØs as a result of CL depletion of tissue-resident AMØ. Percent GFP⁺ indicated within the respective box in red. Flow plot is a representative sample of n=4. **C.** Bar plot represents individual mouse GFP⁻ (tissue-resident AMØ, grey) and GFP⁺ (monocyte-derived AMØ, white) populations, indicating no recruitment of monocyte-derived AMØ following CL depletion. Full flow cytometry gating strategy and antibodies can be found in the supplements (Figure 3).

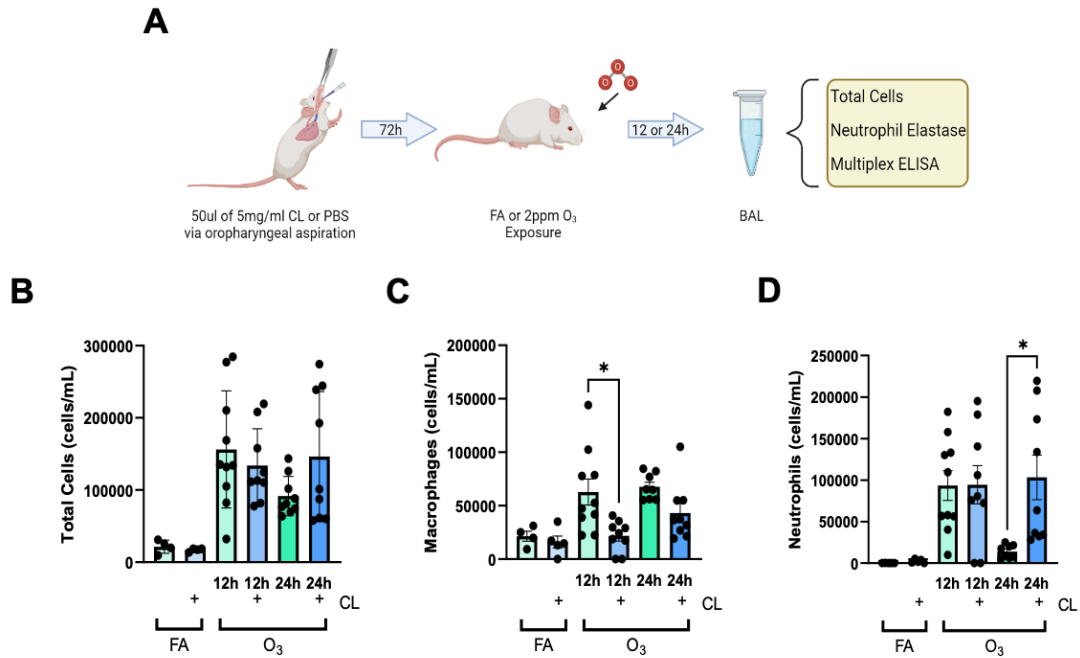


Figure 7. Tissue-Resident AMØ depletion leads to persistent O₃-induced BAL neutrophilia.

A. Male mice were dosed with 50uL of 5mg/ml clodronate liposomes via oropharyngeal aspiration. 72h following clodronate depletion of tissue-resident AMØ, mice were exposed to FA or O₃ (2 ppm) for 3h. Mice were then harvested 12/24h following exposure and the samples were processed for cell differentials and other measures of inflammation. Schematic made with BioRender.com. **B.** BAL total cells, **(C.)** macrophages, and **(D.)** neutrophils were enumerated following PBS or Clodronate (CL) administration and FA or O₃ exposure. Bars shaded green indicate PBS/vehicle control while blue indicates CL administration. By total cell numbers, CL exposed mice exhibited a reduction of macrophages at 12h and increased neutrophils at 24h. n=4-10 mice per group/exposure/timepoint *p<0.05. ANOVA analysis was conducted using Tukey's Honestly Significant Difference Test post-hoc.

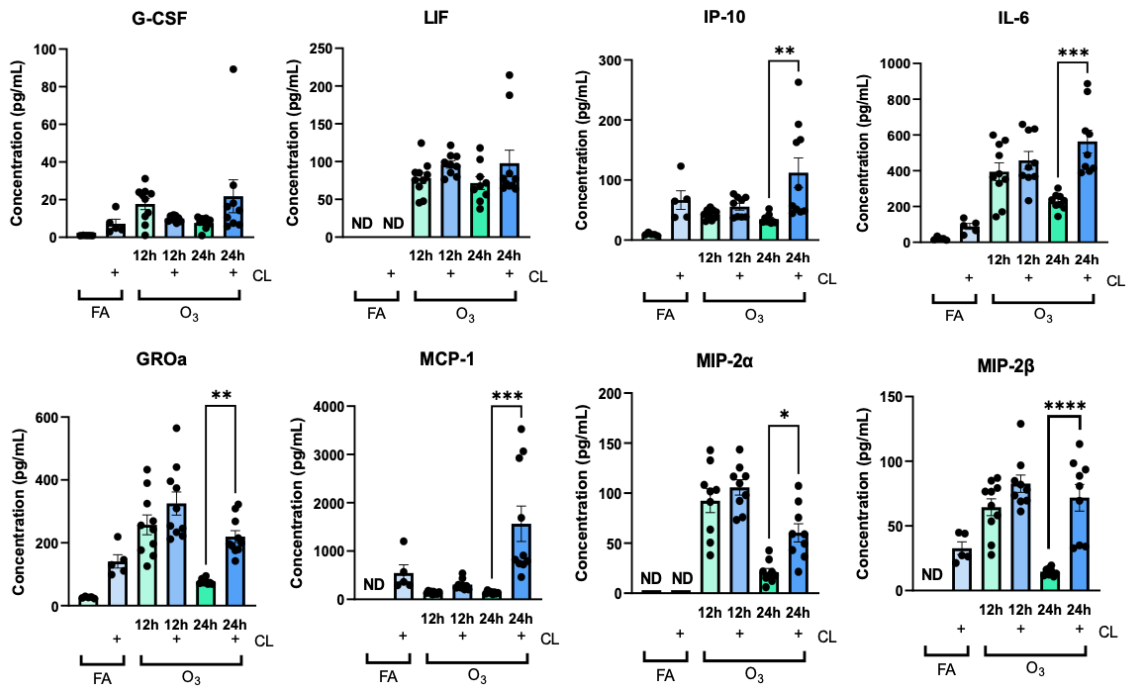


Figure 8. Increased BAL cytokines associated with neutrophil recruitment in O₃-exposed tissue-resident AMØ depleted mice.

BAL fluid from PBS or Clodronate and FA or O₃ (2ppm) exposed male mice was assessed for cytokine expression by multiplex ELISA for inflammatory cytokines and known neutrophilic chemotactic factors. Bars shaded green indicate PBS/vehicle control while blue indicates CL administration. n=4-10 mice per group/exposure/timepoint *p<0.05. ANOVA analysis was conducted using Tukey's Honestly Significant Difference Test post-hoc. ND indicates samples below the assay limit of detection.

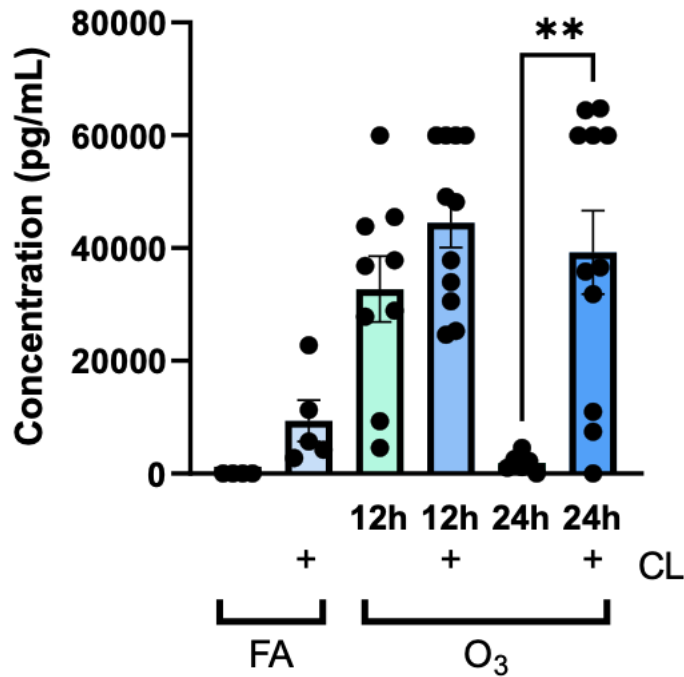


Figure 9. Neutrophil elastase is persistently elevated in tissue-resident AMØ depleted mice.

PBS or Clodronate (CL) was administered to male C57BL/6J mice 72h prior to FA or O₃ (2 ppm) for 3h. Mice were harvested at 12 and 24h post exposure and BAL was collected and processed. Bars shaded green indicate PBS/vehicle control while blue shades indicate CL administration. BAL fluid from PBS or CL and FA/O₃ exposed mice was assessed for neutrophil elastase concentration. n=4-10 mice per group/exposure/timepoint *p<0.05. ANOVA analysis was conducted using Tukey's Honestly Significant Difference Test post-hoc.

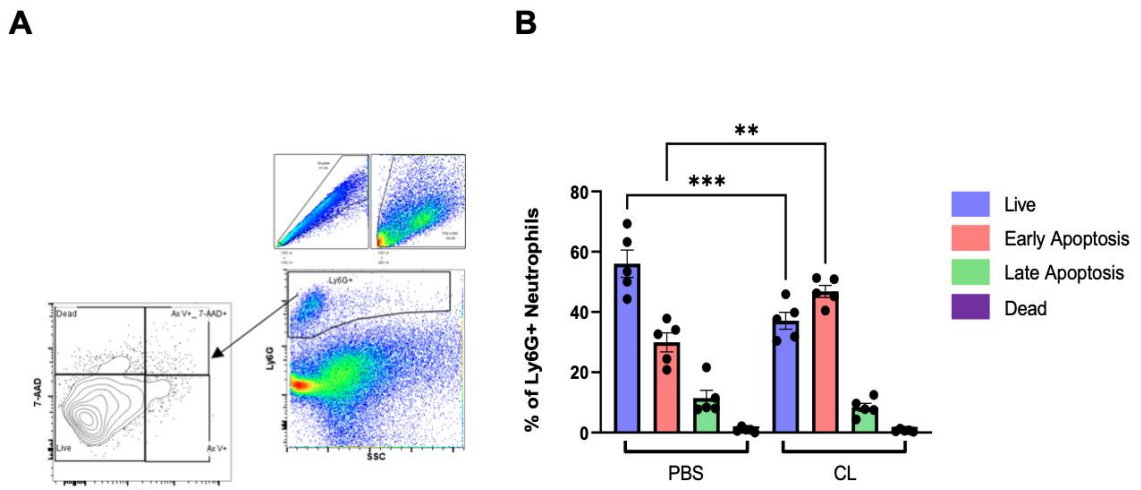


Figure 10. Tissue-resident AMØ depletion increased the proportion of apoptotic neutrophils following O₃ exposure.

A. The gating strategy to delineate neutrophil populations. Flow plots are a representative example of n=5 samples per condition. **B.** PBS or Clodronate (CL) was administered to male C57BL/6J mice 72h prior to O₃ (2 ppm) for 3h. 24h post-exposure, BAL was collected, stained with Ly6G, 7AAD and Annexin V and analyzed by flow cytometry. Neutrophils were defined as Ly6G⁺ cells and then assessed for 7AAD and Annexin V staining. “Live” neutrophils were defined as Ly6G⁺, 7AAD⁻, Annexin V⁻, “Early Apoptosis” neutrophils were defined as Ly6G⁺, 7AAD⁻, Annexin V⁺, “Late Apoptosis” neutrophils were defined as Ly6G⁺, 7AAD⁺, Annexin V⁺, and “Dead” neutrophils were categorized as Ly6G⁺, 7AAD⁺, Annexin V⁻. **p<0.005, ***p<0.0005

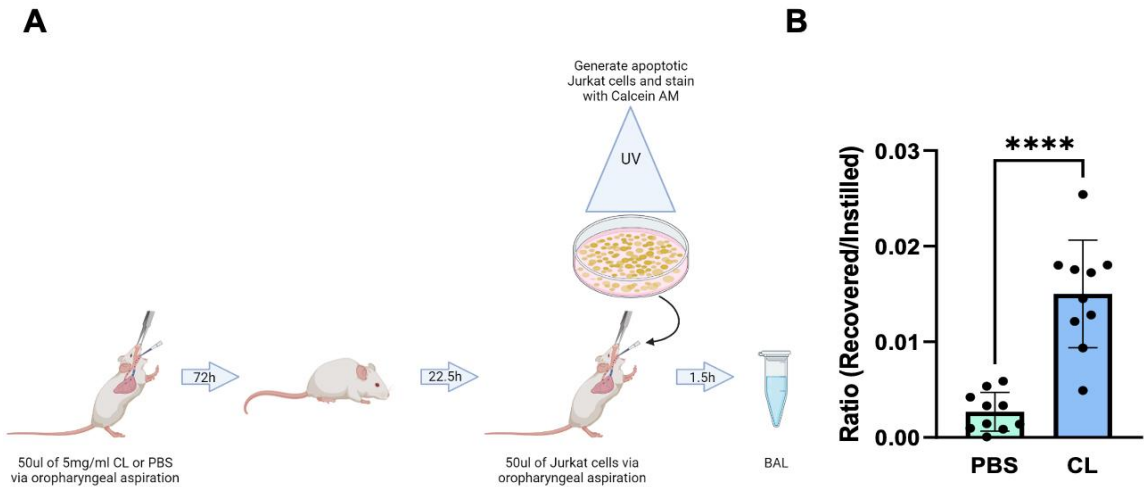


Figure 11. Tissue-resident alveolar macrophage (AMØ) depletion decreased efferocytosis.

A. C57BL/6J male mice were dosed with CL or PBS. The mice were then instilled with apoptotic immortalized T cells, Jurkat cells, via oropharyngeal aspiration 22.5h after exposure for 1.5h immediately prior to the harvest. During the harvest, 24h post-exposure, BAL was collected and prepared for use in flow cytometry. Schematic made with BioRender.com. **B.** Apoptotic cell clearance was defined using Calcein AM, positive cells indicating live or early apoptotic cells. Healthy cells would not be engulfed by AMØs, thus decreased Calcein AM positive cells indicate clearance of apoptotic cells (efferocytosis). The graphs depict the ratio of counted recovered vs. instilled cells from the collected BAL. Bars shaded green indicate PBS/vehicle control while blue indicates CL administration. An unpaired T-test was conducted with n=10 mice per group/exposure/timepoint *p<0.05.

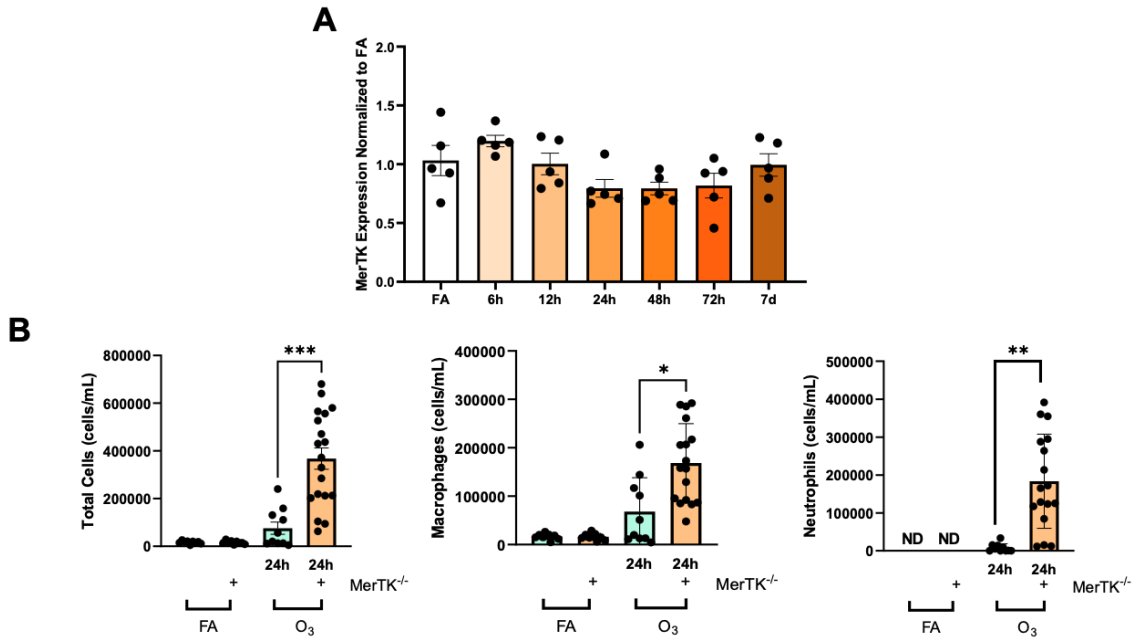


Figure 12. MerTK^{-/-} mice have increased O₃-induced airspace inflammation.

A. C57BL/6J male mice were exposed to O₃ (2 ppm) for 3h and harvested 6h, 12h, 24h, 48h, 72h, and 7days later. mRNA expression of MerTK was assessed using the collected BAL cells. n=5 mice per time point. **B.** MerTK^{-/-} mice and C57BL/6J mice (wildtype) were exposed to FA or O₃ (2 ppm) for 3h. The mice were harvested 24h post-exposure and the BAL was collected and processed for total cell counts and differentials. Green bars indicate the C57BL/6J mice while the orange indicates the MerTK^{-/-} genotype. n=9-19 mice per group. *p<0.05. ANOVA analysis was conducted using Tukey's Honestly Significant Difference Test post-hoc. ND indicates samples below the limit of assay detection.

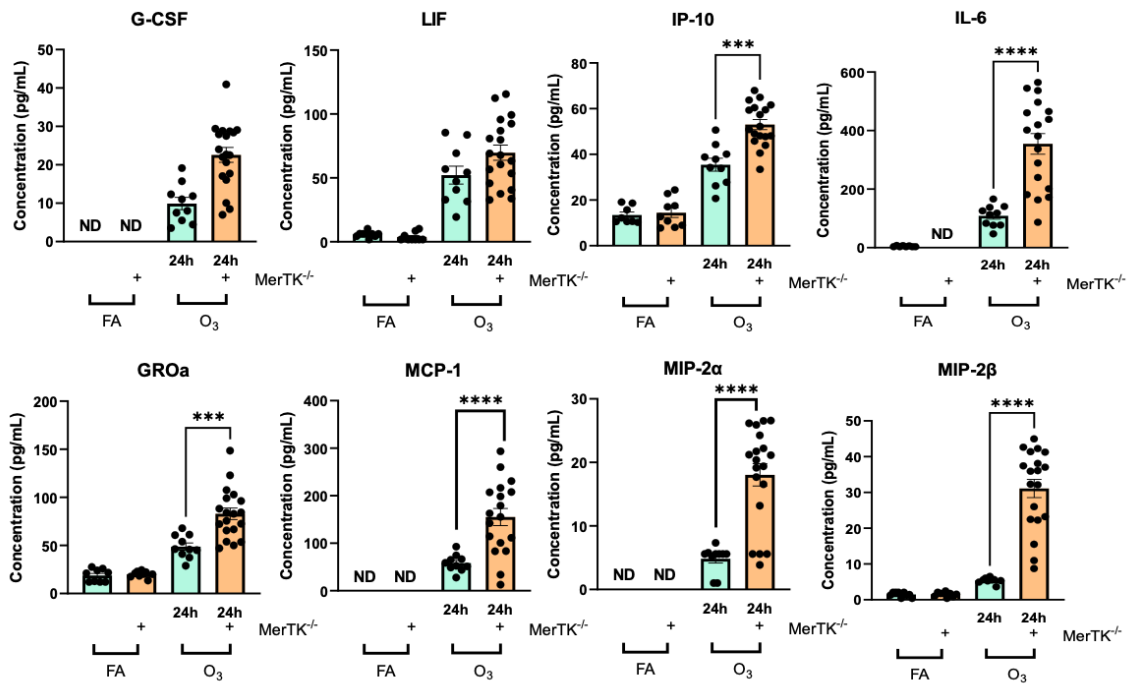


Figure 13. Increased BAL cytokines associated with neutrophil recruitment in O₃-exposed MerTK^{-/-} mice.

BAL fluid from C57BL/6J and MerTK^{-/-} mice FA or O₃ (2ppm) exposed mice was assessed for cytokine expression by multiplex ELISA for inflammatory cytokines and known neutrophilic chemotactic factors. Green bars indicate the C57BL/6J mice while the orange indicates the MerTK^{-/-} genotype. n=8-19 mice per group/exposure/timepoint. *p<0.05. ANOVA analysis was conducted using Tukey's Honestly Significant Difference Test post-hoc. ND indicates samples below the limit of assay detection.

Table 1. Immunophenotyping: Mouse: Antibodies and Staining reagents.

Mouse Target	Clone	Isotype	Conjugate	Working Dilution	Vendor	Catalogue#
CD31 (PECAM-1)	MEC13.3	Rat IgG2a, κ	PerCP-Cy5.5	1:400	Biolegend	102522
Ly6C	HK1.4	Rat IgG2a, κ	PerCP-Cy5.5	1:200	Biolegend	128012
B220 (CD45R)	RA3-6B2	Rat IgG2a, κ	PE	1:100	Biolegend	103208
CD49b	DX5	Rat IgM, κ	PE	1:100	Biolegend	108908
Siglec-F (CD170)	E50-2440	Rat IgG2a, κ	PE-CF594	1:1500	BD Horizon™	562757
F4/80 (Ly71)	BM8	Rat IgG2a, κ	PE-Cy7	1:400	Biolegend	123114
CD163	S15049I	Rat IgG2a, κ	APC	1:200	Biolegend	155306
CD169 (Siglec-1)	3D6.112	Rat IgG2a, κ	APC	1:100	Biolegend	142418
CD206	C068C2	Rat IgG2a, κ	APC	1:100	Biolegend	141708
MERTK (Mer)	2B10C42	Rat IgG2a, κ	APC	1:50	Biolegend	151508
Isotype Control	RTK2758	Rat IgG2a, κ	APC	1:50	Biolegend	400512
Ly6G	1A8	Rat IgG2a, κ	AF700	1:200	Biolegend	127622
CD11b	M1/70	Rat IgG2a, κ	APC-Cy7	1:150	Biolegend	101226
CD64 (FcγRI)	X54-5/7.1	Rat IgG2a, κ	BV421	1:50	Biolegend	139309
CD3ε	145-2C11	Rat IgG2a, κ	BV510	1:100	Biolegend	100353
CD103	2E7	Rat IgG2a, κ	BV510	1:100	Biolegend	121423
CD45	30-F11	Rat IgG2a, κ	BV605	1:500	Biolegend	103155

I-A/I-E	M5/114.15.2	Rat IgG2b, κ	BV650	1:1500	Biolegend	107641
CD24	M1/69	Rat IgG2b, κ	BV711	1:800	Biolegend	563450
CD11c	N418	AH IgG	BV785	1:100	Biolegend	117336
CD8_BUV395	53-6.7	Rat IgG2a, κ		1:100	BD Horizon™	563786
Zombie UV™		Fixable viability dye	350ex / 459em	1:1000	Biolegend	423108
CD4_BUV805	GK1.5	Rat IgG2b, κ		1:100	BD Horizon™	612900

Table 2. LSRFortessa X-20 configuration.

Detector	PMT	Mirror/ Beam Splitter	Band Pass Filter	Fluorochrome
770LP_820_60	A	770	820_60	BUV805
450LP_515_30	B	450	515_30	Zombie UV
379_28	C	----	379_28	BUV395
750LP_780_60	A	750	780_60	BV786
690LP_710_50	C	690	710_50	BV711
635LP_670_30	D	635	670_30	BV650
600LP_610_20	E	600	610_20	BV605
495LP_525_50	G	495	525_50	BV510
450_50	H	----	450_50	BV421
635LP_710_50	A	685	695/40	PerCP-Cy5.5
495LP_525_50	B	505	525_50	GFP
488_10	C	----	488_10	Side Scatter (SSC)
Diode	FSC			
Diode	SSC			
735LP_780_60	A	735	780_60	PE-Cy7
655LP_710_50	B	655	710_50	--
635LP_695_40	C	635	695_40	--
595LP_610_20	D	595	610_20	PE-CF594
575_26	E	----	575_26	PE
750LP_780_60	A	750	780_60	APC-Cy7
710LP_730_45	B	710	730_45	AF700
660_20	C	----	670_30	APC

Table 3. Human: Flow cytometry panel used for BAL sample phenotyping

Antigen	Clone	Fluorochrome	Manufacturer	Cat #
CD4	RPA-T4	BUV395	BD	564724
CD19	HIB19	BUV395	BD	740287
CD25	2A3	BUV737	BD	564385
CD56	NCAM16.2	BUV737	BD	612766
HLA-DR	L243	eFluor450	ThermoFisher	48-9952-42
CD45	HI30	BV510	Biolegend	304036
CD15	HI98	BV786	BD	563838
Live/Dead	Not applicable	SYTOX Green	ThermoFisher	S34860
CD3	SK7	PE	ThermoFisher	12-0036-42
CD127	HIL-7R	PECF594	BD	562397
CD206	19.2	PECy7	ThermoFisher	25-2069-42
CD8	SK1	APC	Biolegend	344721
CD14	M5E2	APC	Biolegend	301808
EpCAM	9C4	APC	Biolegend	324208

3. Spermidine regulation of NF- κ B activation via the NMDA receptor

3.1 Introduction

The functional switch of AM \emptyset s from inflammation to resolution of inflammation is crucial for an individual's health, as prolonged or uncontrolled inflammation can lead to chronic inflammation, and the onset of lung diseases such as asthma, cystic fibrosis, and chronic obstructive pulmonary disease [9,14,19]. As research has focused on uncovering the active process of resolution, it has become clear that there are many factors regulating resolution, including pro-resolution cytokines, bioactive lipids, as well as clearance of cellular debris and apoptotic cells [39,42,46,136]. In the previous chapter, we delved into the cellular-level function of AM \emptyset s in the resolution process following acute O₃ exposure, focusing on efferocytosis via MerTK. These findings led to questions regarding how AM \emptyset s undergo a transition from a pro-inflammatory to a pro-resolution phenotype and what are the intracellular mechanisms driving this phenotypic switch.

An intracellular mechanism that can drive AM \emptyset phenotypic switching to a pro-resolution phenotype occurs following efferocytosis. Prior studies have established links between efferocytosis and activation of intracellular pathways [137,138]. Notably, studies conducted by McCubbrey et al., performed an unbiased metabolomic screen of AM \emptyset s following efferocytosis. They identified a unique increase in arginine-derived polyamines, spermidine and spermine. They also identified that the increase in these

polyamines was due to the increased import of the polyamines from the environment, not retained from engulfed apoptotic cells nor *de novo* biosynthesis. Inhibiting polyamine import led to increased expression of pro-inflammatory cytokines, IL-1 β and IL-6, suggesting that the polyamines had an anti-inflammatory effect [139]. This finding is consistent with other macrophage studies demonstrating that arginase-1 derived metabolites of L-arginine function to promote resolution of inflammation and suppress of inflammatory cytokine production [90,140–143]. Beyond AM \emptyset s, L-arginine-derived polyamines, spermidine and spermine, promote resolution of inflammatory bowel disease [143] and are increased in the peripheral blood of asthmatic patients undergoing an exacerbation [144]. Despite their known roles in inflammatory diseases and macrophage function in various organs, the role and mechanism of polyamine-mediated regulation of lung immune responses is poorly understood [84,140–142,145,146].

Another known role of the L-arginine-derived polyamines is that they can inhibit the NMDA receptor by interacting with an allosteric binding site that regulates ion channel influx [147,148]. Additionally, the NMDA receptor has been studied as a regulator of NF- κ B activation [74]. While the NMDA receptor has largely been studied in the context of neurons and neurodegenerative diseases, it also has functions in other organs, including the lung [75–77]. Data suggests that the NMDA receptor is expressed in various pulmonary tissues including AM \emptyset s, alveolar type 2 cells, as well as the

trachea and airways [77,78,149]. While it is known that the NMDA receptor can be inhibited by polyamines and prior studies have shown that the NMDA receptor can regulate NF- κ B activation [74,92,93]; if these are linked and promote resolution of inflammatory signaling is poorly understood.

To address this knowledge gap, we assessed the presence and concentration of L-arginine and its metabolites following acute O₃ exposure. We observed dynamic changes in L-arginine, spermidine, and spermine concentrations following exposure. Specifically, we observed spermidine elevation at 24h post-exposure, the timepoint post-exposure associated with inflammation resolution. This is consistent with the potential role for spermidine in resolving O₃-induced lung inflammation. Based on this observation, we assessed the impact of spermidine administration on O₃-induced lung injury *in vivo*. We identified that spermidine reduces airspace inflammation and injury following O₃ exposure. To define the mechanism for this effect, we performed *in vitro* studies on MH-S cells, an alveolar macrophage-like cell line. MH-S cells were exposed to a canonical activator of NF- κ B, LPS, to define the impact of spermidine on activation of NF- κ B and production of pro-inflammatory cytokines. In agreement with previous work [90,91], we found spermidine administration following LPS exposure reduces NF- κ B activation, cytokine expression, and cytokine release. To then assess NMDA involvement in NF- κ B activation we dosed the MH-S cells with NMDA, an NMDA

receptor agonist. We were then able to show that NMDA agonism activates NF- κ B similarly to LPS. As spermidine has been demonstrated to inhibit the NMDA receptor, this suggests the potential for spermidine as negatively regulating NF- κ B activation via inhibition of NMDA.

3.2 Materials and Methods

3.2.1 Cell Culture

MH-S cells, an immortalized murine alveolar macrophage cell line, was purchased from and maintained per protocols by ATCC (Manassas, Virginia). Cells were thawed from frozen stock and plated on 10cm dishes in complete media (RPMI1640 (Gibco, #cat: 11875), 10% FBS Non-Heat Inactivated, 5mL A/A, 2.8mL Glucose 45%, 5mL HEPES, and 5mL Na Pyruvate) and 2-mercaptoethanol (BME), which was added fresh with each media change. Following the first split, cells were re-plated and grown to confluence (about 1 week). The cells were then scraped off the plates using a cell scraper (Cell Treat), centrifugated (1200 rpm X 5min) and re-suspended in media without FBS (Fetal Bovine Serum). The number of live cells was determined using a Cellometer K2 (Nexcelom Bioscience). 1 day before the experiments, cells were plated at a density of 1.5 million cells per well in a 6-well plate in MH-S complete media without FBS. All exposures and/or treatments were then conducted in MH-S complete media without FBS. Cells were treated with 200 μ M spermidine (Sigma-Aldrich, #cat: S0266) in

pretreatment (1h pre-exposure) and rescue (1h post-exposure) models. As described in each figure legend, the cells also had administration of Ultrapure LPS (25ng/mL) (Invitrogen, #cat:tlrl-3pelps), NMDA (100/300/600uM) (Tocris, #cat:0114), and D-AP5 (500uM) (Tocris, #cat:0106). The individual MH-S cell experiments had different exposure times and treatment/exposure lengths which are described in figure legends and results. UltraPure LPS was utilized as it removes contaminants that can be found in non-pure LPS, which can include other lipoproteins which would then lead to non-specific inflammatory activation [150]. Following exposure and/or treatment, the MH-S cells were then collected to measure inflammation/resolution markers including multiplex ELISA for cytokines/chemokines (#cat: PPX-08-MX47XMC), western blots, and real time-PCR.

3.2.2 Experimental Animals

C57Bl/6J male mice were purchased from Jackson Laboratories. All mice were 8-10 weeks old at the time of exposure. Animal breeding and study procedures were performed under an approved institutional animal care and use committee (IACUC) protocol at Duke University (A053-21-03). All animal experiments were conducted in accordance with the American Association for the Accreditation of Laboratory Animal Care guidelines.

3.2.3 Rodent Exposures

Mice were exposed to filtered air (FA) and ozone (O₃) as described in section 2.2.2. For *in vivo* spermidine experiments, spermidine (Sigma-Aldrich, #cat: S0266) was administered via intraperitoneal injections, 25mg/kg, 50mg/kg, or 100mg/kg 1h before FA or O₃ exposure. Control mice were given DI water intraperitoneal injections in the same manner.

3.2.4 Mouse bronchoalveolar lavage and measures of inflammation and injury

Bronchoalveolar lavage (BAL) was performed as described in section 2.2.3.

3.2.5 Metabolite Analysis

Metabolite analysis was performed as outlined in prior publications [151]. In brief, stock mixture of internal standards (GABA-d₆, MTA-d₃, N8-acetylspermidine-d₃, diacetylspermine-d₆, and N1-acetylspermine-d₃) was prepared with varied concentrations. A ten-point calibration curve, spanning 0.025-25 μM, was created for each analyte in a solvent mixture of 1:5:1 water:MeOH:CHCl₃, with approximately 1 μM internal standard. Serum reference material (Goldenwest biologicals) was processed by precipitating with a 5x dilution in MeOH:CHCl₃ to achieve a similar final composition. A 400uL aliquot of bronchoalveolar lavage fluid (BALF) each sample were lyophilized and reconstituted in 60uL of 1:5:1 water:MeOH:CHCl₃ to concentrate the sample to about a 6.6x dilution. Samples were then centrifuged at 10000rpm at 4°C for 5 min,

allowing for 50uL to be transferred to a 96 well plate, and 10uL to be used as an internal standard for each sample. The plate was shaken at 800 rpm for 20min prior to analysis. Utilizing a custom LC-MS/MS method for arginine pathway metabolites, previously published by the Duke Metabolomic and Proteomic Core Facility [151], the following compounds in the L-arginine pathway were measured: L-arginine, L-citrulline, agmatine, L-ornithine, 5'-deoxy-5'-methylthioadenosine (MTA), methionine, S-(5'-Adenosyl)-L-methionine chloride (SAM), S-adenosylhomocysteine (SAH), γ -aminobutyric acid (GABA), spermidine, and spermine. 1uL of the sample was analyzed on an Acquity UPLC interfaced to a Xevo TQ-S mass spectrometer (Waters Corporation). Tune parameters were set to spray voltage 3.0 kV, desolvation gas 1000 L/hr, cone voltage 20 V, desolvation temperature 400°C and cone gas flow 150 L/hr. The mass spectrometer was set in multiple reaction monitoring mode, monitoring for each analyte. The data was then imported to skyline for calibration and concentration calculations. The prepared serial dilution curve was used to make a linear regression with 1/x weighting for analytes, using ratios based on the internal standard measures. Then, principal component analysis and outlier detection was conducted to evaluate and account for variability. Once this data was processed, samples were then plotted and analyzed utilizing GraphPad PRISM.

3.2.6 Western Blot

Cells were collected and processed for intracellular protein measurements via western blot. The supernatant was discarded and cell plates were rinsed 2 times with PBS, then immediately scraped with 300uL of a collection buffer (1mL RIPA (Sigma-Aldrich, #cat:R0278), 10uL HALT Protease and Phosphatase Inhibitor Cocktail (Thermo Scientific, #cat:1861281), 10uL EDTA (Thermo Scientific, #cat:1861274)). To lyse cells, samples were placed on a rocker at 4C for 45min, then sonicated for 20sec, and centrifuged (1,500rpm X 10min). Following this, protein was quantified utilizing a Pierce 660nm Protein Assay Reagent kit (Thermo Scientific, #cat:22660) per the manufacturer's protocol. Samples were then prepared for western blotting per instructions accompanying the gel (10% bis-tris gels, Invitrogen). In brief, the samples were prepared with Bolt LDS Sample Buffer (4x) (Novex, #cat: B0007), NuPage Reducing Agent (10x) (Invitrogen, #cat:NP0009), and DI water and then boiled for 5min at 85C and cooled immediately afterward on ice for 15min. The samples and the Spectra Multicolor Broad Range Protein Ladder (Thermo Scientific, #cat:26634) were loaded into 10% bis-tris gels (Invitrogen, NW00100BOX) with MES SDS Running Buffer (Invitrogen, #cat:B0002) and 1mL per gel basin of NuPage Antioxidant (Invitrogen, #cat: NP0005). The gels were run at 130V for 75min on the Invitrogen Bolt System. Immediately following this, the gels were prepared for transfer utilizing PVDF Membrane Filter Paper Sandwich (Invitrogen,

#cat:LC2002) and Transfer Buffer (Invitrogen, #cat:B00061) and underwent a transfer for 70min at 30V. Following this, the membranes with the bands were cut and prepared for staining. Using TBS (Bio-Rad, #cat: 1706435), and TBST, TBS with Tween 20 (Bio-Rad, #cat: 170-6531), we stained for pNF κ Bp65 (Primary: Cell Signaling, #cat: 3033S, Secondary: Cell Signaling, #cat:7074S) and β actin (Primary: Milipore, #cat:A5441 Secondary: Cell Signaling, #cat: 7076S). This was done using, BSA (Sigma-Aldrich, #cat:A7906), Re-Blot Plus Mild Solution (Milipore, #cat:2502), Nonfat dry milk (Blotting-Grade Blocker, Bio-Rad, #cat: 1706404), ECL Prime Western Blotting Detection Reagents (Cytiva, #cat:17757269), and a fluorescent gel imager (Bio-Rad).

3.2.7 Real-Time PCR

Total RNA was collected utilizing RNeasy Plus Mini Kit (Qiagen) per the manufacturer's protocol. Following extraction, RNA samples were reverse transcribed into cDNA using Maxima H Minus cDNA Synthesis Master Mix (thermos scientific). PCR amplification was completed using the following program: 20uL reaction volume; 50°C, 2min; 95°C, 2min; 40 cycles, 95°C 1 sec, 60°C 30 sec. All real time quantitative PCR reactions were completed using the Quant Studio 6 Flex (Applied Biosystems). The reactions utilized SyBR Green reagent (Applied Biosystems), sterile UltraPure Distilled water (Invitrogen), and primers, as listed in Table 4. Gene expression values were

normalized to 18S as a housekeeper and presented as a fold change normalized again to media control.

3.2.8 Statistics

Statistical testing is as noted in the figure legends. In most settings, an ANOVA with post-hoc multiple comparisons analysis was conducted in PRISM 9 (GraphPad, Boston, MA) using Tukey's Honestly Significant Difference Test to reveal individual comparisons within groups on both cell types and cytokines. A p-value of less than 0.05 was considered statistically significant. Data in figures are presented as individual data points \pm standard error of the mean.

3.3 Results

3.3.1 Spermidine is increased in the bronchoalveolar lavage fluid following acute O₃ exposure

We first defined the concentration of L-arginine and its metabolites within BALF of C57Bl/6J mice exposed to acute O₃. C57Bl/6J mice were exposed to FA or O₃ (2ppm) for 3h and harvested at 12, 24, and 72h post-exposure. We performed BAL at timepoints critical to inflammation and resolution; 12h being associated with peak airspace neutrophilia, 24h associated with reduced neutrophilia and peak AMØs, and 72h being associated with resolution of acute inflammation [152–154]. The BALF from these mice was collected and analysis of L-arginine and its metabolites were assessed by the Duke Metabolomic and Proteomic Core Facility. The samples were then analyzed utilizing a

previously published [151] specialized mass spectroscopy panel developed for the assessment of L-arginine metabolites. L-arginine was reduced at 12h and then returned to baseline at 24h and 72h (Figure 14). While there was no significant difference in the concentrations of agmatine, ornithine, and citrulline, there was an interesting biologic trend of increased citrulline at 72h post exposure. Due to the recycling that occurs in this pathway, the later increase of L-citrulline could indicate potential recycling then back into L-arginine [82]. It was seen in some downstream parts of the pathway, methionine, SAM, and MTA, that there was an increase in concentration at 24h. Similarly, it was seen in the concentrations of SAH and GABA, while not significantly different, there was a trend toward an increase at 24h. The polyamines spermine and spermidine were not different at 12h, but then increased at 24h and returned to baseline at 72h post-exposure.

3.3.2 Spermidine administration reduces O₃-induced lung injury *in vivo*

As we observed an early reduction in L-arginine during peak O₃-induced inflammation and then an increase in spermidine during the time point associated with resolution of O₃-induced lung inflammation, this led us to perform experiments to determine if spermidine regulates O₃-induced lung inflammation. To assess the effect of spermidine treatment *in vivo* following acute O₃ exposure, C57BL/6J mice were pretreated with spermidine at doses of 25mg/kg, 50mg/kg, or 100mg/kg via intraperitoneal injection 1hr prior to exposure to FA or O₃ (2 ppm for 3h). Based on

literature within the field, we decided on our range of doses between 25-100mg/kg [155,156]. The O₃ exposure dose is based on the lab's prior publications and known deposition fractions between mice and humans [157]. Given the increase of spermidine, *in vivo* following O₃ exposure (Figure 14) at 24h post-exposure, we hypothesized that spermidine plays a role in resolution or decreased activation of inflammation. Using the 24h point, which is a standard time point to assess O₃-induced lung inflammation and was the timepoint our prior studies identified as critical for inflammation resolution, we then wanted to assess other inflammatory immune responses. Markers of airspace inflammation and injury including infiltrating inflammatory cells and BALF total protein/albumin were assessed. The mice exposed to FA, regardless of spermidine dosing, exhibited no significant recruitment of inflammatory cells (total cells, AMØs, and neutrophils) (Figure15). Following O₃ exposure, the mice pretreated with control DI water demonstrated increased O₃-induced inflammation defined by an increase in total cells and AMØs (Figure15). Mice treated with 25mg/kg and 50 mg/kg of spermidine had reduced recruitment of total inflammatory cells, specifically macrophages; however, when compared to FA there was an increase in neutrophils at the 50mg/kg dose. The cohort of mice treated with 100mg/kg of spermidine had a distinct reduction in the total cell, macrophage, and neutrophil counts where differences between the FA and O₃ exposed groups are negligible (Figure 15).

In addition to airspace inflammation, we assessed BALF total protein and albumin. Total protein was measured for all doses while albumin was only measured on samples collected from control mice and those pretreated with 50mg/kg of spermidine. All mice exposed to FA had a relatively low level of BALF total protein. Following O₃ exposure, the mice with the 25 mg/kg and 50mg/kg spermidine treatment, when compared to DI water control, had no significant change in total protein concentrations. Notable, a significant decrease in total protein present in the airspace was seen when comparing mice exposed to FA or O₃ pretreated with 100mg/kg of spermidine (Figure 16A). Then assessing albumin concentration via the mouse albumin ELISA, we utilized the cohorts of mice treated with the DI water control and 50 mg/kg spermidine, exposed to FA or O₃. In both cohorts, the mice exposed to FA had a relatively low level of albumin within the airspace; however, following acute O₃ exposure, the mice pretreated with 50 mg/kg spermidine had a reduced albumin concentration (Figure 16B). Overall, this data supports that spermidine pre-treatment reduces O₃-induced lung inflammation.

3.3.3 Spermidine pretreatment decreases LPS-induced NF-κB activation

Given the increased airspace concentration of spermidine as well as the reduced inflammatory response *in vivo*, we wanted to define mechanisms by which spermidine could be impacting AMØs function to promote resolution of inflammation. We utilized

MH-S cells exposed to LPS, since it causes the production of pro-inflammatory cytokines via activation of canonical NF- κ B signaling. To assess the impact of spermidine on LPS responses in MH-S cells, we administered 200 μ M spermidine for an hour prior to exposure to 25ng/mL LPS. We defined this as a pre-treatment model (Figure 17A). To define NF- κ B activation following LPS, we measured phosphorylated-NF κ Bp65 (pNF κ Bp65) staining by western blot. pNF κ Bp65 is present when the NF- κ B-heterodimer is activated, as it has been liberated from its natural inhibitor, I κ B α . The "freeing" of the heterodimer, signals its movement into the nucleus to initiate the NF- κ B inflammatory cascade [71,72]. Following the exposure, the cells were then collected and processed for western blotting. The LPS control had more pNF κ Bp65 present in comparison to what we measured in the media and spermidine control, which had no added inflammatory stimulus. The blots and its semi-quantitative densitometry analysis demonstrated that there was a decrease in pNF κ Bp65 at 5 and 15min following "LPS + Spermidine" exposure (Figure 17B and 17C). The reduction in pNF κ Bp65 in the LPS exposed MH-S cells treated with spermidine, supports that spermidine administration causes a reduction in LPS-mediated NF- κ B activation.

3.3.4 Spermidine rescue treatment decreases NF- κ B associated cytokine expression and concentration

To understand how the expression and release of these cytokines' changes following spermidine treatment, we changed the treatment model. In the rescue model

25ng/mL of LPS was given for 1hr and then a treatment plus exposure of 200uM of spermidine and 25ng/mL LPS or 25ng/mL LPS was given, respectively (Figure 18A). These samples were collected and processed to run both real-time PCR and multiplex ELISAs. We initially evaluated mRNA expression after administering rescue spermidine treatment. The data is a 3-hour time course, with samples collected at one-hour intervals. The data collected was then analyzed so that it was normalized to the house-keeper gene 18s. Then the cohorts were normalized to the media control, as that is considered the negative control. In comparison to media control, which had low expression, an increase of MIP2, TNF α , and IL-6 expression was observed in samples exposed to 1-3h of 25ng/mL of LPS. Notably, the samples administered the rescue spermidine treatment for 2h or 3h trended toward decreased mRNA expression (Figure 18B).

In addition to the mRNA expression showing decreases following the spermidine rescue, similar trends were seen in the concentration of cytokines from the culture supernatant, assessed by a multiplex ELISA. In our assessment of cytokines, we focused on pro-inflammatory macrophage-derived cytokines and chemokines including Granulocyte colony-stimulating factor (G-CSF), Leukemia inhibitory factor (LIF), IP-10 (also known as CXCL10), interleukin (IL)-6, GRO α (also known as CXCL1), Monocyte chemoattractant protein-1 (MCP-1 or CCL2), Macrophage inflammatory protein 2-alpha (MIP-2 α), and Macrophage inflammatory protein-2 beta (MIP-2 β). At 1h IP-10, IL-6,

MCP-1, MIP-2 α , and MIP-2 β trended lower than the media control while G-CSF, GRO α , and LIF concentrations were similar. In the samples exposed to LPS for 2h, when compared to media controls, IL-6, GRO α , MCP-1, and MIP-2 β trended toward increased concentration; while G-CSF, LIF, IP-10, and MIP-2 α had a similar concentration to the control. In contrast, samples administered a spermidine rescue treatment had a significantly lower concentration in G-CSF, IP-10, GRO α , MCP-1, MIP-2 α , and MIP-2 β with a trending decreased concentration in IL-6 when compared to 25ng/mL of LPS for 2h (Figure 19). Additionally, we assessed later cytokine responses at 3h of 25ng/mL of LPS exposure and 3h rescue spermidine treatment. A similar trend was seen where a statistically lower concentration of IP-10, IL-6, GRO α , MCP-1, MIP-2 α , and MIP-2 β was observed in the spermidine rescue treatment groups (Figure 20). Overall, this cytokine data was consistent with our observation of reduced NF- κ B activation. Furthermore, this data set demonstrated that spermidine rescue treatment appeared to have similar inflammation resolving effects to spermidine pre-treatment.

3.3.5 NMDA receptor agonist activates NF- κ B

Given this data demonstrating the link between spermidine and NF- κ B as well as the known interaction of spermidine binding to the allosteric binding site of the NMDA receptor, we wanted to define if activation of the NMDA receptor could activate NF- κ B signaling. To assess this (Figure 21A), we administered to MH-S cells an NMDA agonist

at 3 doses, 100, 300, and 600uM and collected cells at 5 or 15min following exposure (Figure 20B). NMDA doses were determined based on use in prior publications [77,158]. These samples were collected and processed for western blotting where we blotted for pNF κ Bp65, as a marker for NF- κ B activation. In the media control samples, we observed less pNF κ Bp65 protein expression on the blot. At both 5 and 15 min there was an increase in pNF κ Bp65 present in the samples exposed to NMDA at all doses, indicating increased NF- κ B activation (Figure 21C). This demonstrates that NMDA agonism causes NF- κ B activation in MH-S cells.

We then worked to test the efficacy in inhibiting NF- κ B activation by the NMDA receptor antagonist, D-AP5, as well as assess the response following a spermidine treatment with an NMDA exposure. The dose of D-AP5 was determined based on findings in prior studies [77]. The antagonist D-AP5 was administered as a pretreatment 1h prior to exposure of 25ng/mL of LPS and the cells were harvested at 5 or 15min post-LPS (Figure 22A). To test the direct effects of spermidine on NMDA activation of NF- κ B, we administered a 1h pretreatment of spermidine, followed by exposure to the NMDA receptor agonist, NMDA (Figure 22D). Though we observed potential impacts on NF- κ B activation, we were unable to produce reliable western blots from either of these experiments due to technical limitations. In particular, there was an issue of incomplete β actin staining, making us uncertain of our loading controls. Despite several attempts to

adjust the blotting techniques, antibody concentrations, and transfer methods this data is not conclusive (Figures 22 B, C, E, F, and G); rather theories and future work will be addressed in the discussion.

3.4 Discussion

AMØs have roles both in the initiation and support of inflammation but also in the resolution of inflammation. Though their roles in inflammation have been well-characterized, the specific mechanisms that drive AMØs to support resolution of inflammation have been less well defined. Therefore, this study focused on defining intracellular mechanisms within AMØs that drive signaling promoting the resolution of inflammation. We focused on the potential of spermidine to promote resolution of inflammation and a mechanism for this effect via NMDA receptor signaling. We first defined the concentration of L-arginine and its metabolites after acute O₃ exposure. In O₃-exposed mice, we observed a decrease in L-arginine concentration at 12h and an increase of polyamines, such as spermidine, at 24h. Having confirmed that acute O₃ exposure impacts the concentration of L-arginine and its metabolites, we then assessed the *in vivo* function of spermidine in resolution of O₃-induced lung inflammation. In mice exposed to O₃ and treated with spermidine, there was a reduction in inflammatory cell recruitment and decreased total protein found within the BAL fluid. Following this, we aimed to understand a potential mechanism by which spermidine promotes

resolution. To define this, we performed *in vitro* studies with LPS in MH-S cells. We observed that spermidine administration post-LPS exposure reduced NF- κ B activation, cytokine expression, and cytokine release. We then confirmed that NMDA agonism activates NF- κ B similarly to LPS, suggesting the potential of spermidine to negatively regulate NF- κ B activation through NMDA inhibition. Overall, the data support that there is a potential mechanism in which spermidine promotes resolution of O₃-induced lung inflammation via spermidine-mediated inhibition of NMDA receptor activation and downstream NF- κ B activation.

While the arginine pathway has been recently probed more due to its potential therapeutic role in varied diseases [90,140–143], it has been largely understudied in the context of understanding the specific mechanisms by which it mediates resolution. L-arginine can be metabolized by NOS2, leading to pro-inflammation intermediates, or by arginase-1, which has been understood to promote inflammation resolution [85,89,159,160]. Following O₃ exposure, prior research observed an increase in NOS and citrulline in mouse models [161,162]. Furthermore, Sunil et. al. observed in O₃-exposed rats an increase in epithelial expression of inducible NOS2 and arginase 1 [163]. Consistent with our data, this demonstrated that arginase-1 expression is impacted by O₃ exposure (Figure 14). However, expression of the enzymes NOS2 or Arg-1 does not define function; rather, their effects are defined by their metabolites. Prior to our

research, the dynamics of L-arginine and its metabolites following O₃ exposure had not been defined. This understanding is crucial for comprehending the impact of increased NOS2 and Arg-1 expression. To define the impact of O₃ exposure on L-arginine metabolism via arginase-1, we performed LC/MS analysis of L-arginine metabolites in BALF. Using this assay, we defined an initial decrease in L-arginine concentration at 12h post-exposure. This suggests that L-arginine is being metabolized, presumably to generate metabolites, though specific labeling and tracking of L-arginine metabolism was not directly studied in our experiments. Interestingly, L-arginine levels returned to baseline by 24h. This suggests that there is a compensatory increase in L-arginine. The source of this increased L-arginine is not clear but could come from intracellular recycling from citrulline or from endogenous sources [160,164,165]. The source and dynamics of L-arginine flux following O₃ exposure remains to be defined. At 24h post-exposure, there was an observed increase in the polyamines, spermine and spermidine, as well as SAM, MTA, and methionine, which are critical for intermediates in polyamine production [166]. This elevation in polyamines and their intermediates then decreased by 72h post exposure. Interestingly, at this time point there was a biologic, though not statistically significant, increase in citrulline. The significance of this observation is not clear but could support a potential source of L-arginine recycling as has been observed in other studies [160,164,165]. The finding of an increase in arginase-1 derived L-arginine

metabolites suggested it may have a role in O₃-induced immune signaling. Given that the 24h time point is typically one that associates with resolution from O₃-induced lung injury, this made us consider if spermidine promoted resolution of O₃-induced lung injury.

While prior research supports spermidine involvement in pro-resolution functions and NF-κB activation [90,91], to the author's knowledge, this is the first study addressing its potential role in the resolution of acute O₃-induced lung inflammation. To define direct effects of spermidine on O₃-induced lung injury, we performed a dose-response study with spermidine administration prior to *in vivo* FA or O₃ exposure. Overall, we observed a decrease in O₃-induced inflammation and injury responses as demonstrated by reduced airspace inflammation (Figure 15) and decreased BALF total protein and albumin (Figure 16). Furthermore, while at 25mg/kg and 50 mg/kg we observed some reductions in inflammation, at 100 mg/kg the effect was much more prominent, suggesting a therapeutic threshold. We observed that O₃ exposed mice with the 100 mg/kg spermidine dose had reduced BALF inflammatory cells and total protein to the point that there was no difference between FA and O₃ exposure (Figure 15 and 16). This data suggests spermidine has a role in decreasing O₃-induced injury. This data is consistent with other research defining spermidine as a pro-resolution mediator for inflammation and inflammatory diseases [142,144]. Consistent with lung effects,

Wawrzyniak et al. found in a house dust mite allergic airway model. They observed that mice orally treated with spermidine (15 mg/kg) had a reduced allergic airway inflammation [145]. Overall, this suggests spermidine and L-arginine metabolism via arginase-1 may be a promising therapeutic target to reduce and/or resolve lung inflammation.

Given the observation of increased spermidine-mediated resolution of O₃ induced lung inflammation, we were interested to confirm the potential mechanism of this response. We focused on spermidine's effects on NF-κB. NF-κB is a central regulator of inflammation and its activation in AMØ is associated with production of pro-inflammatory cytokines [36,71,72]. In addition, NF-κB activation is noted following O₃ exposure and inhibition of NF-κB has been associated with reduced O₃-induced lung inflammation [69,152]. To assess for impacts of spermidine on NF-κB activation, we utilized LPS as a canonical NF-κB activator and translated our *in vivo* findings into defining the mechanism via *in vitro* studies. Consistent with prior studies [145,167,168], we observed that spermidine reduced LPS-mediated NF-κB associated cytokines and chemokines, expression and concentration (Figure 18-20). In addition, we identified that spermidine decreased the activation of NF-κB activation surrogate, pNFκBp65 (Figure 17).

Though we were not able to fully tie spermidine regulation of NMDA-mediated NF- κ B activation together in this study set (Figure 22), we were able to identify an agonist of the NMDA receptor, NMDA, as an activator of NF- κ B in MH-S cells (Figure 21). Furthermore, while there are clear technical issues with the blot developed to demonstrate spermidine reducing NF- κ B activation via NMDA, there is a trend showing that the pretreatment of spermidine had less pNF κ Bp65 (Figure 22). There are several limitations and potential areas to improve the experimental design for future work. One such consideration is the concentration of LPS. In our study we utilized 25ng/mL since we identified it as the lowest dose to provide a robust cytokine response (data not shown). However, in other studies defining NF- κ B activation via translocation of p65 on western blots, doses of 100ng/mL-500ng/mL were used [90,169]. While we were concerned with identifying a low dose initially to not quench or mute a spermidine response, potentially having less protein in general due to the more mild response, made differences between groups harder to identify and quantify. Additionally, while it was of interest to utilize D-AP5 as an antagonist to the NMDA receptor, in future work if a robust difference is not seen another established inhibitor of the NMDA receptor can be used. This is inclusive of MK-801 (dizocilpine) or memantine, both of which bind selectively to the active form of the receptor and have commercially been used as pharmaceuticals for Alzheimer's Disease [80,170,171]. Finally, we acknowledge that in

spite of several iterative troubleshooting steps, there is a potential for there to be a technical issue with the laboratory protein transfer set up and protocol. A future step in addressing this was determined to utilize a collaborator's set up and protocol to address internal individual errors.

Though we were able to define a direct effect of spermidine on O₃-induced lung injury in mouse models, we acknowledge limitations in the method of exposure for the spermidine *in vivo*. Due to it being given via intraperitoneal injection, it is not directly impacting the lung space. This method of exposure can then lead to questions regarding how much of the dose is specifically impacting the lung and its cellular responses versus a non-specific/whole-body, inflammation and injury response. This question could in part be answered by collecting BALF samples from these mice, similar to what was seen in Figure 14, to address the concentration of spermidine that is then found in the airspace and presumably active. Furthermore, while intraperitoneal studies have been done using spermidine [155], for the purpose of more specific responses within the lung, future experiments can transition to utilizing oropharyngeal aspiration. Additionally, it is worth exploring and testing a 75mg/kg dose of spermidine for a pretreatment. While this data is preliminary, conducted on a limited number of mice, there was a mouse within the 100mg/kg dose group that died following spermidine treatment and O₃ exposure. However, that time point also gave the most distinct difference regarding

injury and inflammatory markers measured. Thus, it would be of interest to not only add to the number of mice per group, but also better define the therapeutic dose of spermidine and any potential off-target toxicity. In addition, there is still a missing link between this response and the NMDA receptor. It is of interest to determine whether the decreased *in vivo* injury response following acute O₃ exposure, respectively, is due to spermidine interacting with the NMDA receptor and then decreasing NF-κB activation. This can be defined by using available NMDA receptor agonists and antagonists, similar to what was done *in vitro* or by utilizing an NMDA knockout mouse to assess differences in the inflammation response in the absence of this receptor.

3.5 Conclusion

In summary, our study focused on an intracellular mechanism in AMØs with potential to resolve pro-inflammatory signaling via reduced NF-κB activation. We focused on arginase-1 derived metabolites of L-arginine based on the observation that there was a dynamic increase in spermidine at 24h post O₃ exposure, a time point associated with resolution of O₃-induced lung inflammation. We confirmed the potential role of spermidine in resolving O₃-induced lung inflammation by administration of spermidine to rodents undergoing *in vivo* O₃ exposure. To define mechanisms of spermidine's effects on AMØs, we focused on spermidine effects on NF-κB activation in MH-S cells. We observed that spermidine inhibited LPS-induced NF-κB activation,

cytokine expression, and release. Furthering this assessment, we determine that an NMDA agonist, similarly activated NF- κ B, and in preliminary studies there was a suggestion that spermidine could inhibit NMDA-mediated NF- κ B activation. Overall, this highlights the potential role of spermidine in resolving inflammation associated with air pollution exposure. Furthermore, it highlights a potential mechanistic relationship in AM \emptyset s where spermidine inhibits NMDA signaling to reduce NF- κ B activation and thereby promote a transition in AM \emptyset s from a pro-inflammatory phenotype to one that can promote the resolution of inflammatory stimuli. These studies could identify a potential therapeutic target that might promote the resolution of lung inflammation and/or limit the adverse lung inflammatory effects of air pollution exposure.

3.6 Acknowledgements

The authors acknowledge the contributions of the Duke Metabolomic and Proteomic Core Facility.

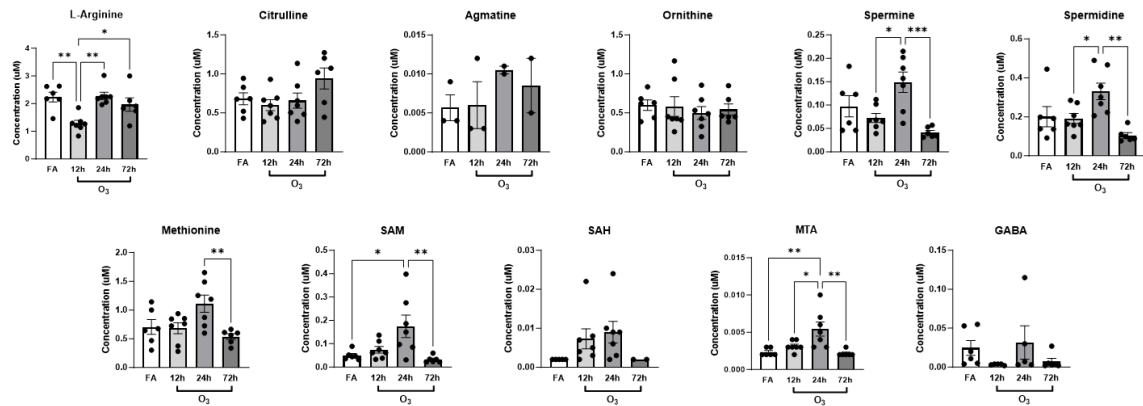


Figure 14. L-Arginine metabolites fluctuated following O₃ exposure.

Male C57BL/6J mice were exposed to FA or O₃ (2 ppm) for 3h. Mice were then harvested 12/24/72h following exposure and the samples were collected and processed for metabolite processing via the Duke Proteomics and Metabolomics Core Facility. Via LC-MS/MS l-arginine metabolites were quantified from BALF samples of the mice. Concentrations at the respective timepoints for l-arginine and its metabolites are represented in grey, darker indicating later timepoints. n=2-7 mice per group/exposure/timepoint *p<0.05. ANOVA analysis was conducted using Tukey's Honestly Significant Difference Test post-hoc.

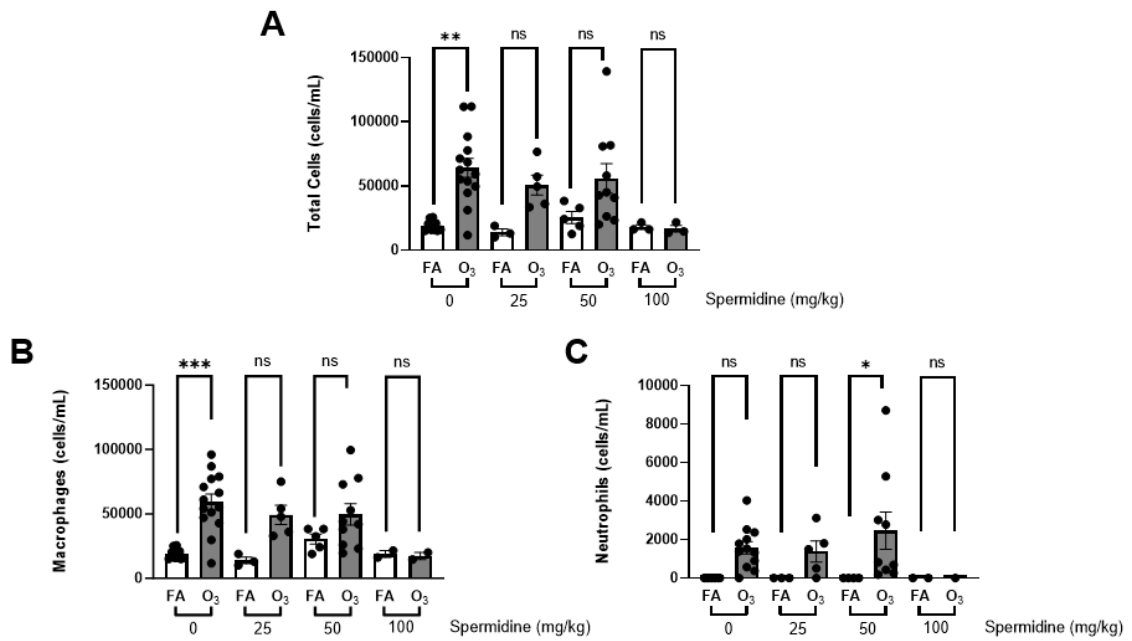


Figure 15. *In vivo* spermidine treatment trended toward decreased inflammatory cell recruitment.

Male mice were treated with spermidine (25/50/100mg/kg) or DI water (control) via intraperitoneal injections 1h before FA or O₃ (2 ppm) exposure. Mice were then harvested 24h following exposure and the samples were processed for cell differentials and other measures of inflammation. BAL total cells (A), macrophages (B), and neutrophils (C) were enumerated following pretreatment and exposure to FA or O₃ exposure. Bars shaded grey indicate O₃ exposure while white indicates FA exposure. n=3-14 mice per group/exposure/timepoint *p<0.05. ANOVA analysis was conducted using Tukey's Honestly Significant Difference Test post-hoc.

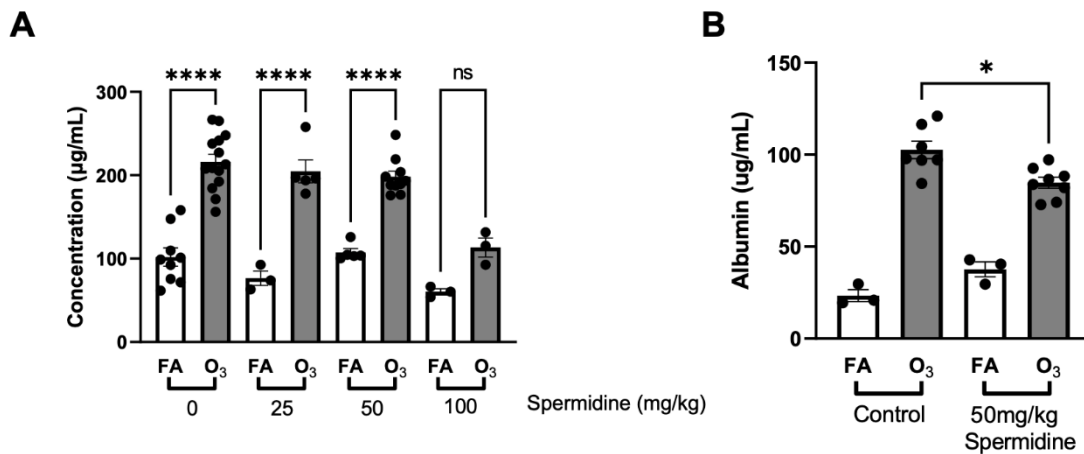


Figure 16. Spermidine treatment decreased total protein and albumin in the airspace following O₃ exposure.

A. Male mice were treated with spermidine (25/50/100mg/kg) or DI water (control) via intraperitoneal injections 1h before FA or O₃ (2 ppm) exposure. Mice were then harvested 24h following exposure. BAL fluid was processed for total protein measurements. **B.** A subset of samples was assessed utilizing a mouse albumin ELISA to measure more specifically the amount of albumin, a protein found in vasculature and an indicator of lung injury, is present in the airspace. Bars shaded grey indicate O₃ exposure while white indicates FA exposure. n=3-14 mice per group/exposure/timepoint *p<0.05. ANOVA analysis was conducted using Tukey's Honestly Significant Difference Test post-hoc.

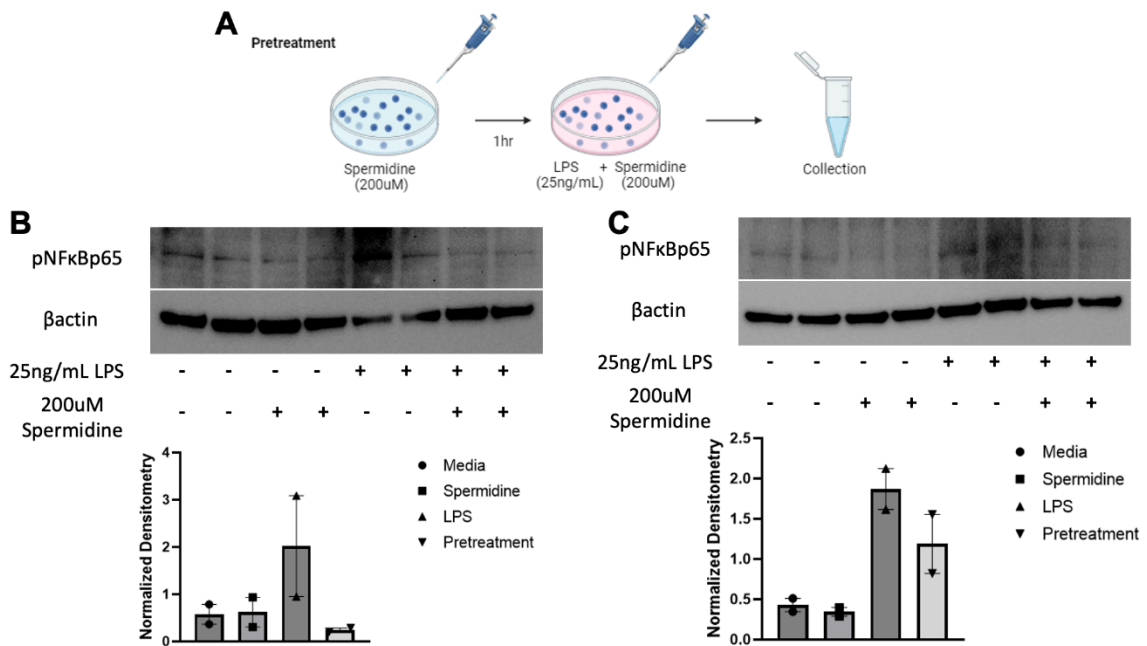


Figure 17. Pretreatment of spermidine decreased NF-κB activation.

A. MH-S cells were pretreated with 200uM spermidine 1hr before being exposed to 25ng/mL of LPS and 200uM spermidine. Following the exposure, cells were collected and processed for analysis and measures of NF-κB activation. Schematic made on BioRender.com. The cells were collected (**B.**) 5 min or (**C.**) 15 min after exposure to LPS+ spermidine and processed for western blotting. The membranes were probed for pNFκBp65, indicating activation of NF-κB, and βactin as a housekeeper. Densitometry was done and is seen underneath each corresponding western blot.

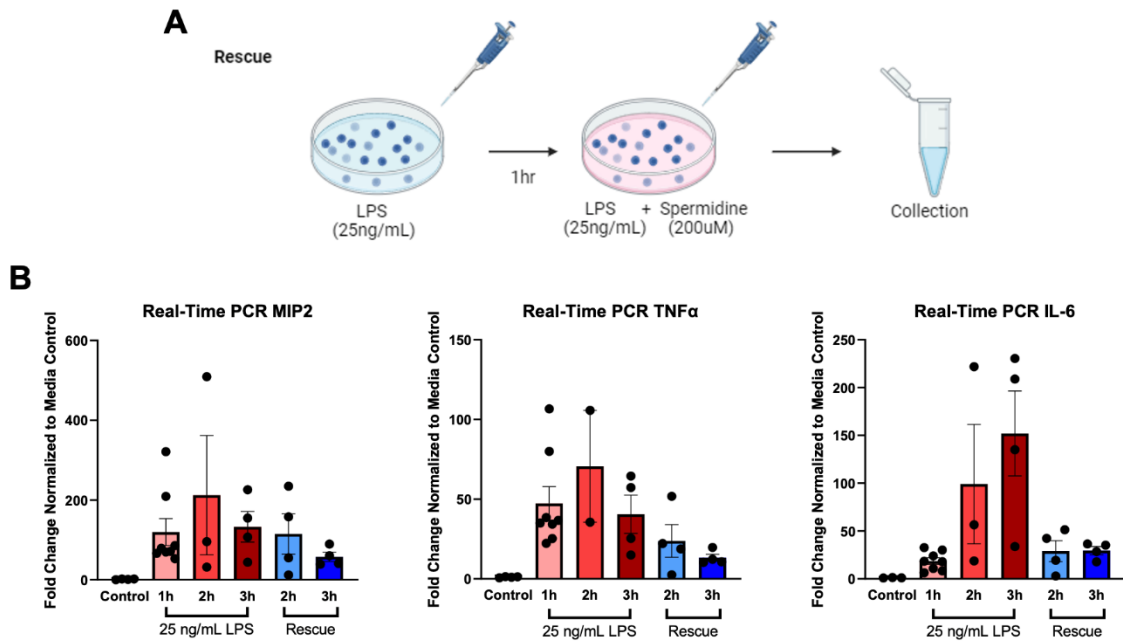


Figure 18. Rescue treatment of spermidine decreased expression of NF- κ B associated cytokines.

A. MH-S cells were exposed to 25ng/mL of LPS for 1hr and then treated with 200uM of spermidine in addition to the 25ng/mL of LPS. Following exposure, cells were collected and processed for analysis and measures of NF- κ B activation. Schematic made on BioRender.com. **B.** The cells were collected and processed for real time-PCR quantification of MIP2, TNF α , and IL-6. Bars shaded red indicate exposure to 25ng/mL of LPS, 1/2/3h, while blue indicates spermidine rescue treatment, 1h of 25ng/mL of LPS followed by a treatment of 200uM of spermidine plus an exposure of 25ng/mL of LPS for 1/2h. n=2-8 per exposure/timepoint *p<0.05. ANOVA analysis was conducted using Tukey's Honestly Significant Difference Test post-hoc.

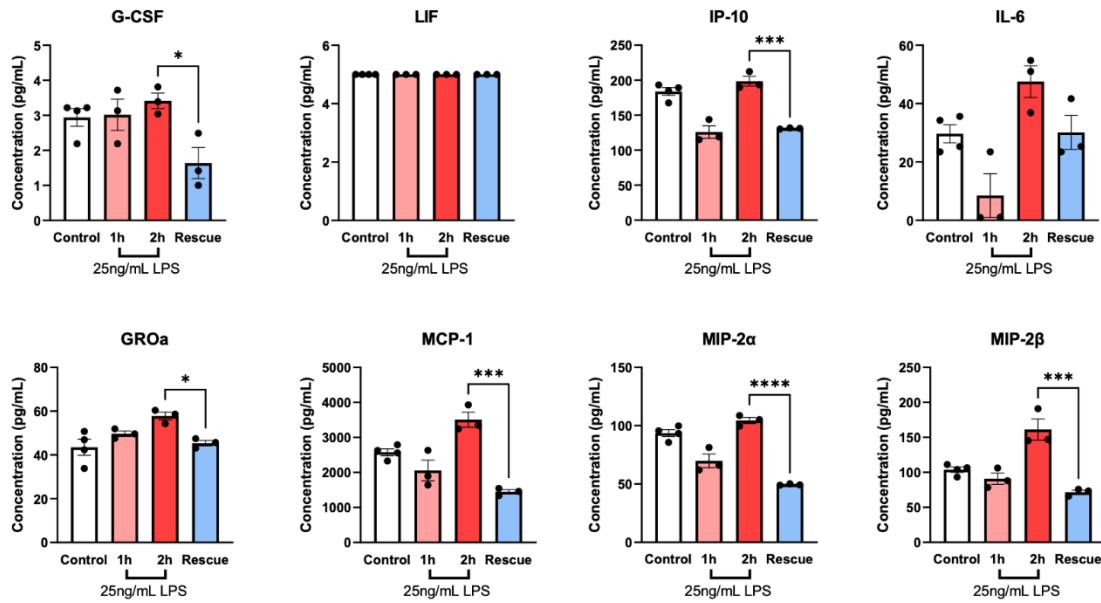


Figure 19. Decrease of inflammatory cytokines following a 2h spermidine rescue treatment.

Supernatant from MH-S cell culture was assessed for cytokine expression by multiplex ELISA for inflammatory cytokines and known neutrophilic chemotactic factors. Bars shaded red indicate exposure to 25ng/mL of LPS, 1h and 2h, while blue indicates spermidine rescue treatment, 1h of 25ng/mL of LPS followed by a treatment of 200uM of spermidine plus an exposure of 25ng/mL of LPS for 1h. n=3-4 per exposure/timepoint *p<0.05. ANOVA analysis was conducted using Tukey's Honestly Significant Difference Test post-hoc.

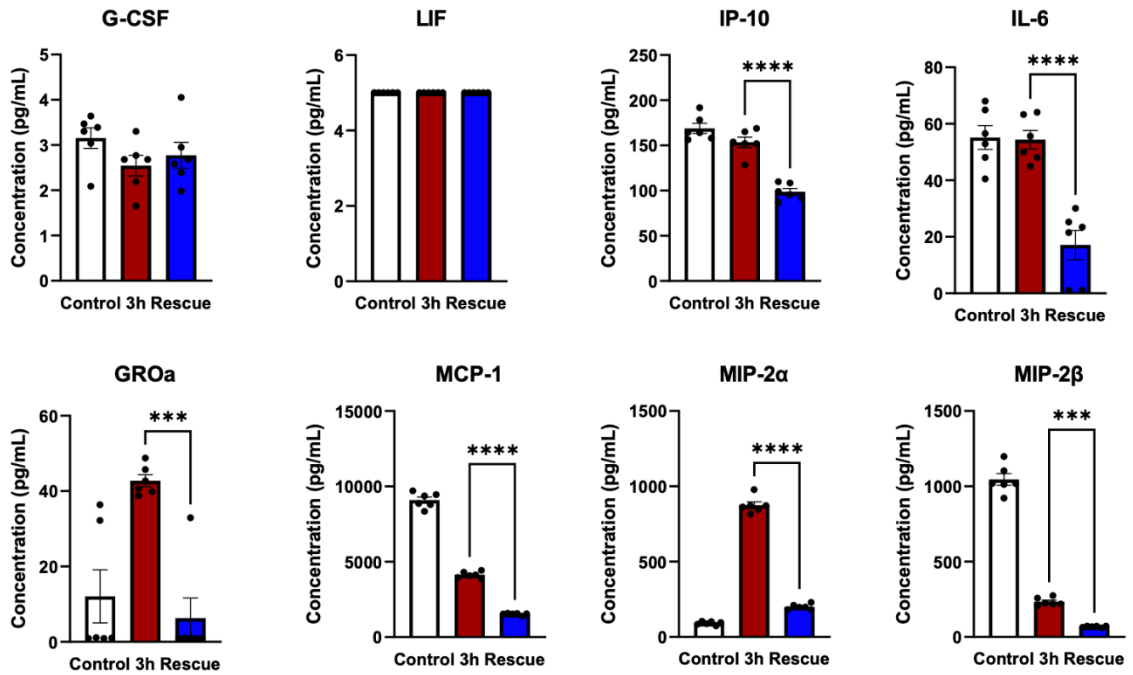


Figure 20. Decrease of inflammatory cytokines following a 3h spermidine rescue treatment.

Supernatant from MH-S cell culture was assessed for cytokine expression by multiplex ELISA for inflammatory cytokines and known neutrophilic chemotactic factors. Bars shaded red indicate 3h exposure to 25ng/mL of LPS while blue indicates spermidine rescue treatment, 1h of 25ng/mL of LPS followed by a treatment of 200uM of spermidine plus an exposure of 25ng/mL of LPS for 2h. n=6 per exposure/timepoint *p<0.05. ANOVA analysis was conducted using Tukey's Honestly Significant Difference Test post-hoc.

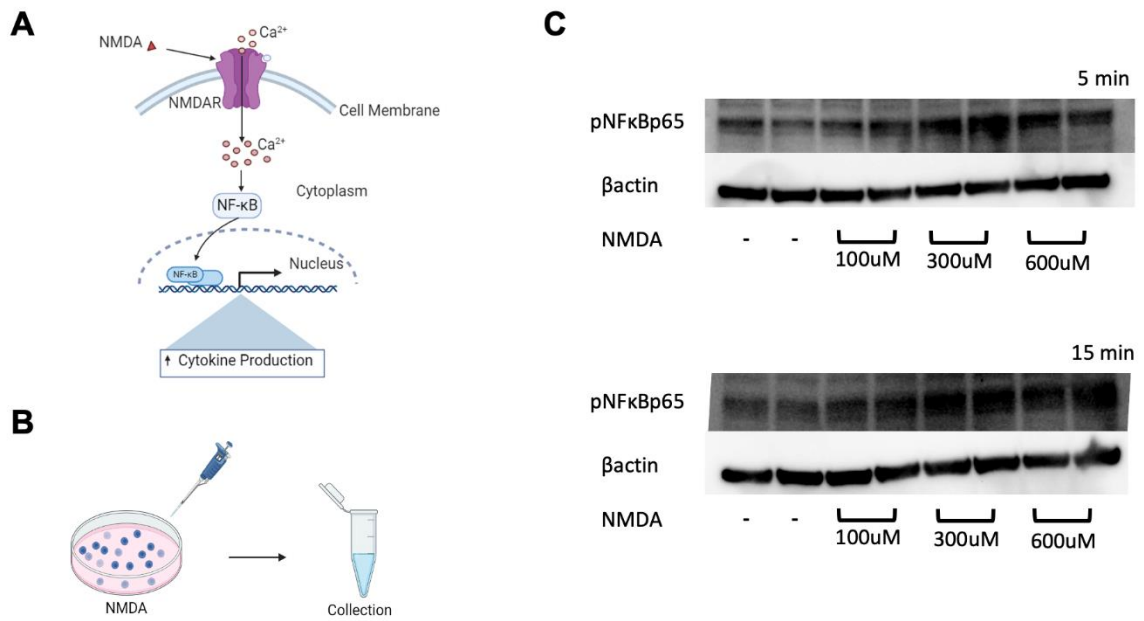


Figure 21. NMDA activates NF-κB.

A. Hypothesized pathway in which the NMDA receptor agonist, NMDA, will activate NF-κB, leading to increased inflammation responses such as cytokine responses. **B.** MH-S cells were exposed to NMDA at 100/300/600uM then collected for NF-κB activation measurements. Schematics were made on BioRender.com. Following exposure, cells were collected and processed for analysis and measures of NF-κB activation. Schematic made on BioRender.com. **C.** The cells were collected 5 min or 15 min after exposure to NMDA and processed for western blotting. The membranes were probed for pNFκBp65, indicating activation of NF-κB, and βactin as a housekeeper.

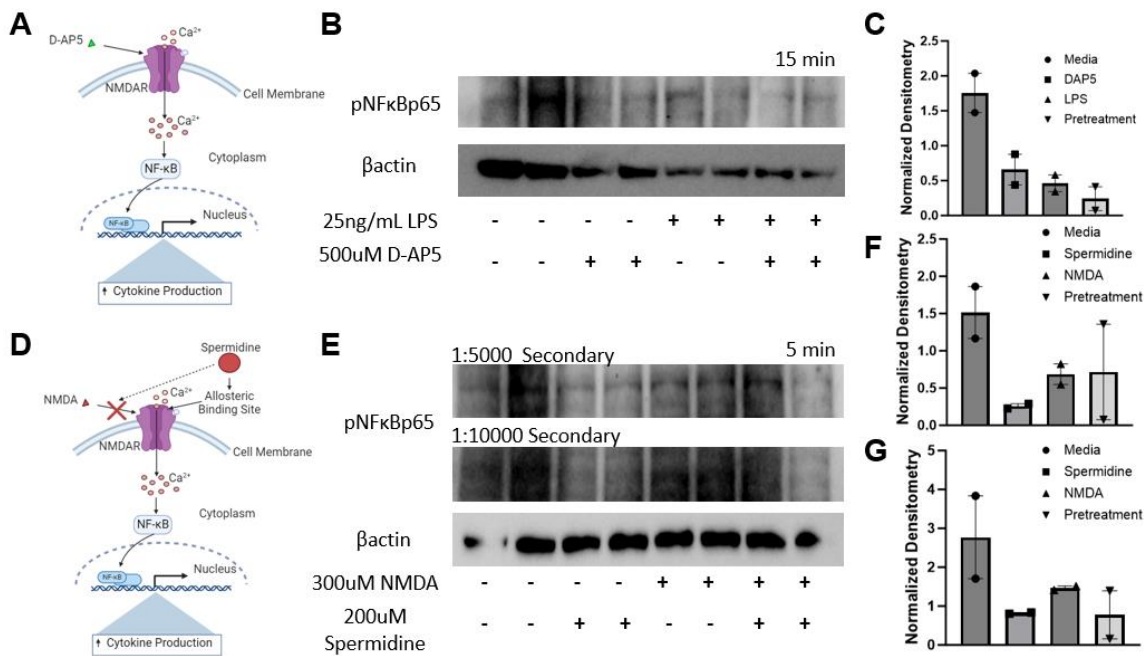


Figure 22. Technical limitations in showing D-AP5 decreases LPS-induced NF-κB activation and spermidine decreases NMDA-induced NF-κB activation.

A. Hypothesized pathway in which the NMDA receptor antagonist, D-AP5, will decrease NF-κB activation leading to decreased inflammation responses such as cytokines. MH-S cells were exposed to then collected for NF-κB activation measurements. Following the exposure, cells were collected and processed for analysis and measures of NF-κB activation.

B. The cells were pretreated with 500uM D-AP5 for 1hr then exposed to 25ng/mL LPS. They were then collected 15 min after exposure and processed for western blotting. The membranes were probed for pNFκBp65, indicating activation of NFκB, and βactin as a housekeeper.

C. Densitometry was also done utilizing ImageJ to create a quantitative assessment of the blots.

D. Hypothesized pathway in which the spermidine will decrease NMDA-mediated activation of NF-κB. MH-S cells were exposed to then collected for NF-κB activation measurements. Following the exposure, cells were collected and processed for analysis and measures of NF-κB activation.

E. The cells were pretreated with 200uM spermidine for 1hr then exposed to 300uM NMDA. They were then collected 5 min after exposure and processed for western blotting. The membranes were probed for pNFκBp65, indicating activation of NFκB, and βactin as a housekeeper. 2 blots are shown, with differing secondary concentrations denoted, due to technical issues making the band fainter than typically seen. Densitometry was also done utilizing ImageJ to create a quantitative assessment of

the blots, (F) 1:5000 and (G) 1:10000, both blots probing pNF κ Bp65 were measured and plotted. Schematics were made on BioRender.com.

Table 4. RT-PCR primer sequences used for proinflammatory cytokine expression.

Gene	Vendor	Forward Sequence	Reverse Sequence
MIP2	Sigma-Aldrich	5'- GGGTTGACTTCAAGAAC ATC-3'	5'- CCTTGCCTTTGTTTCAGTATC- 3'
IL6	Integrated DNA Technologies	5'- TTGGTCCTTAGCCACTCC TTC-3'	5'- TAGTCCTTCCTACCCCAATT TCC-3'
TNF α	Sigma-Aldrich	5'- CTATGTCTCAGCCTCTTC TC-3'	5'- CATTGGGAACTTCTCATCC -3'
18s	Integrated DNA Technologies	5'- TTGACGGAAGGGCACCA CCAG-3'	5'- GCACCACCACCCACGGAAT CG-3'

4. Conclusion

4.1 Summary

The goals of this dissertation research were to explore both cellular and intercellular pathways of inflammation resolution, with a particular focus on the role of alveolar macrophages (AMØs). It is well-established that air pollution, such as O₃, causes detrimental effects and poses a significant health risk, particularly in individuals who are most susceptible to air pollution's adverse effects [24,26,30]. While generally air pollutants induce inflammation that can be considered mild and resolving, in some individuals these injuries can lead to prolonged and exacerbated inflammation and lung disease [98]. Lung inflammation and resolution following injury is a highly regulated and active process which is mediated in part by AMØs [95,99]. While AMØ functions in injury have been extensively studied, understanding which AMØs, based on ontogeny, function following different injury sources and severities has not been well defined. Furthermore, understanding mechanisms which promote the functional transition of AMØs from pro-inflammation to pro-resolution phenotype has not been well studied. These gaps in knowledge have prompted our in-depth investigation into the mechanisms responsible for resolving environmental-induced lung inflammation. To address this, we performed separate but conceptually integrated studies that focused on

cellular mechanisms of AMØ function (chapter 2) and intracellular mechanisms in AMØ (chapter 3) both of which promote a resolution of O₃-induced lung inflammation.

In chapter 2, we worked to understand the AMØ cellular response using mouse models (including lineage-labeled, and genetic knockouts) and data from O₃-exposed human volunteers. We identified that the predominant AMØ subset responsible for resolution of inflammation following acute O₃ exposure are tissue-resident. Depletion of these tissue-resident AMØs led to prolonged neutrophil presence in the alveolar space after O₃ exposure, indicating impaired clearance of neutrophils and prolonged inflammation. This impaired clearance was associated with reduced efferocytosis, as the cells not cleared were apoptotic. We were then able to identify that this impairment was due to the reduction of the MerTK receptor, which is found on AMØs and crucial for resolving inflammation.

In chapter 3, we investigated a potential mediator of an intracellular mechanism of resolution within AMØs. While nitric oxide synthase-mediated L-arginine metabolism can promote inflammatory responses, arginase-1 generates metabolites, aiding inflammation resolution [82,84–86]. We found that spermidine, a known anti-inflammatory metabolite, was increased following acute O₃ exposure. Given the increased presence within the airspace of spermidine, we examined for its inhibitory effect on the NMDA receptor. Although previous studies suggest a link between NMDA

activation, NF- κ B activation, and spermidine's anti-inflammatory properties, direct connections have not been shown. By using MH-S cells, AM \emptyset -like cells, we were able to test this paradigm and connect these pathways and receptors. Pretreatment with spermidine decreased NF- κ B activation following LPS exposure, a canonical NF- κ B activator. Additionally, NMDA, an agonist for the NMDA receptor, activated NF- κ B, establishing a direct link between the pathways. Evaluation of the NMDA receptor antagonist, along with NMDA and spermidine co-treatment, elucidated the interplay between the NMDA receptor and NF- κ B activation, highlighting spermidine's ability to mitigate this response.

In summary, this research underscores the crucial role of tissue-resident AM \emptyset s in resolving O₃-induced inflammation and explores spermidine's potential as a therapeutic agent for environmental-induced lung inflammation.

4.2 Implications and Future Directions

Acute increases in ambient O₃ levels have been linked to increased illness, mortality, and greater severity of lung diseases [24,26]. Elevated ground-level O₃ concentrations contribute significantly to a rise in hospital admissions, posing significant health and economic challenges [14,27–29]. Prior research has found that an increase of 10ppb in daily O₃ exposure led to approximately 0.87% increase in total mortality [30]. Given the increase in both global average temperature and the frequency of severe

climate events, the need to further understand mechanisms of resolution is critical to the health and well-being of individuals. This study specifically explores the mechanisms that govern the resolution of environmentally-induced lung inflammation through AMØs.

One of the resolution pathways discussed in this thesis was MerTK mediated efferocytosis. As one of the principal functions of AMØs, efferocytosis is particularly important because ineffective clearance of apoptotic cells can lead to exacerbations of lung pathologies following injury and ultimately can cause and exacerbate chronic lung diseases [39,42,66]. Additionally, ineffective clearance of neutrophils can lead to diseases such as autoimmunity when neutrophil exposure is prolonged [39,172]. While healthy individuals are able to undergo “typical” inflammation and resolution responses, some are more sensitive to environmental exposures, and this could be driven by having differing macrophage sub-populations that are less effective in pro-resolving functions such as efferocytosis.

Consistent with this potential, when we were assessing profiles of healthy individuals aged 20-36, we observed significant inter-individual differences in immune cell compositions in the FA exposure samples. This highlights baseline variability in airspace immune cell composition between subjects (Figure 5A and 5D). Furthermore, we observed additional variability in FA to O₃ exposure responses (Figure 5D). This

suggests that there is not only intra-individual variability in baseline immune cell composition but also in the changes in immune cell composition following exposure. A limitation of the observation in these pilot studies is that these baseline effects or exposure responses were not linked to phenotypic exposure responses. Future studies should consider if this baseline composition predicts the exposure responses or if exposure immune cell profiles predict an individual's response to exposure. In future studies it would be interesting to address if individuals may have different base-line populations of AMØs, leading to different susceptibilities to O₃-induced lung injury.

In addition to studying differences seen between individuals and their response to injury, it is important to understand a susceptibility factor that impacts everyone, aging. Prior studies have shown that tissue-resident AMØs and their functionality decrease as individuals age; however, the full implication of what a reduced tissue-resident AMØ population means for health is not yet well understood [173,174]. In part, the reduction of inflammatory cells can result in a less vigorous immune response, leading to a persistence of disease [175]. In support of this, work conducted by DeMaeyer et al. described a failure of the immune system of elderly people to be an inability to effectively clear acute inflammation via efferocytosis [176]. This can potentially lead to systemic issues such as "inflammaging," where there is a low, yet chronic, inflammation found within the body [175,177]. In humans and mice,

polyamines, such as spermidine, can be found in circulation, and their levels have shown to decrease with age [178,179]. Thus, another potential avenue to study spermidine in regard to resolution is how it can supplement endogenous polyamines to increase the presence of anti-inflammatory signals, potentially reducing “inflammaging.” In future studies, defining portions of the resolution pathway, cellular and intracellular, that can be targeted for therapeutics is critical for the health and wellbeing of susceptible individuals.

Expanding on the importance of understanding how polyamines can support vulnerable individuals by promoting pro-resolution factors, the studies in this thesis shed light on a potential mechanism for this process. The next crucial step involves finalizing studies that directly establish the link between spermidine, decreased NMDA activation, and reduced NF- κ B activation. While previous research has identified polyamines, like spermidine, as anti-inflammatory factors [84,86,134], the absence of a targetable mechanism makes it difficult to effectively utilize it as a therapeutic. This challenge is exacerbated by the highly recycled nature of components in the L-arginine pathway and their variable half-lives, contingent upon their location (organ/circulation) [160,164,165,180,181]. Achieving effective targeting is therefore essential for the future use of polyamines as both a pro-resolution factor and therapeutic agent.

These studies suggest a need for a more in-depth examination of tissue resident cells in inflammation induced by air pollution. It is essential to consider not only the dynamics of these cells as they clear debris but also the specific signals enabling them to initiate and resolve inflammatory responses. Additionally, there is a necessity to enhance our understanding of how pollutants alter these normal responses, causing an inability to return to homeostasis.

More broadly, this thesis contributes to the understanding that inflammation resolution is an "active" process. While previous studies primarily concentrated on the initiation and propagation of inflammation, a broader examination of resolution now includes active processes. This expansion enables more comprehensive investigations into potential mechanisms and cellular pathways. As illustrated in this thesis, resolution operates on multiple levels, demanding specific features within cellular subsets and mechanistic pathways that actively downregulate signals promoting inflammation. Defining these will be critical to understanding how air pollution promotes inflammation, how it might perturb resolution of inflammation and ultimately enable improved identification of at-risk individuals for adverse health effects that can be addressed with targeted therapeutics.

References

1. Fuller R, Landrigan PJ, Balakrishnan K, Bathan G, Bose-O'Reilly S, Brauer M, et al. Pollution and health: a progress update. *Lancet Planet Heal* [Internet]. Elsevier B.V.; 2022 [cited 2023 May 30];6:e535–47. Available from: <http://www.thelancet.com/article/S2542519622000900/fulltext>
2. Environmental Protection Agency U. Clean Air Act Requirements and History | US EPA [Internet]. 2023 [cited 2024 Jan 7]. Available from: <https://www.epa.gov/clean-air-act-overview/clean-air-act-requirements-and-history>
3. Environmental Protection Agency U. AQI Basics | AirNow.gov [Internet]. 2023 [cited 2024 Jan 9]. Available from: <https://www.airnow.gov/aqi/aqi-basics/>
4. Environmental Protection Agency U. Air Quality Index - A Guide to Air Quality and Your Health. Brochure 2014. EPA-456/F-14-002. Air Qual. Index - A Guid. to Air Qual. Your Heal. Broch. 2014. EPA-456/F-14-002. 2014.
5. Liao H, Chen WT, Seinfeld JH. Role of climate change in global predictions of future tropospheric ozone and aerosols. *J Geophys Res Atmos* [Internet]. Blackwell Publishing Ltd; 2006 [cited 2020 Oct 19];111. Available from: <https://agupubs.onlinelibrary.wiley.com/doi/full/10.1029/2005JD006852>
6. Riera Romo M, Pérez-Martínez D, Castillo Ferrer C. Innate immunity in vertebrates: an overview. *Immunology* [Internet]. Blackwell Publishing Ltd; 2016 [cited 2021 Feb 9];148:125–39. Available from: </pmc/articles/PMC4863567/>
7. Bauer RN, Diaz-Sanchez D, Jaspers I. Effects of air pollutants on innate immunity: The role of Toll-like receptors and nucleotide-binding oligomerization domain-like receptors [Internet]. *J. Allergy Clin. Immunol.* Mosby Inc.; 2012 [cited 2021 Feb 9]. p. 26. Available from: </pmc/articles/PMC4341993/>
8. Estrella B, Naumova EN, Cepeda M, Voortman T, Katsikis PD, Drexhage HA. Effects of Air Pollution on Lung Innate Lymphoid Cells: Review of In Vitro and In Vivo Experimental Studies [Internet]. *Int. J. Environ. Res. Public Health.* MDPI AG; 2019 [cited 2021 Feb 9]. Available from: </pmc/articles/PMC6650824/>
9. Anenberg SC, Henze DK, Tinney V, Kinney PL, Raich W, Fann N, et al. Estimates of the Global Burden of Ambient PM_{2.5}, Ozone, and NO₂ on Asthma Incidence and

- Emergency Room Visits. *Environ Health Perspect* [Internet]. Public Health Services, US Dept of Health and Human Services; 2018 [cited 2021 Feb 9];126. Available from: [/pmc/articles/PMC6371661/](#)
10. Halonen JI, Lanki T, Tiittanen P, Niemi J V., Loh M, Pekkanen J. Ozone and cause-specific cardiorespiratory morbidity and mortality. *J Epidemiol Community Health* [Internet]. BMJ Publishing Group Ltd; 2010 [cited 2021 Feb 9];64:814–20. Available from: <http://jech.bmj.com/>
 11. Holst GJ, Pedersen CB, Thygesen M, Brandt J, Geels C, Bønløkke JH, et al. Air pollution and family related determinants of asthma onset and persistent wheezing in children: Nationwide case-control study. *BMJ* [Internet]. BMJ Publishing Group; 2020 [cited 2021 Feb 9];370. Available from: [/pmc/articles/PMC7437497/](#)
 12. Chatkin J, Correa L, Santos U. External Environmental Pollution as a Risk Factor for Asthma. *Clin Rev Allergy Immunol* [Internet]. Springer; 2021 [cited 2021 Feb 9];1:18. Available from: [/pmc/articles/PMC7801569/](#)
 13. Tiotiu AI, Novakova P, Nedeva D, Chong-Neto HJ, Novakova S, Steiropoulos P, et al. Impact of Air Pollution on Asthma Outcomes. *Int J Environ Res Public Health* [Internet]. MDPI AG; 2020 [cited 2021 Feb 9];17:1–29. Available from: [/pmc/articles/PMC7503605/](#)
 14. Medina-Ramón M, Zanobetti A, Schwartz J. The Effect of Ozone and PM10 on Hospital Admissions for Pneumonia and Chronic Obstructive Pulmonary Disease: A National Multicity Study. *Am J Epidemiol* [Internet]. Oxford Academic; 2006 [cited 2021 Feb 9];163:579–88. Available from: <http://academic.oup.com/aje/article/163/6/579/87717/The-Effect-of-Ozone-and-PM10-on-Hospital>
 15. Wang M, Aaron CP, Madrigano J, Hoffman EA, Angelini E, Yang J, et al. Association between Long-term Exposure to Ambient Air Pollution and Change in Quantitatively Assessed Emphysema and Lung Function. *JAMA - J Am Med Assoc* [Internet]. American Medical Association; 2019 [cited 2021 Feb 9];322:546–56. Available from: [/pmc/articles/PMC6692674/](#)
 16. Doiron D, de Hoogh K, Probst-Hensch N, Fortier I, Cai Y, De Matteis S, et al. Air

- pollution, lung function and COPD: results from the population-based UK Biobank study. *Eur Respir J* [Internet]. NLM (Medline); 2019 [cited 2021 Feb 9];54. Available from: <https://doi.org/10.1183/13993003.02140-2018>
17. Elbarbary M, Oganesyanyan A, Honda T, Kelly P, Zhang Y, Guo Y, et al. Ambient air pollution, lung function and COPD: Cross-sectional analysis from the WHO Study of AGEing and adult health wave 1. *BMJ Open Respir Res* [Internet]. BMJ Publishing Group; 2020 [cited 2021 Feb 9];7. Available from: </pmc/articles/PMC7747603/>
 18. Duan R-R, Hao K, Yang T. Air pollution and chronic obstructive pulmonary disease. *Chronic Dis Transl Med* [Internet]. Elsevier BV; 2020 [cited 2021 Feb 9];6:260–9. Available from: </pmc/articles/PMC7729117/>
 19. Szczesniak R, Rice JL, Brokamp C, Ryan P, Pestian T, Ni Y, et al. Influences of environmental exposures on individuals living with cystic fibrosis. *Expert Rev Respir Med* [Internet]. Taylor and Francis Ltd; 2020 [cited 2021 Feb 9];14:737–48. Available from: <https://www.tandfonline.com/doi/abs/10.1080/17476348.2020.1753507>
 20. Brugha R, Edmondson C, Davies JC. Outdoor air pollution and cystic fibrosis. *Paediatr Respir Rev*. W.B. Saunders Ltd; 2018;28:80–6.
 21. Farhat SCL, Almeida MB, Silva-Filho LVRF, Farhat J, Rodrigues JC, Braga ALF. Ozone is Associated With an Increased Risk of Respiratory Exacerbations in Patients With Cystic Fibrosis. *Chest* [Internet]. American College of Chest Physicians; 2013 [cited 2021 Feb 9];144:1186–92. Available from: </pmc/articles/PMC7172612/>
 22. Thurston GD, Balmes JR, Garcia E, Gilliland FD, Rice MB, Schikowski T, et al. Outdoor Air Pollution and New-Onset Airway Disease: An Official American Thoracic Society Workshop Report. *Ann Am Thorac Soc* [Internet]. American Thoracic Society; 2020 [cited 2021 Feb 9]. p. 387–98. Available from: </pmc/articles/PMC7175976/>
 23. Zhang JJ, Wei Y, Fang Z. Ozone pollution: A major health hazard worldwide. *Front Immunol*. Frontiers Media S.A.; 2019;10:492681.

24. Jerrett M, Burnett RT, Pope CA, Ito K, Thurston G, Krewski D, et al. Long-Term Ozone Exposure and Mortality. *N Engl J Med* [Internet]. Massachusetts Medical Society; 2009 [cited 2024 Jan 11];360:1085–95. Available from: <https://www.nejm.org/doi/full/10.1056/NEJMoa0803894>
25. Moller D. The tropospheric ozone problem. *Archives of industrial hygiene and toxicology* 55, 11-23. *Arh Hig Rada Toksikol.* 2004;55:11–23.
26. Hollingsworth JW, Kleeberger SR, Foster WM. Ozone and Pulmonary Innate Immunity. *Proc Am Thorac Soc* [Internet]. 2007 [cited 2020 Sep 7];4:240–6. Available from: www.atsjournals.org
27. Di Q, Wang Y, Zanobetti A, Wang Y, Koutrakis P, Choirat C, et al. Air Pollution and Mortality in the Medicare Population. *N Engl J Med* [Internet]. Massachusetts Medical Society; 2017 [cited 2023 Jul 18];376:2513–22. Available from: <https://www.nejm.org/doi/full/10.1056/nejmoa1702747>
28. Moore K, Neugebauer R, Lurmann F, Hall J, Brajer V, Alcorn S, et al. Ambient ozone concentrations cause increased hospitalizations for asthma in children: an 18-year study in Southern California. *Environ Health Perspect* [Internet]. *Environ Health Perspect*; 2008 [cited 2024 Jan 12];116:1063–70. Available from: <https://pubmed.ncbi.nlm.nih.gov/18709165/>
29. Lin S, Liu X, Le LH, Hwang SA. Chronic exposure to ambient ozone and asthma hospital admissions among children. *Environ Health Perspect* [Internet]. *Environ Health Perspect*; 2008 [cited 2024 Jan 12];116:1725–30. Available from: <https://pubmed.ncbi.nlm.nih.gov/19079727/>
30. Bell ML, McDermott A, Zeger SL, Samet JM, Dominici F. Ozone and short-term mortality in 95 US urban communities, 1987-2000. *J Am Med Assoc* [Internet]. NIH Public Access; 2004 [cited 2020 Oct 19];292:2372–8. Available from: <https://pubmed.ncbi.nlm.nih.gov/15444444/>
31. Camalier L, Cox W, Dolwick P. The effects of meteorology on ozone in urban areas and their use in assessing ozone trends. *Atmos Environ.* Pergamon; 2007;41:7127–37.
32. Wynn TA, Vannella KM. Macrophages in Tissue Repair, Regeneration, and

- Fibrosis. *Immunity* [Internet]. *Immunity*; 2016 [cited 2024 Jan 12];44:450–62. Available from: <https://pubmed.ncbi.nlm.nih.gov/26982353/>
33. Arsalane K, Gosset P, Vanhee D, Voisin C, Hamid Q, Tonnel A-B, et al. Ozone stimulates synthesis of inflammatory cytokines by alveolar macrophages in vitro. *Am J Respir Cell Mol Biol*. 1995;13:60–8.
 34. Ishii Y, Yang H, Sakamoto T, Nomura A, Hasegawa S, Hirata F, et al. Rat Alveolar Macrophage Cytokine Production and Regulation of Neutrophil Recruitment Following Acute Ozone Exposure. *Toxicol Appl Pharmacol*. Academic Press; 1997;147:214–23.
 35. Hollingsworth JW, Cook DN, Brass DM, Walker JKL, Morgan DL, Foster WM, et al. The Role of Toll-like Receptor 4 in Environmental Airway Injury in Mice. *Am J Respir Crit Care Med*. 2004;170:126–32.
 36. Miyata R, van Eeden SF. The innate and adaptive immune response induced by alveolar macrophages exposed to ambient particulate matter. *Toxicol Appl Pharmacol*. 2011;257:209–26.
 37. Patial S, Saini Y. Lung macrophages: current understanding of their roles in Ozone-induced lung diseases. *Crit Rev Toxicol* [Internet]. Taylor and Francis Ltd; 2020 [cited 2021 Feb 10];50:310–23. Available from: <https://pubmed.ncbi.nlm.nih.gov/32458707/>
 38. Chen L, Deng H, Cui H, Fang J, Zuo Z, Deng J, et al. Inflammatory responses and inflammation-associated diseases in organs. *Oncotarget* [Internet]. Impact Journals, LLC; 2018 [cited 2024 Jan 12];9:7204. Available from: </pmc/articles/PMC5805548/>
 39. Sugimoto MA, Sousa LP, Pinho V, Perretti M, Teixeira MM. Resolution of Inflammation: What Controls Its Onset? *Front Immunol* [Internet]. Frontiers Media SA; 2016 [cited 2024 Jan 12];7:160. Available from: </pmc/articles/PMC4845539/>
 40. Nathan C, Ding A. Nonresolving inflammation. *Cell* [Internet]. *Cell*; 2010 [cited 2024 Jan 12];140:871–82. Available from: <https://pubmed.ncbi.nlm.nih.gov/20303877/>
 41. Lawrence T, Gilroy DW. Chronic inflammation: a failure of resolution? *Int J Exp*

- Pathol [Internet]. *Int J Exp Pathol*; 2007 [cited 2024 Jan 12];88:85–94. Available from: <https://pubmed.ncbi.nlm.nih.gov/17408451/>
42. Laskin DL, Malaviya R, Laskin JD. Role of Macrophages in Acute Lung Injury and Chronic Fibrosis Induced by Pulmonary Toxicants. *Toxicol Sci* [Internet]. Oxford University Press; 2019 [cited 2021 Feb 10];168:287–301. Available from: <https://pubmed.ncbi.nlm.nih.gov/30590802/>
43. Singh Gangwar R, Vinayachandran V, Rengasamy P, Chan R, Park B, Diamond-Zaluski R, et al. Differential contribution of bone marrow-derived infiltrating monocytes and resident macrophages to persistent lung inflammation in chronic air pollution exposure. *Sci Rep* [Internet]. 2020;10:14348. Available from: <https://doi.org/10.1038/s41598-020-71144-1>
44. Bekki K, Ito T, Yoshida Y, He C, Arashidani K, He M, et al. PM2.5 collected in China causes inflammatory and oxidative stress responses in macrophages through the multiple pathways. *Environ Toxicol Pharmacol* [Internet]. Elsevier B.V.; 2016 [cited 2020 Nov 5];45:362–9. Available from: <http://dx.doi.org/10.1016/j.etap.2016.06.022>
45. Raji H, Riahi A, Borsi SH, Masoumi K, Khanjani N, Ahmadiangali K, et al. Acute effects of air pollution on hospital admissions for asthma, copd, and bronchiectasis in ahvaz, Iran. *Int J COPD* [Internet]. Dove Medical Press Ltd.; 2020 [cited 2020 Nov 6];15:501–14. Available from: </pmc/articles/PMC7061718/?report=abstract>
46. Kilburg-Basnyat B, Reece SW, Crouch MJ, Luo B, Boone AD, Yaeger M, et al. Specialized pro-resolving lipid mediators regulate ozone-induced pulmonary and systemic inflammation. *Toxicol Sci* [Internet]. Oxford University Press; 2018 [cited 2020 Nov 6];163:466–77. Available from: <https://academic.oup.com/toxsci/article/163/2/466/4870160>
47. Epelman S, Lavine KJ, Randolph GJ. Origin and Functions of Tissue Macrophages. *Immunity* [Internet]. Cell Press; 2014 [cited 2021 Feb 10];41:21–35. Available from: <https://pubmed.ncbi.nlm.nih.gov/25035951/>
48. Gordon S, Plüddemann A. Tissue macrophages: Heterogeneity and functions. *BMC Biol* [Internet]. BioMed Central Ltd.; 2017 [cited 2021 Feb 10];15. Available from: <https://pubmed.ncbi.nlm.nih.gov/28662662/>

49. Patel VI, Metcalf JP. Airway Macrophage and Dendritic Cell Subsets in the Resting Human Lung. *Crit Rev Immunol* [Internet]. Begell House Inc.; 2018 [cited 2021 Feb 10];38:303–31. Available from: <https://pubmed.ncbi.nlm.nih.gov/30806245/>
50. Schyns J, Bureau F, Marichal T. Lung Interstitial Macrophages: Past, Present, and Future. *J Immunol Res* [Internet]. Hindawi Limited; 2018 [cited 2021 Feb 10];2018. Available from: <https://pubmed.ncbi.nlm.nih.gov/29854841/>
51. Tighe RM, Misharin A V., Jakubzick C V., Brinkman R, Curtis JL, Duggan R, et al. Improving the Quality and Reproducibility of Flow Cytometry in the Lung. An Official American Thoracic Society Workshop Report. *Am J Respir Cell Mol Biol* [Internet]. American Thoracic Society; 2019 [cited 2021 Feb 10];61:150–61. Available from: <https://pubmed.ncbi.nlm.nih.gov/31368812/>
52. Mould KJ, Moore CM, McManus SA, McCubbrey AL, McClendon JD, Griesmer CL, et al. Airspace Macrophages and Monocytes Exist in Transcriptionally Distinct Subsets in Healthy Adults. *Am J Respir Crit Care Med* [Internet]. American Thoracic Society; 2020 [cited 2021 Feb 10]; Available from: <https://pubmed.ncbi.nlm.nih.gov/33079572/>
53. Lavrich KS, Speen AM, Ghio AJ, Bromberg PA, Samet JM, Alexis NE. Macrophages from the upper and lower human respiratory tract are metabolically distinct. *Am J Physiol - Lung Cell Mol Physiol* [Internet]. American Physiological Society; 2018 [cited 2021 Feb 10];315:L752–64. Available from: <https://pubmed.ncbi.nlm.nih.gov/30091382/>
54. Hume PS, Gibbings SL, Jakubzick C V., Tudor RM, Curran-Everett D, Henson PM, et al. Localization of Macrophages in the Human Lung via Design-based Stereology. *Am J Respir Crit Care Med* [Internet]. American Thoracic Society; 2020 [cited 2021 Feb 10];201:1209–17. Available from: <https://pubmed.ncbi.nlm.nih.gov/32197050/>
55. Venosa A, Malaviya R, Gow AJ, Hall L, Laskin JD, Laskin DL. Protective role of spleen-derived macrophages in lung inflammation, injury, and fibrosis induced by nitrogen mustard. *Am J Physiol - Lung Cell Mol Physiol* [Internet]. American Physiological Society; 2015 [cited 2021 Feb 10];309:L1487–98. Available from: <https://pubmed.ncbi.nlm.nih.gov/26475734/>

56. Francis M, Guo G, Kong B, Abramova E V., Cervelli JA, Gow AJ, et al. Regulation of Lung Macrophage Activation and Oxidative Stress Following Ozone Exposure by Farnesoid X Receptor. *Toxicol Sci* [Internet]. Oxford University Press; 2020 [cited 2021 Feb 10];177:441–53. Available from: <https://pubmed.ncbi.nlm.nih.gov/32984886/>
57. Choudhary I, Vo T, Paudel K, Patial S, Saini Y. Compartment-specific transcriptomics of ozone-exposed murine lungs reveals sex- and cell type-associated perturbations relevant to mucoinflammatory lung diseases. *Am J Physiol Cell Mol Physiol* [Internet]. American Physiological Society; 2021 [cited 2021 Feb 10];320:L99–125. Available from: <https://pubmed.ncbi.nlm.nih.gov/33026818/>
58. Birukova A, Cyphert-Daly J, Cumming RI, Yu YR, Gowdy KM, Que LG, et al. Sex modifies acute ozone-mediated airway physiologic responses. *Toxicol Sci*. Oxford University Press; 2019;169:499–510.
59. Venosa A, Malaviya R, Choi H, Gow AJ, Laskin JD, Laskin DL. Characterization of Distinct Macrophage Subpopulations during Nitrogen Mustard-Induced Lung Injury and Fibrosis. *Am J Respir Cell Mol Biol* [Internet]. American Thoracic Society; 2016 [cited 2021 Feb 10];54:436–46. Available from: <https://pubmed.ncbi.nlm.nih.gov/26273949/>
60. Martin CJ, Peters KN, Behar SM. Macrophages clean up: Efferocytosis and microbial control. *Curr. Opin. Microbiol.* Elsevier Current Trends; 2014. p. 17–23.
61. Underhill DM, Goodridge HS. Information processing during phagocytosis [Internet]. *Nat. Rev. Immunol.* Nature Publishing Group; 2012 [cited 2021 Jan 6]. p. 492–502. Available from: www.nature.com/reviews/immunol
62. Karavitis J, Kovacs EJ. Macrophage phagocytosis: effects of environmental pollutants, alcohol, cigarette smoke, and other external factors. *J Leukoc Biol* [Internet]. Wiley; 2011 [cited 2021 Feb 10];90:1065–78. Available from: <https://pubmed.ncbi.nlm.nih.gov/21878544/>
63. Soukup JM, Becker S. Human alveolar macrophage responses to air pollution particulates are associated with insoluble components of coarse material, including

- particulate endotoxin. *Toxicol Appl Pharmacol* [Internet]. Academic Press Inc.; 2001 [cited 2021 Feb 10];171:20–6. Available from: <https://pubmed.ncbi.nlm.nih.gov/11181108/>
64. Sweeney S, Grandolfo D, Ruenraroengsak P, Tetley TD. Functional consequences for primary human alveolar macrophages following treatment with long, but not short, multiwalled carbon nanotubes. *Int J Nanomedicine* [Internet]. Dove Medical Press Ltd.; 2015 [cited 2021 Feb 10];10:3115–29. Available from: <https://pubmed.ncbi.nlm.nih.gov/25960651/>
65. Doran AC, Yurdagul Jr A, Tabas I. Efferocytosis in health and disease. *Nat Rev Immunol* [Internet]. Nature Research; 2020 [cited 2021 Feb 10];20:254–67. Available from: <https://pubmed.ncbi.nlm.nih.gov/31822793/>
66. Grabiec AM, Denny N, Doherty JA, Happonen KE, Hankinson J, Connolly E, et al. Diminished airway macrophage expression of the Axl receptor tyrosine kinase is associated with defective efferocytosis in asthma. *J Allergy Clin Immunol* [Internet]. Mosby Inc.; 2017 [cited 2021 Jan 6];140:1144-1146.e4. Available from: <http://dx.doi.org/10.1016/j.jaci.2017.03.024>
67. de Souza Xavier Costa N, Ribeiro Júnior G, Dos Santos Alemany AA, Belotti L, Schalch AS, Cavalcante MF, et al. Air pollution impairs recovery and tissue remodeling in a murine model of acute lung injury. *Sci Rep* [Internet]. Nature Research; 2020 [cited 2021 Feb 10];10. Available from: <https://pubmed.ncbi.nlm.nih.gov/32943719/>
68. Hodge MX, Reece SW, Madenspacher JH, Gowdy KM. In vivo assessment of alveolar macrophage efferocytosis following ozone exposure. *J Vis Exp* [Internet]. Journal of Visualized Experiments; 2019 [cited 2021 Jan 6];2019:60109. Available from: www.jove.com/url:https://www.jove.com/video/60109
69. Fakhrzadeh L, Laskin JD, Laskin DL. Ozone-induced production of nitric oxide and TNF- α and tissue injury are dependent on NF- κ B p50. *Am J Physiol Cell Mol Physiol* [Internet]. American Physiological Society; 2004 [cited 2020 Nov 13];287:L279–85. Available from: <https://www.physiology.org/doi/10.1152/ajplung.00348.2003>
70. Mishra V, Banga J, Silveyra P. Oxidative stress and cellular pathways of asthma

and inflammation: Therapeutic strategies and pharmacological targets. *Pharmacol Ther* [Internet]. NIH Public Access; 2018 [cited 2021 Jan 13];181:169. Available from: [/pmc/articles/PMC5743757/?report=abstract](https://pubmed.ncbi.nlm.nih.gov/30000000/)

71. Liu T, Zhang L, Joo D, Sun S-C. NF- κ B signaling in inflammation. *Nat Publ Gr* [Internet]. 2017 [cited 2019 Dec 16];2. Available from: www.nature.com/sigtrans
72. Oeckinghaus A, Ghosh S. The NF-kappaB family of transcription factors and its regulation. *Cold Spring Harb Perspect Biol* [Internet]. Cold Spring Harbor Laboratory Press; 2009 [cited 2021 Jan 14];1:a000034. Available from: <http://cshperspectives.cshlp.org/>
73. Laskin DL, Sunil V, Guo Y, Heck DE, Laskin JD. Increased nitric oxide synthase in the lung after ozone inhalation is associated with activation of NF-kappa B. *Environ Health Perspect* [Internet]. Environ Health Perspect; 1998 [cited 2024 Feb 6];106 Suppl 5:1175–8. Available from: <https://pubmed.ncbi.nlm.nih.gov/9788894/>
74. Tang F, Yue S, Luo Z, Feng D, Wang M, Qian C, et al. Role of N-methyl-D-aspartate Receptor in Hyperoxia-Induced Lung Injury. *Pediatr Pulmonol* [Internet]. 2005 [cited 2020 Oct 20];40:437–44. Available from: <http://doi.wiley.com/10.1002/ppul.20299>
75. Li X, Li C, Tang Y, Huang Y, Cheng Q, Huang X, et al. NMDA receptor activation inhibits the antifibrotic effect of BM-MSCs on bleomycin-induced pulmonary fibrosis. *Am J Physiol - Lung Cell Mol Physiol* [Internet]. American Physiological Society; 2018 [cited 2021 Jan 14];315:L404–21. Available from: www.ajplung.org
76. Skerry TM, Genever PG. Glutamate signalling in non-neuronal tissues. *Trends Pharmacol. Sci.* Elsevier Ltd; 2001. p. 174–81.
77. Anaparti V, Ilarraza R, Orihara K, Stelmack GL, Ojo OO, Mahood TH, et al. NMDA receptors mediate contractile responses in human airway smooth muscle cells. *Am J Physiol Cell Mol Physiol* [Internet]. American Physiological Society; 2015 [cited 2021 Jan 14];308:L1253–64. Available from: <https://www.physiology.org/doi/10.1152/ajplung.00402.2014>
78. Dickman KG, Youssef JG, Mathew SM, Said SI. Ionotropic Glutamate Receptors in Lungs and Airways: Molecular Basis for Glutamate Toxicity. *Am J Respir Cell Mol*

- Biol [Internet]. American Thoracic Society; 2004 [cited 2020 Aug 11];30:139–44. Available from: <http://www.atsjournals.org/doi/abs/10.1165/rcmb.2003-0177OC>
79. Said SI, Berisha HI, Pakbaz H. Excitotoxicity in the lung: N-Methyl-D-aspartate-induced, nitric oxide-dependent, pulmonary edema is attenuated by vasoactive intestinal peptide and by inhibitors of poly(ADP-ribose) polymerase. *Proc Natl Acad Sci U S A* [Internet]. National Academy of Sciences; 1996 [cited 2020 Sep 16];93:4688–92. Available from: [/pmc/articles/PMC39340/?report=abstract](http://pmc/articles/PMC39340/?report=abstract)
80. Cheng Q, Fang L, Feng D, Tang S, Yue S, Huang Y, et al. Memantine ameliorates pulmonary inflammation in a mice model of COPD induced by cigarette smoke combined with LPS. *Biomed Pharmacother* [Internet]. Elsevier Masson SAS; 2019 [cited 2020 Aug 19];109:2005–13. Available from: <https://doi.org/10.1016/j.biopha.2018.11.002>
81. Willard SS, Koochekpour S. Glutamate, Glutamate Receptors, and Downstream Signaling Pathways. *Int J Biol Sci* [Internet]. 2013 [cited 2021 Jan 17];9. Available from: <http://www.ijbs.com948>
82. Rodriguez PC, Ochoa AC, Al-Khami AA. Arginine metabolism in myeloid cells shapes innate and adaptive immunity. *Front Immunol*. Frontiers Research Foundation; 2017;8:239508.
83. Yurdagul Jr. A, Subramanian M, Wang X, Crown SB, Ilkayeva OR, Darville L, et al. Macrophage Metabolism of Apoptotic Cell-Derived Arginine Promotes Continual Efferocytosis and Resolution of Injury. *Cell Metab*. Cell Press; 2020;31:518-533.e10.
84. Bronte V, Zanovello P. Regulation of Immune Responses By L-Arginine Metabolism. *Nat Rev Immunol*. 2005;5:641–54.
85. MacMicking J, Xie QW, Nathan C. NITRIC OXIDE AND MACROPHAGE FUNCTION. <https://doi.org/10.1146/annurev.immunol151323> [Internet]. Annual Reviews 4139 El Camino Way, P.O. Box 10139, Palo Alto, CA 94303-0139, USA ; 2003 [cited 2024 Jan 13];15:323–50. Available from: <https://www.annualreviews.org/doi/abs/10.1146/annurev.immunol.15.1.323>
86. Pesce JT, Ramalingam TR, Mentink-Kane MM, Wilson MS, El Kasmi KC, Smith

- AM, et al. Arginase-1-Expressing Macrophages Suppress Th2 Cytokine-Driven Inflammation and Fibrosis. Kazura JW, editor. PLoS Pathog [Internet]. 2009 [cited 2020 Jan 8];5:e1000371. Available from: <https://dx.plos.org/10.1371/journal.ppat.1000371>
87. Jost MM, Ninci E, Meder B, Kempf C, Royen N van, Hua J, et al. Divergent effects of GM-CSF and TGF β 1 on bone marrow- derived macrophage arginase-1 activity, MCP-1 expression, and matrix-metalloproteinase-12: a potential role during arteriogenesis. FASEB J [Internet]. John Wiley & Sons, Ltd; 2003 [cited 2024 Jan 13];17:2281–3. Available from: <https://onlinelibrary.wiley.com/doi/full/10.1096/fj.03-0071fje>
88. Boutard V, Havouis R, Fouqueray B, Philippe C, Moulinoux JP, Baud L. Transforming growth factor-beta stimulates arginase activity in macrophages. Implications for the regulation of macrophage cytotoxicity. J Immunol [Internet]. American Association of Immunologists; 1995 [cited 2024 Jan 13];155:2077–84. Available from: <https://dx.doi.org/10.4049/jimmunol.155.4.2077>
89. El Kasmi KC, Qualls JE, Pesce JT, Smith AM, Thompson RW, Henao-Tamayo M, et al. Toll-like receptor-induced arginase 1 in macrophages thwarts effective immunity against intracellular pathogens. Nat Immunol 2008 9:12 [Internet]. Nature Publishing Group; 2008 [cited 2024 Jan 13];9:1399–406. Available from: <https://www.nature.com/articles/ni.1671>
90. Jeong JW, Cha HJ, Han MH, Hwang SJ, Lee DS, Yoo JS, et al. Spermidine protects against oxidative stress in inflammation models using macrophages and Zebrafish. Biomol Ther [Internet]. Korean Society of Applied Pharmacology; 2018 [cited 2020 Sep 17];26:146–56. Available from: [/pmc/articles/PMC5839493/?report=abstract](https://pubmed.ncbi.nlm.nih.gov/30000000/)
91. Yang Q, Zheng C, Cao J, Cao G, Shou P, Lin L, et al. Spermidine alleviates experimental autoimmune encephalomyelitis through inducing inhibitory macrophages. Cell Death Differ. Nature Publishing Group; 2016;23:1850–61.
92. Williams K, Romano C, Molinoff PB. Effects of polyamines on the binding of [3H]MK-801 to the N-methyl-D-aspartate receptor: pharmacological evidence for the existence of a polyamine recognition site. Mol Pharmacol. 1989;36.
93. Williams K, Romano C, Dichter MA, Molinoff PB. Modulation of the NMDA

- receptor by polyamines. *Life Sci. Pergamon*; 1991. p. 469–98.
94. Meng Q, Cooney M, Yepuri N, Cooney RN. L-arginine attenuates Interleukin-1 β (IL-1 β) induced Nuclear Factor Kappa-Beta (NF- κ B) activation in Caco-2 cells. 2017 [cited 2020 Jan 8]; Available from: <https://doi.org/10.1371/journal.pone.0174441>
95. Guttenberg MA, Vose AT, Tighe RM. Role of Innate Immune System in Environmental Lung Diseases. *Curr Allergy Asthma Rep* [Internet]. Springer; 2021 [cited 2021 May 10];21:34. Available from: <https://link.springer.com/10.1007/s11882-021-01011-0>
96. Lim CC, Hayes RB, Ahn J, Shao Y, Silverman DT, Jones RR, et al. Long-term exposure to ozone and cause-specific mortality risk in the United States. *Am J Respir Crit Care Med* [Internet]. American Thoracic Society; 2019 [cited 2023 Jun 1];200:1022–31. Available from: www.atsjournals.org.
97. Samet JM, Zeger SL, Dominici F, Curriero F, Coursac I, Dockery DW, et al. The National Morbidity, Mortality, and Air Pollution Study. Part II: Morbidity and mortality from air pollution in the United States - PubMed [Internet]. 2000 Jun. Available from: <https://pubmed.ncbi.nlm.nih.gov/11354823/>
98. Ciencewicki J, Trivedi S, Kleeberger SR. Oxidants and the pathogenesis of lung diseases. *J Allergy Clin Immunol* [Internet]. *J Allergy Clin Immunol*; 2008 [cited 2023 Aug 31];122:456–68. Available from: <https://pubmed.ncbi.nlm.nih.gov/18774381/>
99. Hussell T, Bell TJ. Alveolar macrophages: Plasticity in a tissue-specific context [Internet]. *Nat. Rev. Immunol.* Nature Publishing Group; 2014 [cited 2021 Jan 9]. p. 81–93. Available from: www.nature.com/reviews/immunol
100. Guilliams M, De Kler I, Henri S, Post S, Vanhoutte L, De Prijck S, et al. Alveolar macrophages develop from fetal monocytes that differentiate into long-lived cells in the first week of life via GM-CSF. *J Exp Med* [Internet]. The Rockefeller University Press; 2013 [cited 2023 Jul 18];210:1977. Available from: [/pmc/articles/PMC3782041/](https://pmc/articles/PMC3782041/)
101. Hashimoto D, Chow A, Noizat C, Teo P, Beasley MB, Leboeuf M, et al. Tissue resident macrophages self-maintain locally throughout adult life with minimal

- contribution from circulating monocytes. *Immunity* [Internet]. NIH Public Access; 2013 [cited 2023 Jul 18];38:792–804. Available from: [/pmc/articles/PMC3853406/](#)
102. Janssen WJ, Barthel L, Muldrow A, Oberley-Deegan RE, Kearns MT, Jakubzick C, et al. Fas Determines Differential Fates of Resident and Recruited Macrophages during Resolution of Acute Lung Injury. *Am J Respir Crit Care Med* [Internet]. American Thoracic Society; 2011 [cited 2023 Jul 3];184:547. Available from: [/pmc/articles/PMC3175550/](#)
103. Maus UA, Janzen S, Wall G, Srivastava M, Blackwell TS, Christman JW, et al. Resident Alveolar Macrophages Are Replaced by Recruited Monocytes in Response to Endotoxin-Induced Lung Inflammation. <https://doi.org/10.1165/rcmb.2005-0241OC> [Internet]. American Thoracic Society; 2012 [cited 2023 Jul 13];35:227–35. Available from: www.atsjournals.org
104. Mould KJ, Barthel L, Mohning MP, Thomas SM, McCubbrey AL, Danhorn T, et al. Cell Origin Dictates Programming of Resident versus Recruited Macrophages during Acute Lung Injury. *Am J Respir Cell Mol Biol* [Internet]. *Am J Respir Cell Mol Biol*; 2017 [cited 2023 Jul 12];57:294–306. Available from: <https://pubmed.ncbi.nlm.nih.gov/28421818/>
105. Misharin A V., Morales-Nebreda L, Reyfman PA, Cuda CM, Walter JM, McQuattie-Pimentel AC, et al. Monocyte-derived alveolar macrophages drive lung fibrosis and persist in the lung over the life span. *J Exp Med* [Internet]. The Rockefeller University Press; 2017 [cited 2022 Mar 15];214:2404. Available from: [/pmc/articles/PMC5551573/](#)
106. Joshi N, Watanabe S, Verma R, Jablonski RP, Chen CI, Cheres P, et al. A spatially restricted fibrotic niche in pulmonary fibrosis is sustained by M-CSF/M-CSFR signalling in monocyte-derived alveolar macrophages. *Eur Respir J* [Internet]. European Respiratory Society; 2020 [cited 2023 Jun 2];55. Available from: <https://erj.ersjournals.com/content/55/1/1900646>
107. Yona S, Kim KW, Wolf Y, Mildner A, Varol D, Breker M, et al. Fate mapping reveals origins and dynamics of monocytes and tissue macrophages under homeostasis. *Immunity* [Internet]. *Immunity*; 2013 [cited 2023 Aug 30];38:79–91. Available from: <https://pubmed.ncbi.nlm.nih.gov/23273845/>

108. Madenspacher JH, Morrell ED, Gowdy KM, McDonald JG, Thompson BM, Muse G, et al. Cholesterol 25-hydroxylase promotes efferocytosis and resolution of lung inflammation. *JCI Insight* [Internet]. American Society for Clinical Investigation; 2020 [cited 2023 Jul 14];5. Available from: [/pmc/articles/PMC7308063/](https://pubmed.ncbi.nlm.nih.gov/35075603/)
109. Scott RS, McMahon EJ, Pop SM, Reap EA, Caricchio R, Cohen PL, et al. Phagocytosis and clearance of apoptotic cells is mediated by MER. *Nat* 2001 411:207–11. Available from: <https://www.nature.com/articles/35075603>
110. Tighe RM, Birukova A, Yaeger MJ, Reece SW, Gowdy KM. Euthanasia- and Lavage-mediated Effects on Bronchoalveolar Measures of Lung Injury and Inflammation. *Am J Respir Cell Mol Biol* [Internet]. Am J Respir Cell Mol Biol; 2018 [cited 2023 Jun 25];59:257–66. Available from: <https://pubmed.ncbi.nlm.nih.gov/29481287/>
111. Tighe RM, Li Z, Potts EN, Frush S, Liu N, Gunn MD, et al. Ozone Inhalation Promotes CX3CR1-dependent Maturation of Resident Lung Macrophages which Limit Oxidative Stress and Inflammation. *J Immunol* [Internet]. NIH Public Access; 2011 [cited 2022 Mar 15];187:4800. Available from: [/pmc/articles/PMC3197861/](https://pubmed.ncbi.nlm.nih.gov/26938654/)
112. Albright M, Guttenberg MA, Tighe RM. Ozone-Induced Models of Airway Hyperreactivity and Epithelial Injury. *Methods Mol Biol* [Internet]. Humana Press Inc.; 2022 [cited 2023 Feb 3];2506:67–81. Available from: https://link.springer.com/protocol/10.1007/978-1-0716-2364-0_5
113. Yu YRA, O’Koren EG, Hotten DF, Kan MJ, Kopin D, Nelson ER, et al. A Protocol for the Comprehensive Flow Cytometric Analysis of Immune Cells in Normal and Inflamed Murine Non-Lymphoid Tissues. *PLoS One* [Internet]. PLoS One; 2016 [cited 2023 Jun 25];11. Available from: <https://pubmed.ncbi.nlm.nih.gov/26938654/>
114. Grant RA, Morales-Nebreda L, Markov NS, Swaminathan S, Querrey M, Guzman ER, et al. Circuits between infected macrophages and T cells in SARS-CoV-2 pneumonia. *Nat* 2021 590:7847 [Internet]. Nature Publishing Group; 2021 [cited 2023 Sep 10];590:635–41. Available from: <https://www.nature.com/articles/s41586-020-03148-w>
115. Yaeger MJ, Reece SW, Kilburg-Basnyat B, Hodge MX, Pal A, Dunigan-Russell K,

- et al. Sex Differences in Pulmonary Eicosanoids and Specialized Pro-Resolving Mediators in Response to Ozone Exposure. *Toxicol Sci* [Internet]. Oxford Academic; 2021 [cited 2021 Nov 22];183:170–83. Available from: <https://academic.oup.com/toxsci/article/183/1/170/6310193>
116. Nguyen J, Deering-Rice CE, Armstrong BS, Massa C, Reilly CA, Venosa A. Parenchymal and Inflammatory Cell Responses to Single and Repeated Ozone Exposure in Healthy and Surfactant Protein-C Mutant Lung. *Toxicol Sci* [Internet]. *Toxicol Sci*; 2022 [cited 2023 Jun 29];189:107–23. Available from: <https://pubmed.ncbi.nlm.nih.gov/35866636/>
117. Mould KJ, Moore CM, McManus SA, McCubbrey AL, McClendon JD, Griesmer CL, et al. Airspace macrophages and monocytes exist in transcriptionally distinct subsets in healthy adults. *Am J Respir Crit Care Med* [Internet]. American Thoracic Society; 2021 [cited 2023 Jul 13];203:946–56. Available from: <https://healthy-bal.cells.ucsc.edu>.
118. Al-Hegelan M, Tighe RM, Castillo C, Hollingsworth JW. Ambient ozone and pulmonary innate immunity. *Immunol Res* [Internet]. 2011 [cited 2020 Jun 10];49:173–91. Available from: <http://link.springer.com/10.1007/s12026-010-8180-z>
119. Francis M, Groves AM, Sun R, Cervelli JA, Choi H, Laskin JD, et al. Editor’s Highlight: CCR2 Regulates Inflammatory Cell Accumulation in the Lung and Tissue Injury following Ozone Exposure. *Toxicol Sci* [Internet]. *Toxicol Sci*; 2017 [cited 2023 Jun 25];155:474–84. Available from: <https://pubmed.ncbi.nlm.nih.gov/27837169/>
120. Francis M, Sun R, Cervelli JA, Choi H, Mandal M, Abramova E V., et al. Editor’s Highlight: Role of Spleen-Derived Macrophages in Ozone-Induced Lung Inflammation and Injury. *Toxicol Sci* [Internet]. *Toxicol Sci*; 2017 [cited 2023 Jun 25];155:182–95. Available from: <https://pubmed.ncbi.nlm.nih.gov/27708193/>
121. Jakubzick C, Gautier EL, Gibbings SL, Sojka DK, Schlitzer A, Johnson TE, et al. Minimal differentiation of classical monocytes as they survey steady-state tissues and transport antigen to lymph nodes. *Immunity* [Internet]. *Immunity*; 2013 [cited 2023 Jun 29];39:599–610. Available from: <https://pubmed.ncbi.nlm.nih.gov/24012416/>

122. Rawat K, Tewari A, Li X, Mara AB, King WT, Gibbings SL, et al. CCL5-producing migratory dendritic cells guide CCR5+ monocytes into the draining lymph nodes. *J Exp Med* [Internet]. *J Exp Med*; 2023 [cited 2023 Jul 7];220. Available from: <https://pubmed.ncbi.nlm.nih.gov/36946983/>
123. Byrne AJ, Powell JE, O'Sullivan BJ, Ogger PP, Hoffland A, Cook J, et al. Dynamics of human monocytes and airway macrophages during healthy aging and after transplant. *J Exp Med* [Internet]. Rockefeller University Press; 2020 [cited 2023 Aug 31];217. Available from: <https://doi.org/10.1084/jem.20191236>
124. Novak CM, Tighe RM, Ballinger MN. What is 'Normal' When Examining Myeloid Cells in Human Airways? *Am J Respir Crit Care Med* [Internet]. American Thoracic Society; 2020 [cited 2021 Feb 10]; Available from: <https://pubmed.ncbi.nlm.nih.gov/33181037/>
125. Li X, Kolling FW, Aridgides D, Mellinger D, Ashare A, Jakubzick C V. ScRNA-seq expression of IFI27 and APOC2 identifies four alveolar macrophage superclusters in healthy BALF. *Life Sci alliance* [Internet]. Life Sci Alliance; 2022 [cited 2023 Aug 31];5. Available from: <https://pubmed.ncbi.nlm.nih.gov/35820705/>
126. Runyan CE, Welch LC, Lecuona E, Shigemura M, Amarelle L, Abdala-Valencia H, et al. Impaired Phagocytic Function in CX3CR1+ Tissue-Resident Skeletal Muscle Macrophages Prevents Muscle Recovery After Influenza A Virus-Induced Pneumonia in Old Mice. *Aging Cell* [Internet]. John Wiley & Sons, Ltd; 2020 [cited 2023 Jan 1];19:e13180. Available from: <https://onlinelibrary.wiley.com/doi/full/10.1111/ace1.13180>
127. Misharin A V., Morales-Nebreda L, Mutlu GM, Budinger GRS, Perlman H. Flow Cytometric Analysis of Macrophages and Dendritic Cell Subsets in The Mouse Lung. *Am J Respir Cell Mol Biol* [Internet]. American Thoracic Society; 2013 [cited 2022 Dec 31];49:503–10. Available from: [/pmc/articles/PMC3824047/](https://pubmed.ncbi.nlm.nih.gov/24382407/)
128. Wagner JG, Barkauskas CE, Vose A, Lewandowski RP, Harkema JR, Tighe RM. Repetitive Ozone Exposures and Evaluation of Pulmonary Inflammation and Remodeling in Diabetic Mouse Strains. *Environ Health Perspect* [Internet]. Environmental Health Perspectives; 2020 [cited 2023 Jul 18];128:117009-1-117009–11. Available from: <https://ehp.niehs.nih.gov/doi/10.1289/EHP7255>

129. Tovar A, Smith GJ, Nalesnik MB, Thomas JM, McFadden KM, Harkema JR, et al. A Locus on Chromosome 15 Contributes to Acute Ozone-induced Lung Injury in Collaborative Cross Mice. *Am J Respir Cell Mol Biol* [Internet]. *Am J Respir Cell Mol Biol*; 2022 [cited 2023 Jul 18];67:528–38. Available from: <https://pubmed.ncbi.nlm.nih.gov/35816602/>
130. van de Laar L, Saelens W, De Prijck S, Martens L, Scott CL, Van Isterdael G, et al. Yolk Sac Macrophages, Fetal Liver, and Adult Monocytes Can Colonize an Empty Niche and Develop into Functional Tissue-Resident Macrophages. *Immunity* [Internet]. *Immunity*; 2016 [cited 2023 Jul 3];44:755–68. Available from: <https://pubmed.ncbi.nlm.nih.gov/26992565/>
131. Fujimori T, Grabiec AM, Kaur M, Bell TJ, Fujino N, Cook PC, et al. The Axl receptor tyrosine kinase is a discriminator of macrophage function in the inflamed lung. *Mucosal Immunol* [Internet]. Nature Publishing Group; 2015 [cited 2023 Jul 14];8:1021. Available from: </pmc/articles/PMC4430298/>
132. Penberthy KK, Ravichandran KS. Apoptotic cell recognition receptors and scavenger receptors. *Immunol Rev* [Internet]. NIH Public Access; 2016 [cited 2023 Jul 14];269:44. Available from: </pmc/articles/PMC4685734/>
133. Liang S, Sun Q, Du Z, Ren X, Xu Q, Sun Z, et al. PM2.5 induce the defective efferocytosis and promote atherosclerosis via HIF-1 α activation in macrophage. <https://doi.org/10.1080/1743539020222083995> [Internet]. Taylor & Francis; 2022 [cited 2023 Sep 12];16:290–309. Available from: <https://www.tandfonline.com/doi/abs/10.1080/17435390.2022.2083995>
134. Culemann S, Knab K, Euler M, Wegner A, Garibagaoglu H, Ackermann J, et al. Stunning of neutrophils accounts for the anti-inflammatory effects of clodronate liposomes. *J Exp Med* [Internet]. *J Exp Med*; 2023 [cited 2023 Jul 7];220. Available from: <https://pubmed.ncbi.nlm.nih.gov/36976180/>
135. Akalu YT, Mercau ME, Ansems M, Hughes LD, Nevin J, Alberto EJ, et al. Tissue-specific modifier alleles determine Mertk loss-of-function traits. *Elife*. eLife Sciences Publications Ltd; 2022;11.
136. Dunigan-Russell K, Yaeger MJ, Hodge MX, Kilburg-Basnyat B, Reece SW, Birukova A, et al. Scavenger receptor BI attenuates oxidized phospholipid-induced

- pulmonary inflammation. *Toxicol Appl Pharmacol* [Internet]. Academic Press; 2023 [cited 2023 Feb 3];116381. Available from: <https://linkinghub.elsevier.com/retrieve/pii/S0041008X23000194>
137. Morioka S, Perry JSA, Raymond MH, Medina CB, Zhu Y, Zhao L, et al. Efferocytosis induces a novel SLC program to promote glucose uptake and lactate release. *Nat* 2018 5637733 [Internet]. Nature Publishing Group; 2018 [cited 2024 Jan 18];563:714–8. Available from: <https://www.nature.com/articles/s41586-018-0735-5>
138. Fond AM, Lee CS, Schulman IG, Kiss RS, Ravichandran KS. Apoptotic cells trigger a membrane-initiated pathway to increase ABCA1. *J Clin Invest. American Society for Clinical Investigation*; 2015;125:2748–58.
139. McCubbrey AL, McManus SA, McClendon JD, Thomas SM, Chatwin HB, Reisz JA, et al. Polyamine import and accumulation causes immunomodulation in macrophages engulfing apoptotic cells. *Cell Rep* [Internet]. Elsevier B.V.; 2022 [cited 2024 Jan 18];38. Available from: <http://www.cell.com/article/S2211124721017265/fulltext>
140. Latour YL, Gobert AP, Wilson KT. The role of polyamines in the regulation of macrophage polarization and function [Internet]. *Amino Acids*. Springer; 2020 [cited 2020 Nov 13]. p. 151–60. Available from: <https://doi.org/10.1007/s00726-019-02719-0>
141. Zhang M, Caragine T, Wang H, Cohen PS, Botchkina G, Soda K, et al. Spermine Inhibits Proinflammatory Cytokine Synthesis in Human Mononuclear Cells: A Counterregulatory Mechanism that Restrains the Immune Response. *J Exp Med* [Internet]. The Rockefeller University Press; 1997 [cited 2024 Jan 18];185:1759–68. Available from: <http://rupress.org/jem/article-pdf/185/10/1759/1680627/5525.pdf>
142. Li X, Zhou X, Liu X, Li X, Jiang X, Shi B, et al. Spermidine protects against acute kidney injury by modulating macrophage NLRP3 inflammasome activation and mitochondrial respiration in an eIF5A hypusination-related pathway. *Mol Med* [Internet]. The Feinstein Institute for Medical Research; 2022 [cited 2024 Jan 18];28:103. Available from: [/pmc/articles/PMC9441050/](https://pubmed.ncbi.nlm.nih.gov/35441050/)
143. Liu R, Li X, Ma H, Yang Q, Shang Q, Song L, et al. Spermidine endows macrophages anti-inflammatory properties by inducing mitochondrial superoxide-

dependent AMPK activation, Hif-1 α upregulation and autophagy. *Free Radic Biol Med*. Pergamon; 2020;161:339–50.

144. Kurosawa M, Shimizu Y, Tsukagoshi H, Ueki M. Elevated levels of peripheral-blood, naturally occurring aliphatic polyamines in bronchial asthmatic patients with active symptoms. *Allergy* [Internet]. John Wiley & Sons, Ltd; 1992 [cited 2024 Jan 18];47:638–43. Available from: <https://onlinelibrary.wiley.com/doi/full/10.1111/j.1398-9995.1992.tb02388.x>
145. Wawrzyniak M, Groeger D, Frei R, Ferstl R, Wawrzyniak P, Krawczyk K, et al. Spermidine and spermine exert protective effects within the lung. *Pharmacol Res Perspect* [Internet]. John Wiley & Sons, Ltd; 2021 [cited 2024 Jan 18];9:e00837. Available from: <https://onlinelibrary.wiley.com/doi/full/10.1002/prp2.837>
146. Hoet PHM, Nemery B. Polyamines in the lung: Polyamine uptake and polyamine-linked pathological or toxicological conditions [Internet]. *Am. J. Physiol. - Lung Cell. Mol. Physiol.* American Physiological Society; 2000 [cited 2020 Sep 17]. Available from: <http://www.ajplung.org>
147. Brackley P, Goodnow R, Nakanishi K, Sudan HL, Usherwood PNR. Spermine and philanthotoxin potentiate excitatory amino acid responses of *Xenopus* oocytes injected with rat and chick brain RNA. *Neurosci Lett*. Elsevier; 1990;114:51–6.
148. Usherwood PNR. Natural and synthetic polyamines: modulators of signalling proteins. *Farm*. Elsevier Masson; 2000;55:202–5.
149. Shang LH, Luo ZQ, Deng XD, Wang MJ, Huang FR, Feng DD, et al. Expression of N-methyl-d-aspartate receptor and its effect on nitric oxide production of rat alveolar macrophages. *Nitric Oxide - Biol Chem* [Internet]. Elsevier Inc.; 2010;23:327–31. Available from: <http://dx.doi.org/10.1016/j.niox.2010.09.004>
150. Hirschfeld M, Ma Y, Weis JH, Vogel SN, Weis JJ. Cutting Edge: Repurification of Lipopolysaccharide Eliminates Signaling Through Both Human and Murine Toll-Like Receptor 2. *J Immunol* [Internet]. American Association of Immunologists; 2000 [cited 2024 Jan 15];165:618–22. Available from: <https://dx.doi.org/10.4049/jimmunol.165.2.618>
151. Adams KJ, Pratt B, Bose N, Dubois LG, St. John-Williams L, Perrott KM, et al.

Skyline for Small Molecules: A Unifying Software Package for Quantitative Metabolomics. *J Proteome Res.* 2020;19:1447–58.

152. Sunil VR, Patel-Vayas K, Shen J, Laskin JD, Laskin DL. Classical and alternative macrophage activation in the lung following ozone-induced oxidative stress. *Toxicol Appl Pharmacol.* Academic Press; 2012;263:195–202.
153. Holz O, Jörres RA, Timm P, Mücke M, Richter K, Koschyk S, et al. Ozone-induced Airway Inflammatory Changes Differ between Individuals and Are Reproducible. <https://doi.org/10.1164/ajrccm.15939806098> [Internet]. American Thoracic Society New York, NY; 2012 [cited 2024 Jan 17];159:776–84. Available from: www.atsjournals.org
154. Guttenberg MA, Vose AT, Birukova A, Lewars K, Cumming RI, Albright MC, et al. Tissue-resident alveolar macrophages reduce O₃-induced inflammation via MerTK mediated efferocytosis. *bioRxiv* [Internet]. 2023;2023.11.06.565865. Available from: <http://biorxiv.org/content/early/2023/11/06/2023.11.06.565865.abstract>
155. Baek AR, Hong J, Song KS, Jang AS, Kim DJ, Chin SS, et al. Spermidine attenuates bleomycin-induced lung fibrosis by inducing autophagy and inhibiting endoplasmic reticulum stress (ERS)-induced cell death in mice. *Exp Mol Med* [Internet]. Springer Science and Business Media LLC; 2020 [cited 2021 Jan 15];52:2034–45. Available from: <https://doi.org/10.1038/s12276-020-00545-z>
156. Sakurada T, Onodera K, Tadano T, Kisara K. Effects of Polyamines on the Central Nervous System. *Jpn J Pharmacol.* 1975;25:653–61.
157. Hatch GE, Slade R, Harris LP, McDonnell WF, Devlin RB, Koren HS, et al. Ozone dose and effect in humans and rats: A comparison using oxygen-18 labeling and bronchoalveolar lavage. *Am J Respir Crit Care Med* [Internet]. American Thoracic Society; 1994 [cited 2020 Oct 27];150:676–83. Available from: <https://pubmed.ncbi.nlm.nih.gov/8087337/>
158. Huang YA, Grant J, Roper S. Glutamate May Be an Efferent Transmitter That Elicits Inhibition in Mouse Taste Buds. *PLoS One* [Internet]. PLOS; 2012 [cited 2024 Feb 1];7:30662. Available from: [/pmc/articles/PMC3266908/](http://pmc/articles/PMC3266908/)

159. Okamoto T, Gohil K, Finkelstein EI, Bove P, Akaike T, Van Der Vliet A. Multiple contributing roles for NOS2 in LPS-induced acute airway inflammation in mice. *Am J Physiol - Lung Cell Mol Physiol* [Internet]. American Physiological Society; 2004 [cited 2021 Nov 22];286:198–209. Available from: <https://journals.physiology.org/doi/abs/10.1152/ajplung.00136.2003>
160. Morris Jr. SM. Arginine Metabolism Revisited. *J Nutr* [Internet]. 2016 [cited 2020 Apr 17];2579–86. Available from: <https://www.sciencedirect.com/science/article/pii/S0022316623008106?via%3Dihub>
161. Mathews JA, Kasahara DI, Cho Y, Bell LN, Gunst PR, Karoly ED, et al. Effect of acute ozone exposure on the lung metabolomes of obese and lean mice. *PLoS One* [Internet]. Public Library of Science; 2017 [cited 2024 Feb 2];12:e0181017. Available from: <https://journals.plos.org/plosone/article?id=10.1371/journal.pone.0181017>
162. Laskin DL, Fakhrzadeh L, Laskin JD. Nitric oxide and peroxynitrite in ozone-induced lung injury. *Adv Exp Med Biol* [Internet]. Kluwer Academic/Plenum Publishers; 2001 [cited 2024 Feb 2];500:183–90. Available from: https://link.springer.com/chapter/10.1007/978-1-4615-0667-6_24
163. Sunil VR, Vayas KN, Massa CB, Gow AJ, Laskin JD, Laskin DL. Ozone-induced injury and oxidative stress in bronchiolar epithelium are associated with altered pulmonary mechanics. *Toxicol Sci* [Internet]. Oxford Academic; 2013 [cited 2020 Oct 21];133:309–19. Available from: <https://academic.oup.com/toxsci/article/133/2/309/1615834>
164. Wu G, Morris SM. Arginine metabolism: Nitric oxide and beyond. *Biochem J*. 1998;336:1–17.
165. Hecker M, Sessa WC, Harris HJ, Änggård EE, Vane JR. The metabolism of L-arginine and its significance for the biosynthesis of endothelium-derived relaxing factor: Cultured endothelial cells recycle L-citrulline to L-arginine. *Proc Natl Acad Sci U S A* [Internet]. National Academy of Sciences; 1990 [cited 2024 Feb 2];87:8612–6. Available from: <https://www.pnas.org>
166. Szondi DC, Wong JK, Vardy LA, Cruickshank SM. Arginase Signalling as a Key Player in Chronic Wound Pathophysiology and Healing. *Front Mol Biosci* [Internet]. Front Mol Biosci; 2021 [cited 2024 Jan 21];8. Available from:

<https://pubmed.ncbi.nlm.nih.gov/34778380/>

167. Liu G, Designed Research; L RWL, Lian G, Performed Research; L RWL. Proinflammatory signal suppresses proliferation and shifts macrophage metabolism from Myc-dependent to HIF1 α -dependent. 2016 [cited 2019 Feb 11];113. Available from:
<https://www.ncbi.nlm.nih.gov/pmc/articles/PMC4760828/pdf/pnas.201518000.pdf>
168. Choi YH, Park HY. Anti-inflammatory effects of spermidine in lipopolysaccharide-stimulated BV2 microglial cells [Internet]. 2012. Available from:
<http://www.jbiomedsci.com/content/19/1/31>
169. Shi Y, Liu T, Nieman DC, Cui Y, Li F, Yang L, et al. Aerobic Exercise Attenuates Acute Lung Injury Through NET Inhibition. *Front Immunol*. 2020;11:1–12.
170. Song X, Jensen MO, Jogini V, Stein RA, Lee CH, McHaourab HS, et al. Mechanism of NMDA receptor channel block by MK-801 and memantine. *Nature* [Internet]. *Nature*; 2018 [cited 2024 Jan 21];556:515–9. Available from:
<https://pubmed.ncbi.nlm.nih.gov/29670280/>
171. Da Cunha AA, Nunes FB, Lunardelli A, Pauli V, Amaral RH, De Oliveira LM, et al. Treatment with N-methyl-d-aspartate receptor antagonist (MK-801) protects against oxidative stress in lipopolysaccharide-induced acute lung injury in the rat. *Int Immunopharmacol* [Internet]. Elsevier B.V.; 2011;11:706–11. Available from:
<http://dx.doi.org/10.1016/j.intimp.2011.01.016>
172. Abdolmaleki F, Farahani N, Hayat SMG, Pirro M, Bianconi V, Barreto GE, et al. The Role of Efferocytosis in Autoimmune Diseases. *Front Immunol* [Internet]. *Frontiers Media SA*; 2018 [cited 2024 Jan 21];9:1645. Available from:
</pmc/articles/PMC6064952/>
173. Goldstein CKW; CAS; KS; NK; JLK; DR, Smith CA, Sakamoto K, Kaminski N, Koff JL, Goldstein DR. Aging impairs alveolar macrophage phagocytosis and increases influenza-induced mortality in mice. *J Immunol* [Internet]. *NIH Public Access*; 2017 [cited 2024 Jan 21];199:1060. Available from:
</pmc/articles/PMC5557035/>
174. McQuattie-Pimentel AC, Ren Z, Joshi N, Watanabe S, Stoeger T, Chi M, et al. The

- lung microenvironment shapes a dysfunctional response of alveolar macrophages in aging. *J Clin Invest* [Internet]. *J Clin Invest*; 2021 [cited 2024 Jan 21];131. Available from: <https://pubmed.ncbi.nlm.nih.gov/33586677/>
175. Hopkin SJ, Pezhman L, Begum J, Kavanagh D, McGettrick HM, Iqbal AJ, et al. Aging modulates homeostatic leukocyte trafficking to the peritoneal cavity in a sex-specific manner. *J Leukoc Biol*. NLM (Medline); 2023;114:301–14.
176. De Maeyer RPH, van de Merwe RC, Louie R, Bracken O V., Devine OP, Goldstein DR, et al. Blocking elevated p38 MAPK restores efferocytosis and inflammatory resolution in the elderly. *Nat Immunol* 2020 216 [Internet]. Nature Publishing Group; 2020 [cited 2024 Feb 2];21:615–25. Available from: <https://www.nature.com/articles/s41590-020-0646-0>
177. Franceschi C, Garagnani P, Parini P, Giuliani C, Santoro A. Inflammaging: a new immune–metabolic viewpoint for age-related diseases. *Nat Rev Endocrinol* 2018 1410 [Internet]. Nature Publishing Group; 2018 [cited 2024 Feb 2];14:576–90. Available from: <https://www.nature.com/articles/s41574-018-0059-4>
178. Soda K, Kano Y, Sakuragi M, Takao K, Lefor A, Konishi F. Long-Term Oral Polyamine Intake Increases Blood Polyamine Concentrations. *J Nutr Sci Vitaminol (Tokyo)*. Center for Academic Publications Japan; 2009;55:361–6.
179. Madeo F, Eisenberg T, Pietrocola F, Kroemer G. Spermidine in health and disease. *Science (80-.)*. American Association for the Advancement of Science; 2018.
180. Antrup H, Seiler N. On the turnover of polyamines spermidine and spermine in mouse brain and other organs. *Neurochem Res*. 1980;5:123–43.
181. McCormick F. Kinetics of polyamine synthesis and turnover in mouse fibroblasts. *Biochem J* [Internet]. Portland Press Ltd; 1978 [cited 2024 Feb 2];174:427. Available from: </pmc/articles/PMC1185931/?report=abstract>

Biography

Marissa Arielle Guttenberg completed her Bachelor of Science Degree in Nanoscale Science, *summa cum laude*, and minors in Mathematics and Business from SUNY University at Albany College of Nanoscale Science and Engineering in May 2018. She then joined the Integrated Toxicology and Environmental Health Program at Duke University in the Fall of 2018, focusing her doctoral research on macrophage-derived mechanisms of resolution of environmental lung injury in the Robert Tighe Lab.

During her time at Duke, Marissa received several awards, including the Society of Toxicology (SOT) Science Communication Training Award and Visiting Pulmonary Scholar Symposium – First Place Poster Award. She presented her research at various conferences, including the Gordon Research Conference. She also contributed significantly to scientific mentorship, serving in leadership roles such as president of the Duke Graduate Student Chabad and treasurer of the Nicholas School PhD Advocacy Council. Marissa mentored numerous undergraduate and doctoral students and supported peers in their scientific endeavors.

Her dedication to fostering scientific scholarship extended beyond Duke, as she served as a representative on the SOT Inhalation and Respiratory Specialty Section. Marissa's commitment to advancing scientific knowledge and nurturing emerging scientists underscores her aspiration to pursue a career in industry post-graduation.